Chapter 3
Beamforming with Uniform Linear Arrays

Any good microphone array system requires a reliable beamforming algorithm at the outputs of the sensors to enhance a desired signal coming from a known direction. There are many ways to optimize the coefficients of this beamformer depending on what we want and the application at hand. Fundamentally, there are three large classes of conventional beamformers; they are the fixed, adaptive, and differential beamformers. In this chapter, we show how to derive most of their counterparts as well as new approaches with Kronecker product filters. We also show how to combine fixed and adaptive beamforming. While most of these beamformers are rather easy to derive, for some it is necessary to use iterative algorithms. The focus is on ULAs and with the decomposition of the steering vector of Chapter 2.

3.1 Fixed Beamformers

In this first section, we derive many examples of fixed beamformers thanks to the Kronecker product decomposition. We start with the most obvious one.

3.1.1 Delay and Sum

The most well-known and popular fixed beamformer is the so-called delay and sum (DS), which is derived by maximizing the WNG. Given the structure of the WNG of $\mathbf{h}$, it is clear that the maximization of this gain is equivalent to maximizing $\mathcal{W}_1(\mathbf{h}_1)$ and $\mathcal{W}_2(\mathbf{h}_2)$ separately. Taking into account the distortionless constraints, we easily get the DS beamformers at the two subarrays:

J. Benesty et al., *Array Processing*, Springer Topics in Signal Processing 18, https://doi.org/10.1007/978-3-030-15600-8_3

$$\mathbf{h}_{1,\mathrm{DS}} = \frac{\mathbf{d}_{1,\theta_\mathrm{d}}}{M_0}, \tag{3.1}$$

$$\mathbf{h}_{2,\mathrm{DS}} = \frac{\mathbf{d}_{2,\theta_\mathrm{d}}}{M_0}. \tag{3.2}$$

As a consequence, the DS beamformer corresponding to the global ULA is

$$\begin{aligned}\mathbf{h}_{\mathrm{DS}} &= \mathbf{h}_{1,\mathrm{DS}} \otimes \mathbf{h}_{2,\mathrm{DS}} \\ &= \frac{\mathbf{d}_{1,\theta_\mathrm{d}} \otimes \mathbf{d}_{2,\theta_\mathrm{d}}}{M_0^2} \\ &= \frac{\mathbf{d}_{\theta_\mathrm{d}}}{M_0^2},\end{aligned} \tag{3.3}$$

which is, of course, the classical DS beamformer [1], [2]. Here, however, it is shown how the structure of the global steering vector is exploited. In other words, the DS beamformer is determined by $2M_0$ different coefficients only when $M = M_0^2$.

It is obvious that

$$\mathcal{W}\left(\mathbf{h}_{\mathrm{DS}}\right) = M_0^2 = M \tag{3.4}$$

and the beampattern of the DS beamformer is

$$\begin{aligned}\mathcal{B}_\theta\left(\mathbf{h}_{\mathrm{DS}}\right) &= \mathcal{B}_{1,\theta}\left(\mathbf{h}_{1,\mathrm{DS}}\right) \times \mathcal{B}_{2,\theta}\left(\mathbf{h}_{2,\mathrm{DS}}\right) \\ &= \frac{1}{M_0^2}\left(\mathbf{d}_{1,\theta}^H \mathbf{d}_{1,\theta_\mathrm{d}}\right)\left(\mathbf{d}_{2,\theta}^H \mathbf{d}_{2,\theta_\mathrm{d}}\right).\end{aligned} \tag{3.5}$$

Finally, the DF of $\mathbf{h}_{\mathrm{DS}}$ is

$$\mathcal{D}\left(\mathbf{h}_{\mathrm{DS}}\right) = \frac{M_0^4}{\mathbf{d}_{\theta_\mathrm{d}}^H \boldsymbol{\Gamma} \mathbf{d}_{\theta_\mathrm{d}}}. \tag{3.6}$$

3.1.2 Partial Maximum DF

There are different fixed beamformers for which the DF is only maximized in part. We review some possibilities.

In the first approach, we assume that $\mathbf{h}_2$ is fixed. We may take $\mathbf{h}_2 = \mathbf{h}_{2,\mathrm{DS}}$ for the second ULA. Substituting this filter into (2.42), we get

$$\mathcal{D}\left(\mathbf{h}_1 | \mathbf{h}_{2,\mathrm{DS}}\right) = \frac{\left|\mathbf{h}_1^H \mathbf{d}_{1,\theta_\mathrm{d}}\right|^2}{\mathbf{h}_1^H \boldsymbol{\Gamma}_{\mathbf{h}_{2,\mathrm{DS}}} \mathbf{h}_1}, \tag{3.7}$$

where

$$\mathbf{\Gamma}_{\mathbf{h}_{2,\mathrm{DS}}} = \left(\mathbf{I}_{M_0} \otimes \mathbf{h}_{2,\mathrm{DS}}\right)^H \mathbf{\Gamma} \left(\mathbf{I}_{M_0} \otimes \mathbf{h}_{2,\mathrm{DS}}\right). \tag{3.8}$$

The maximization of $\mathcal{D}\left(\mathbf{h}_1|\mathbf{h}_{2,\mathrm{DS}}\right)$ gives the maximum DF beamformer at the first ULA:

$$\mathbf{h}_{1,\mathrm{mDF1}} = \frac{\mathbf{\Gamma}_{\mathbf{h}_{2,\mathrm{DS}}}^{-1}\mathbf{d}_{1,\theta_\mathrm{d}}}{\mathbf{d}_{1,\theta_\mathrm{d}}^H\mathbf{\Gamma}_{\mathbf{h}_{2,\mathrm{DS}}}^{-1}\mathbf{d}_{1,\theta_\mathrm{d}}}. \tag{3.9}$$

Therefore, our first (global) partial maximum DF (PmDF) beamformer is

$$\mathbf{h}_{\mathrm{PmDF1}} = \mathbf{h}_{1,\mathrm{mDF1}} \otimes \mathbf{h}_{2,\mathrm{DS}}. \tag{3.10}$$

We deduce that the WNG and the beampattern are, respectively,

$$\mathcal{W}\left(\mathbf{h}_{\mathrm{PmDF1}}\right) = M_0\mathcal{W}\left(\mathbf{h}_{1,\mathrm{mDF1}}\right) \tag{3.11}$$

and

$$\mathcal{B}_\theta\left(\mathbf{h}_{\mathrm{PmDF1}}\right) = \mathcal{B}_{1,\theta}\left(\mathbf{h}_{1,\mathrm{mDF1}}\right) \times \mathcal{B}_{2,\theta}\left(\mathbf{h}_{2,\mathrm{DS}}\right). \tag{3.12}$$

Figure 3.1 displays the directivity patterns of the first partial maximum DF beamformer, $\mathbf{h}_{\mathrm{PmDF1}}$, for $\theta_\mathrm{d} = 0$, $f = 1$ kHz, $\delta = 1$ cm, and different numbers of sensors $M = M_0^2$. Figure 3.2 shows plots of the DFs and WNGs of the first partial maximum DF beamformer as a function of frequency for $\theta_\mathrm{d} = 0$, $\delta = 1$ cm, and different numbers of sensors. We observe that as the number of sensors increases, the width of the main beam and the level of side lobes decrease, while the DF of the first partial maximum DF beamformer increases. However, using a larger number of sensors increases the WNG of the first partial maximum DF beamformer only for high frequencies, but decreases its WNG for low frequencies.

In the second approach, we assume that $\mathbf{h}_1$ is fixed, i.e., $\mathbf{h}_1 = \mathbf{h}_{1,\mathrm{DS}}$ for the first ULA. Substituting this filter into (2.44), we get

$$\mathcal{D}\left(\mathbf{h}_2|\mathbf{h}_{1,\mathrm{DS}}\right) = \frac{\left|\mathbf{h}_2^H\mathbf{d}_{2,\theta_\mathrm{d}}\right|^2}{\mathbf{h}_2^H\mathbf{\Gamma}_{\mathbf{h}_{1,\mathrm{DS}}}\mathbf{h}_2}, \tag{3.13}$$

where

$$\mathbf{\Gamma}_{\mathbf{h}_{1,\mathrm{DS}}} = \left(\mathbf{h}_{1,\mathrm{DS}} \otimes \mathbf{I}_{M_0}\right)^H \mathbf{\Gamma} \left(\mathbf{h}_{1,\mathrm{DS}} \otimes \mathbf{I}_{M_0}\right). \tag{3.14}$$

The maximization of $\mathcal{D}\left(\mathbf{h}_2|\mathbf{h}_{1,\mathrm{DS}}\right)$ gives the maximum DF beamformer at the second ULA:

$$\mathbf{h}_{2,\mathrm{mDF2}} = \frac{\mathbf{\Gamma}_{\mathbf{h}_{1,\mathrm{DS}}}^{-1}\mathbf{d}_{2,\theta_\mathrm{d}}}{\mathbf{d}_{2,\theta_\mathrm{d}}^H\mathbf{\Gamma}_{\mathbf{h}_{1,\mathrm{DS}}}^{-1}\mathbf{d}_{2,\theta_\mathrm{d}}}. \tag{3.15}$$

As a result, our second partial maximum DF beamformer is

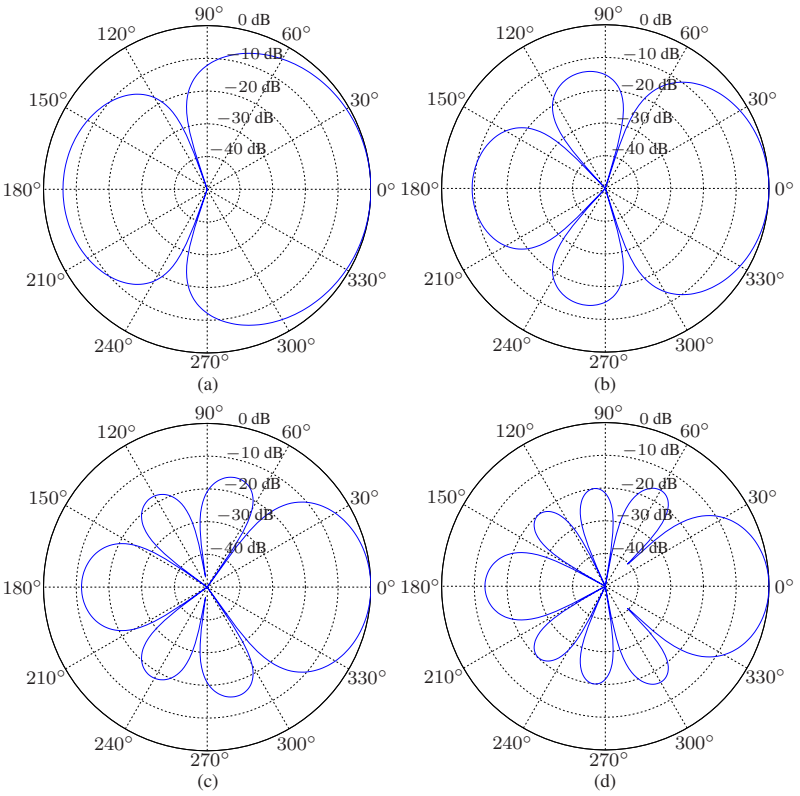

Fig. 3.1 Beampatterns of the first partial maximum DF beamformer, $\mathbf{h}_{\mathrm{PmDF1}}$, for $\theta_{\mathrm{d}} = 0$, $f = 1$ kHz, $\delta = 1$ cm, and different numbers of sensors $M = M_0^2$: (a) $M_0 = 2$, (b) $M_0 = 3$, (c) $M_0 = 4$, and (d) $M_0 = 5$.

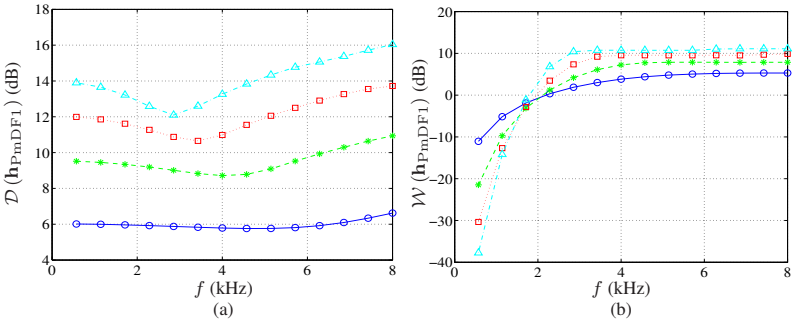

Fig. 3.2 Performance of the first partial maximum DF beamformer, $\mathbf{h}_{\mathrm{PmDF1}}$, as a function of frequency for $\theta_{\mathrm{d}} = 0$, $\delta = 1$ cm, and different numbers of sensors $M = M_0^2$: $M_0 = 2$ (solid line with circles), $M_0 = 3$ (dashed line with asterisks), $M_0 = 4$ (dotted line with squares), and $M_0 = 5$ (dash-dot line with triangles). (a) DF and (b) WNG.

$$\mathbf{h}_{\mathrm{PmDF2}} = \mathbf{h}_{1,\mathrm{DS}} \otimes \mathbf{h}_{2,\mathrm{mDF2}}. \tag{3.16}$$

We deduce that the WNG and the beampattern are, respectively,

$$\mathcal{W}\left(\mathbf{h}_{\mathrm{PmDF2}}\right) = M_0 \mathcal{W}\left(\mathbf{h}_{2,\mathrm{mDF2}}\right) \tag{3.17}$$

and

$$\mathcal{B}_\theta\left(\mathbf{h}_{\mathrm{PmDF2}}\right) = \mathcal{B}_{1,\theta}\left(\mathbf{h}_{1,\mathrm{DS}}\right) \times \mathcal{B}_{2,\theta}\left(\mathbf{h}_{2,\mathrm{mDF2}}\right). \tag{3.18}$$

From the two maximum DF beamformers derived above for the two subarrays, we find the third approach:

$$\mathbf{h}_{\mathrm{PmDF3}} = \mathbf{h}_{1,\mathrm{mDF1}} \otimes \mathbf{h}_{2,\mathrm{mDF2}}. \tag{3.19}$$

Now, we can maximize separately the two DFs, $\mathcal{D}_1\left(\mathbf{h}_1\right)$ and $\mathcal{D}_2\left(\mathbf{h}_2\right)$, of the subarrays. We get

$$\mathbf{h}_{1,\mathrm{mDF}} = \frac{\mathbf{\Gamma}_1^{-1}\mathbf{d}_{1,\theta_\mathrm{d}}}{\mathbf{d}_{1,\theta_\mathrm{d}}^H \mathbf{\Gamma}_1^{-1}\mathbf{d}_{1,\theta_\mathrm{d}}}, \tag{3.20}$$

$$\mathbf{h}_{2,\mathrm{mDF}} = \frac{\mathbf{\Gamma}_2^{-1}\mathbf{d}_{2,\theta_\mathrm{d}}}{\mathbf{d}_{2,\theta_\mathrm{d}}^H \mathbf{\Gamma}_2^{-1}\mathbf{d}_{2,\theta_\mathrm{d}}}. \tag{3.21}$$

As a result, the partial maximum DF beamformer of the fourth approach is simply the Kronecker product of the two above filters, i.e.,

$$\mathbf{h}_{\mathrm{PmDF4}} = \mathbf{h}_{1,\mathrm{mDF}} \otimes \mathbf{h}_{2,\mathrm{mDF}}. \tag{3.22}$$

Figure 3.3 displays the directivity patterns of the fourth partial maximum DF beamformer, $\mathbf{h}_{\mathrm{PmDF4}}$, for $\theta_\mathrm{d} = 0$, $f = 1$ kHz, $\delta = 1$ cm, and different numbers of sensors $M = M_0^2$. Figure 3.4 shows plots of the DFs and WNGs of the fourth partial maximum DF beamformer as a function of frequency for $\theta_\mathrm{d} = 0$, $\delta = 1$ cm, and different numbers of sensors. We observe that as the number of sensors increases, the width of the main beam and the level of side lobes decrease, while the DF of the fourth partial maximum DF beamformer increases. However, using a larger number of sensors decreases the WNG of the fourth partial maximum DF beamformer, especially at low frequencies. For a given number of sensors, the DF of the fourth partial maximum DF beamformer is higher than that of the first partial maximum DF beamformer, but the WNG of the fourth partial maximum DF beamformer is lower than that of the first partial maximum DF beamformer (compare Figs 3.2 and 3.4).

Two other possibilities are

$$\mathbf{h}_{\mathrm{PmDF5}} = \mathbf{h}_{1,\mathrm{mDF}} \otimes \mathbf{h}_{2,\mathrm{DS}} \tag{3.23}$$

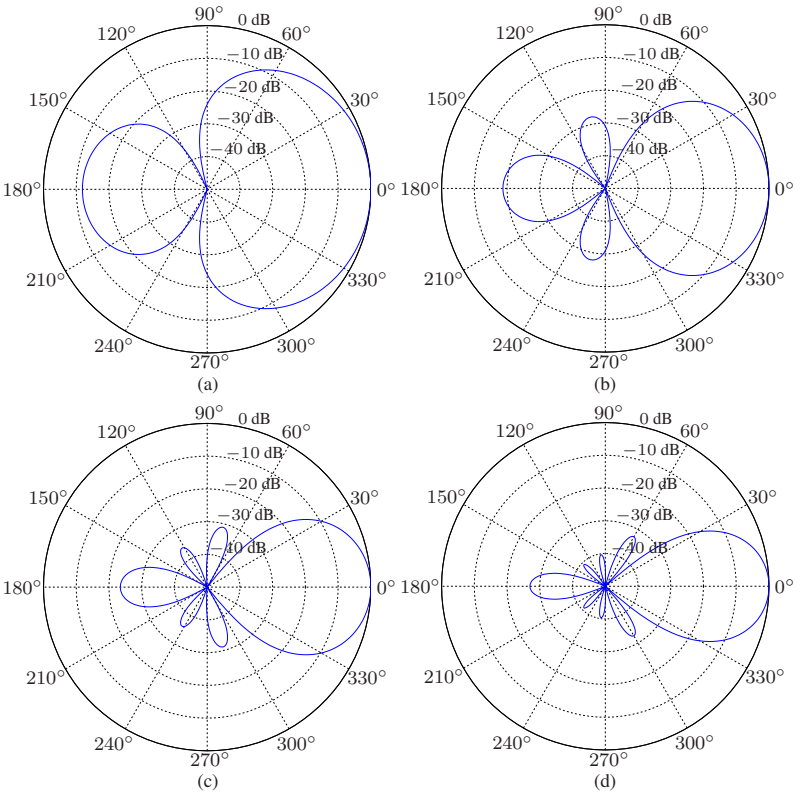

Fig. 3.3 Beampatterns of the fourth partial maximum DF beamformer, $\mathbf{h}_{\mathrm{PmDF4}}$, for $\theta_{\mathrm{d}} = 0$, $f = 1$ kHz, $\delta = 1$ cm, and different numbers of sensors $M = M_0^2$: (a) $M_0 = 2$, (b) $M_0 = 3$, (c) $M_0 = 4$, and (d) $M_0 = 5$.

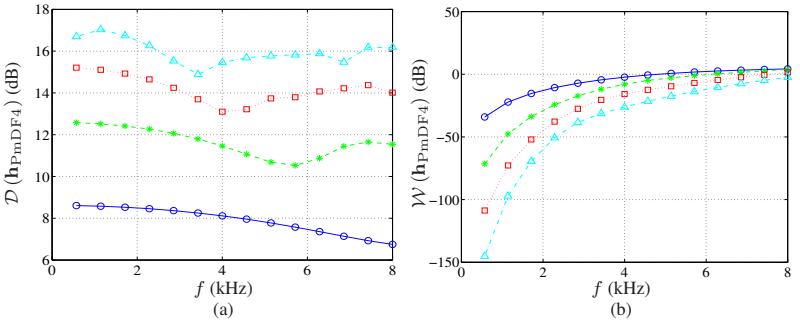

Fig. 3.4 Performance of the fourth partial maximum DF beamformer, $\mathbf{h}_{\mathrm{PmDF4}}$, as a function of frequency for $\theta_{\mathrm{d}} = 0$, $\delta = 1$ cm, and different numbers of sensors $M = M_0^2$: $M_0 = 2$ (solid line with circles), $M_0 = 3$ (dashed line with asterisks), $M_0 = 4$ (dotted line with squares), and $M_0 = 5$ (dash-dot line with triangles). (a) DF and (b) WNG.

and

$$\mathbf{h}_{\mathrm{PmDF6}} = \mathbf{h}_{1,\mathrm{DS}} \otimes \mathbf{h}_{2,\mathrm{mDF}}. \tag{3.24}$$

3.1.3 Maximum DF

From a theoretical point of view, the maximum DF beamformer is obtained by maximizing $\mathcal{D}(\mathbf{h})$ in (2.31) but this DF cannot be maximized directly. Therefore, an iterative algorithm is required for this task.

We start by taking

$$\begin{aligned}\mathbf{h}_2^{(0)} &= \mathbf{h}_{2,\mathrm{mDF}} \\ &= \frac{\mathbf{\Gamma}_2^{-1}\mathbf{d}_{2,\theta_\mathrm{d}}}{\mathbf{d}_{2,\theta_\mathrm{d}}^H\mathbf{\Gamma}_2^{-1}\mathbf{d}_{2,\theta_\mathrm{d}}}.\end{aligned} \tag{3.25}$$

Substituting $\mathbf{h}_2^{(0)}$ into (2.43), we get

$$\mathbf{\Gamma}_{\mathbf{h}_2^{(0)}} = \left(\mathbf{I}_{M_0} \otimes \mathbf{h}_2^{(0)}\right)^H \mathbf{\Gamma} \left(\mathbf{I}_{M_0} \otimes \mathbf{h}_2^{(0)}\right). \tag{3.26}$$

Now, plugging this expression into the DF in (2.42), we obtain at iteration 1:

$$\mathcal{D}\left(\mathbf{h}_1^{(1)}|\mathbf{h}_2^{(0)}\right) = \frac{\left|\left(\mathbf{h}_1^{(1)}\right)^H \mathbf{d}_{1,\theta_\mathrm{d}}\right|^2}{\left(\mathbf{h}_1^{(1)}\right)^H \mathbf{\Gamma}_{\mathbf{h}_2^{(0)}} \mathbf{h}_1^{(1)}}. \tag{3.27}$$

The maximization of $\mathcal{D}\left(\mathbf{h}_1^{(1)}|\mathbf{h}_2^{(0)}\right)$ with respect to $\mathbf{h}_1^{(1)}$ gives

$$\mathbf{h}_1^{(1)} = \frac{\mathbf{\Gamma}_{\mathbf{h}_2^{(0)}}^{-1}\mathbf{d}_{1,\theta_\mathrm{d}}}{\mathbf{d}_{1,\theta_\mathrm{d}}^H\mathbf{\Gamma}_{\mathbf{h}_2^{(0)}}^{-1}\mathbf{d}_{1,\theta_\mathrm{d}}}. \tag{3.28}$$

Using $\mathbf{h}_1^{(1)}$ in (2.45), we get

$$\mathbf{\Gamma}_{\mathbf{h}_1^{(1)}} = \left(\mathbf{h}_1^{(1)} \otimes \mathbf{I}_{M_0}\right)^H \mathbf{\Gamma} \left(\mathbf{h}_1^{(1)} \otimes \mathbf{I}_{M_0}\right). \tag{3.29}$$

As a result, the DF in (2.44) is

$$\mathcal{D}\left(\mathbf{h}_2^{(1)}|\mathbf{h}_1^{(1)}\right) = \frac{\left|\left(\mathbf{h}_2^{(1)}\right)^H \mathbf{d}_{2,\theta_\mathrm{d}}\right|^2}{\left(\mathbf{h}_2^{(1)}\right)^H \mathbf{\Gamma}_{\mathbf{h}_1^{(1)}} \mathbf{h}_2^{(1)}}, \tag{3.30}$$

whose maximization with respect to $\mathbf{h}_2^{(1)}$ gives

$$\mathbf{h}_2^{(1)} = \frac{\mathbf{\Gamma}_{\mathbf{h}_1^{(1)}}^{-1} \mathbf{d}_{2,\theta_\mathrm{d}}}{\mathbf{d}_{2,\theta_\mathrm{d}}^H \mathbf{\Gamma}_{\mathbf{h}_1^{(1)}}^{-1} \mathbf{d}_{2,\theta_\mathrm{d}}}. \tag{3.31}$$

Continuing the iterations up to the iteration n, we easily get for the first filter:

$$\mathbf{h}_1^{(n)} = \frac{\mathbf{\Gamma}_{\mathbf{h}_2^{(n-1)}}^{-1} \mathbf{d}_{1,\theta_\mathrm{d}}}{\mathbf{d}_{1,\theta_\mathrm{d}}^H \mathbf{\Gamma}_{\mathbf{h}_2^{(n-1)}}^{-1} \mathbf{d}_{1,\theta_\mathrm{d}}}, \tag{3.32}$$

with

$$\mathbf{\Gamma}_{\mathbf{h}_2^{(n-1)}} = \left(\mathbf{I}_{M_0} \otimes \mathbf{h}_2^{(n-1)}\right)^H \mathbf{\Gamma} \left(\mathbf{I}_{M_0} \otimes \mathbf{h}_2^{(n-1)}\right), \tag{3.33}$$

and for the second filter:

$$\mathbf{h}_2^{(n)} = \frac{\mathbf{\Gamma}_{\mathbf{h}_1^{(n)}}^{-1} \mathbf{d}_{2,\theta_\mathrm{d}}}{\mathbf{d}_{2,\theta_\mathrm{d}}^H \mathbf{\Gamma}_{\mathbf{h}_1^{(n)}}^{-1} \mathbf{d}_{2,\theta_\mathrm{d}}}, \tag{3.34}$$

with

$$\mathbf{\Gamma}_{\mathbf{h}_1^{(n)}} = \left(\mathbf{h}_1^{(n)} \otimes \mathbf{I}_{M_0}\right)^H \mathbf{\Gamma} \left(\mathbf{h}_1^{(n)} \otimes \mathbf{I}_{M_0}\right). \tag{3.35}$$

Finally, we deduce that the maximum DF beamformer is at iteration n:

$$\mathbf{h}_{\mathrm{mDF}}^{(n)} = \mathbf{h}_1^{(n)} \otimes \mathbf{h}_2^{(n)}. \tag{3.36}$$

Figure 3.5 displays the directivity patterns of the maximum DF beamformer, $\mathbf{h}_{\mathrm{mDF}}^{(n)}$, for $f = 1$ kHz, $\delta = 1$ cm, and $M_0 = 3$, obtained at the iteration n for several values of n. Figure 3.6 shows plots of the DFs and WNGs of the maximum DF beamformer as a function of frequency for $\delta = 1$ cm, $M_0 = 3$, and several values of n. We observe that the DF of the maximum DF beamformer increases at each iteration, and roughly converges after five iterations, while the WNG decreases at each iteration. Compared with the partial maximum DF beamformers, the maximum DF beamformer yields higher DF, but lower WNG (compare Figs 3.4 and 3.6).

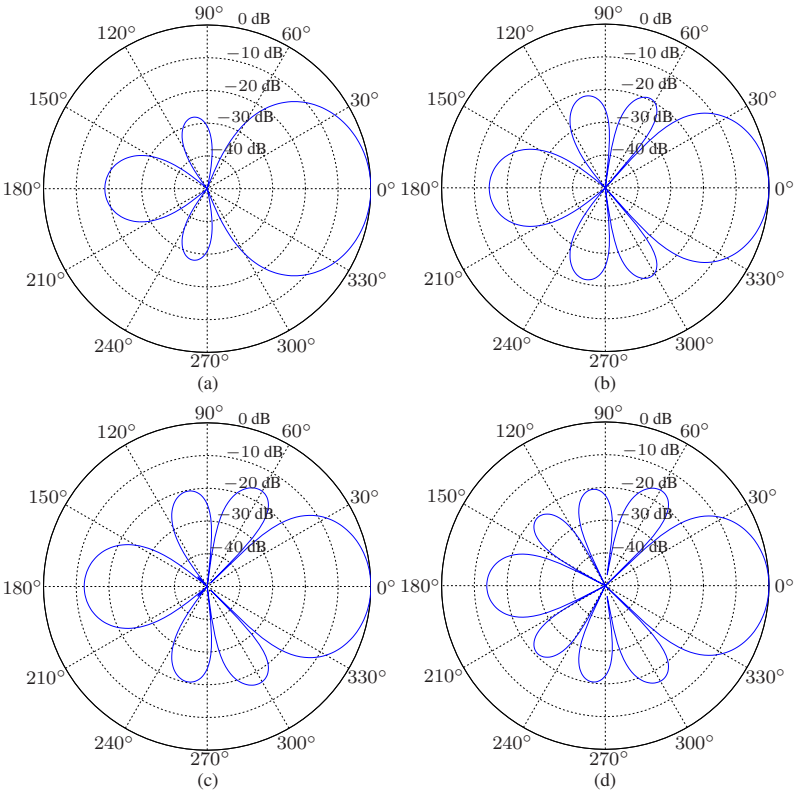

Fig. 3.5 Beampatterns of the maximum DF beamformer, $\mathbf{h}_{\mathrm{mDF}}^{(n)}$, for $f = 1$ kHz, $\delta = 1$ cm, and $M_0 = 3$, obtained at the iteration n: (a) $n = 0$, (b) $n = 1$, (c) $n = 2$, and (d) $n = 5$.

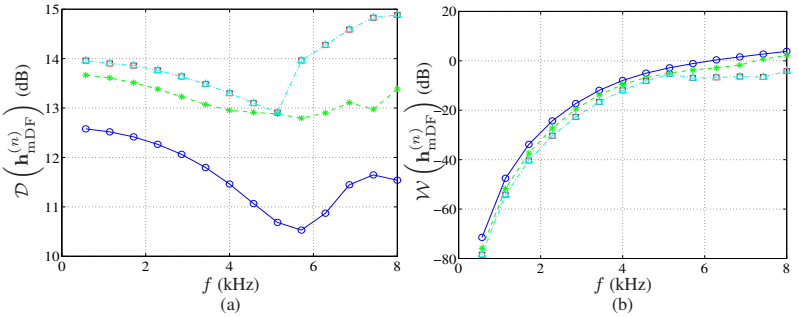

Fig. 3.6 Performance of the maximum DF beamformer, $\mathbf{h}_{\mathrm{mDF}}^{(n)}$, as a function of frequency for $\delta = 1$ cm, $M_0 = 3$, and several values of n: $n = 0$ (solid line with circles), $n = 1$ (dashed line with asterisks), $n = 5$ (dotted line with squares), and $n = 10$ (dash-dot line with triangles). (a) DF and (b) WNG.

If we want to compromise between the WNG and the DF, we should optimize the following criteria:

$$\min_{\mathbf{h}_1^{(n)}} \left(\mathbf{h}_1^{(n)}\right)^H \left(\mathbf{\Gamma}_{\mathbf{h}_2^{(n-1)}} + \epsilon_1 \mathbf{I}_{M_0}\right) \mathbf{h}_1^{(n)} \quad \text{subject to} \quad \left(\mathbf{h}_1^{(n)}\right)^H \mathbf{d}_{1,\theta_\mathrm{d}} = 1, \tag{3.37}$$

$$\min_{\mathbf{h}_2^{(n)}} \left(\mathbf{h}_2^{(n)}\right)^H \left(\mathbf{\Gamma}_{\mathbf{h}_1^{(n)}} + \epsilon_2 \mathbf{I}_{M_0}\right) \mathbf{h}_2^{(n)} \quad \text{subject to} \quad \left(\mathbf{h}_2^{(n)}\right)^H \mathbf{d}_{2,\theta_\mathrm{d}} = 1, \tag{3.38}$$

where $\epsilon_1, \epsilon_2 \geq 0$ are the regularization parameters, and $\mathbf{\Gamma}_{\mathbf{h}_2^{(n-1)}}$ and $\mathbf{\Gamma}_{\mathbf{h}_1^{(n)}}$ are defined in (3.33) and (3.35), respectively. We find that the optimal filters are

$$\mathbf{h}_{1,\epsilon_1}^{(n)} = \frac{\left(\mathbf{\Gamma}_{\mathbf{h}_2^{(n-1)}} + \epsilon_1 \mathbf{I}_{M_0}\right)^{-1} \mathbf{d}_{1,\theta_\mathrm{d}}}{\mathbf{d}_{1,\theta_\mathrm{d}}^H \left(\mathbf{\Gamma}_{\mathbf{h}_2^{(n-1)}} + \epsilon_1 \mathbf{I}_{M_0}\right)^{-1} \mathbf{d}_{1,\theta_\mathrm{d}}} \tag{3.39}$$

and

$$\mathbf{h}_{2,\epsilon_2}^{(n)} = \frac{\left(\mathbf{\Gamma}_{\mathbf{h}_1^{(n)}} + \epsilon_2 \mathbf{I}_{M_0}\right)^{-1} \mathbf{d}_{2,\theta_\mathrm{d}}}{\mathbf{d}_{2,\theta_\mathrm{d}}^H \left(\mathbf{\Gamma}_{\mathbf{h}_1^{(n)}} + \epsilon_2 \mathbf{I}_{M_0}\right)^{-1} \mathbf{d}_{2,\theta_\mathrm{d}}}, \tag{3.40}$$

with the initialization:

$$\mathbf{h}_{2,\epsilon_2}^{(0)} = \frac{\left(\mathbf{\Gamma}_2 + \epsilon_2 \mathbf{I}_{M_0}\right)^{-1} \mathbf{d}_{2,\theta_\mathrm{d}}}{\mathbf{d}_{2,\theta_\mathrm{d}}^H \left(\mathbf{\Gamma}_2 + \epsilon_2 \mathbf{I}_{M_0}\right)^{-1} \mathbf{d}_{2,\theta_\mathrm{d}}}. \tag{3.41}$$

As a result, the robust maximum DF beamformer is at iteration n:

$$\mathbf{h}_{\mathrm{R},\epsilon_1,\epsilon_2}^{(n)} = \mathbf{h}_{1,\epsilon_1}^{(n)} \otimes \mathbf{h}_{2,\epsilon_2}^{(n)}. \tag{3.42}$$

Figure 3.7 displays the directivity patterns of the robust maximum DF beamformer at the iteration $n = 5$, $\mathbf{h}_{\mathrm{R},\epsilon_1,\epsilon_2}^{(5)}$, for $M_0 = 3$, $f = 1$ kHz, $\delta = 1$ cm, and several values of ϵ_1 and ϵ_2. Figure 3.8 shows plots of the DFs and WNGs of the robust maximum DF beamformer at the iteration $n = 5$ as a function of frequency for $M_0 = 3$, $\delta = 1$ cm, and several values of ϵ_1 and ϵ_2. We observe that for larger values of ϵ_1 and ϵ_2, the WNG increases, but the DF decreases and the main lobe becomes wider.

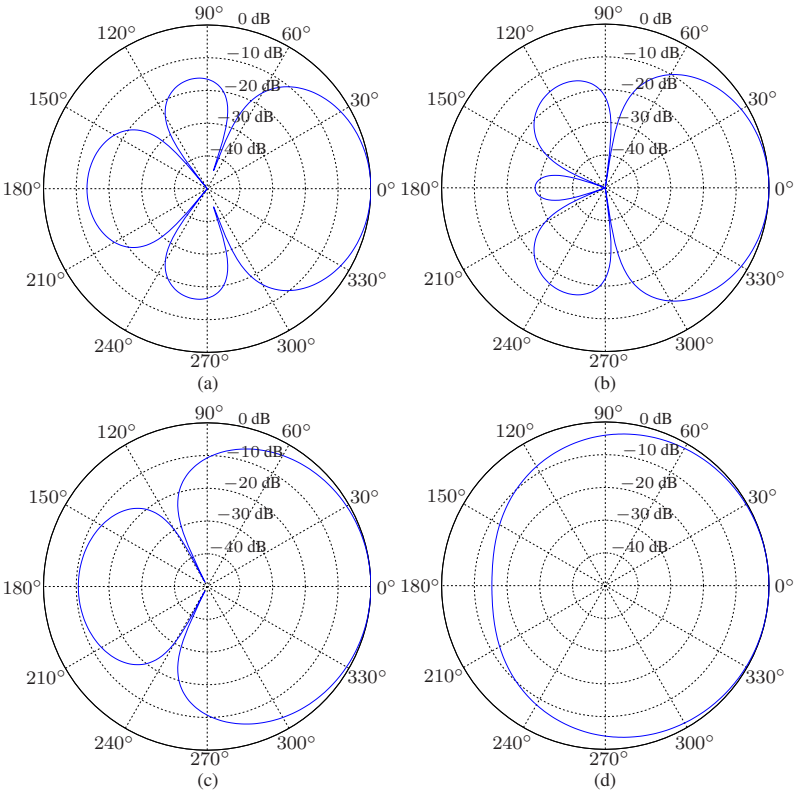

Fig. 3.7 Beampatterns of the robust maximum DF beamformer at the iteration $n = 5$, $\mathbf{h}_{\mathrm{R},\epsilon_1,\epsilon_2}^{(5)}$, for $M_0 = 3$, $f = 1$ kHz, $\delta = 1$ cm, and several values of ϵ_1 and ϵ_2: (a) $\epsilon_1 = \epsilon_2 = 0.001$, (b) $\epsilon_1 = \epsilon_2 = 0.01$, (c) $\epsilon_1 = \epsilon_2 = 0.1$, and (d) $\epsilon_1 = \epsilon_2 = 1$.

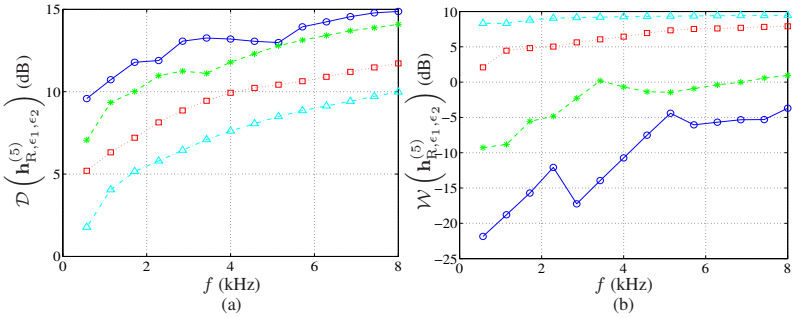

Fig. 3.8 Performance of the robust maximum DF beamformer at the iteration $n = 5$, $\mathbf{h}_{\mathrm{R},\epsilon_1,\epsilon_2}^{(5)}$, as a function of frequency for $M_0 = 3$, $\delta = 1$ cm, and several values of ϵ_1 and ϵ_2: $\epsilon_1 = \epsilon_2 = 0.001$ (solid line with circles), $\epsilon_1 = \epsilon_2 = 0.01$ (dashed line with asterisks), $\epsilon_1 = \epsilon_2 = 0.1$ (dotted line with squares), and $\epsilon_1 = \epsilon_2 = 1$ (dash-dot line with triangles). (a) DF and (b) WNG.

3.1.4 Null Steering

In this subsection, we assume that we have one interference source impinging on the global array from the direction $\theta_0 \neq \theta_\mathrm{d}$ that we would like to completely cancel, i.e., to steer a null in that direction, and, meanwhile, recover the desired source coming from the direction θ_d. There are many ways to do this. First, remember that a null in the beampattern $\mathcal{B}_{1,\theta}(\mathbf{h}_1)$ implies a null in the global beampattern $\mathcal{B}_\theta(\mathbf{h})$. In the same way, a null in the beampattern $\mathcal{B}_{2,\theta}(\mathbf{h}_2)$ implies a null in the global beampattern $\mathcal{B}_\theta(\mathbf{h})$. As a result, the same null in $\mathcal{B}_{1,\theta}(\mathbf{h}_1)$ and in $\mathcal{B}_{2,\theta}(\mathbf{h}_2)$ implies a null in $\mathcal{B}_\theta(\mathbf{h})$ of multiplicity 2. Then, by including the distortionless constraints, we can write the constraint equations as

$$\mathbf{C}_1^H \mathbf{h}_1 = \mathbf{i}_\mathrm{c}, \tag{3.43}$$

$$\mathbf{C}_2^H \mathbf{h}_2 = \mathbf{i}_\mathrm{c}, \tag{3.44}$$

where

$$\mathbf{C}_1 = \left[\, \mathbf{d}_{1,\theta_\mathrm{d}} \; \mathbf{d}_{1,\theta_0} \,\right], \tag{3.45}$$

$$\mathbf{C}_2 = \left[\, \mathbf{d}_{2,\theta_\mathrm{d}} \; \mathbf{d}_{2,\theta_0} \,\right] \tag{3.46}$$

are the constraint matrices of size $M_0 \times 2$ whose two columns are linearly independent and

$$\mathbf{i}_\mathrm{c} = \left[\, 1 \; 0 \,\right]^T \tag{3.47}$$

is a vector of length 2.

In the first approach, we take the DS beamformer for the second filter, i.e., $\mathbf{h}_2 = \mathbf{h}_{2,\mathrm{DS}}$. To find the first filter, we maximize the WNG by taking (3.43) into account, i.e.,

$$\min_{\mathbf{h}_1} \mathbf{h}_1^H \mathbf{h}_1 \quad \text{subject to} \quad \mathbf{C}_1^H \mathbf{h}_1 = \mathbf{i}_\mathrm{c}. \tag{3.48}$$

From this criterion, we get the minimum-norm (MN) beamformer:

$$\mathbf{h}_{1,\mathrm{MN}} = \mathbf{C}_1 \left(\mathbf{C}_1^H \mathbf{C}_1\right)^{-1} \mathbf{i}_\mathrm{c}, \tag{3.49}$$

which is also the minimum-norm solution of (3.43). Therefore, the first (global) proposed null-steering (NS) beamformer is

$$\mathbf{h}_{\mathrm{NS1}} = \mathbf{h}_{1,\mathrm{MN}} \otimes \mathbf{h}_{2,\mathrm{DS}}. \tag{3.50}$$

We deduce that the WNG and the beampattern are, respectively,

$$\mathcal{W}(\mathbf{h}_{\mathrm{NS1}}) = M_0 \mathcal{W}(\mathbf{h}_{1,\mathrm{MN}}) \tag{3.51}$$

and

$$\mathcal{B}_\theta\left(\mathbf{h}_{\mathrm{NS1}}\right)=\mathcal{B}_{1,\theta}\left(\mathbf{h}_{1,\mathrm{MN}}\right)\times\mathcal{B}_{2,\theta}\left(\mathbf{h}_{2,\mathrm{DS}}\right). \tag{3.52}$$

In the second approach, we take the DS beamformer for the first filter, i.e., $\mathbf{h}_1=\mathbf{h}_{1,\mathrm{DS}}$. To find the second filter, we maximize the WNG by taking (3.44) into account. We get

$$\mathbf{h}_{2,\mathrm{MN}}=\mathbf{C}_2\left(\mathbf{C}_2^H\mathbf{C}_2\right)^{-1}\mathbf{i}_{\mathrm{c}}, \tag{3.53}$$

which is also the minimum-norm solution of (3.44). Therefore, the second proposed null-steering beamformer is

$$\mathbf{h}_{\mathrm{NS2}}=\mathbf{h}_{1,\mathrm{DS}}\otimes\mathbf{h}_{2,\mathrm{MN}}. \tag{3.54}$$

We deduce that the WNG and the beampattern are, respectively,

$$\mathcal{W}\left(\mathbf{h}_{\mathrm{NS2}}\right)=M_0\mathcal{W}\left(\mathbf{h}_{2,\mathrm{MN}}\right) \tag{3.55}$$

and

$$\mathcal{B}_\theta\left(\mathbf{h}_{\mathrm{NS2}}\right)=\mathcal{B}_{1,\theta}\left(\mathbf{h}_{1,\mathrm{DS}}\right)\times\mathcal{B}_{2,\theta}\left(\mathbf{h}_{2,\mathrm{MN}}\right). \tag{3.56}$$

Finally, in the third and last approach as far as the maximization of the WNG is concerned, we propose to use the two derived minimum-norm filters, i.e.,

$$\mathbf{h}_{\mathrm{NS3}}=\mathbf{h}_{1,\mathrm{MN}}\otimes\mathbf{h}_{2,\mathrm{MN}}. \tag{3.57}$$

The global beampattern is

$$\mathcal{B}_\theta\left(\mathbf{h}_{\mathrm{NS3}}\right)=\mathcal{B}_{1,\theta}\left(\mathbf{h}_{1,\mathrm{MN}}\right)\times\mathcal{B}_{2,\theta}\left(\mathbf{h}_{2,\mathrm{MN}}\right), \tag{3.58}$$

which has a null of multiplicity 2 in the direction θ_0.

Figure 3.9 displays the directivity patterns of the third null-steering beamformer, $\mathbf{h}_{\mathrm{NS3}}$, for $\theta_{\mathrm{d}}=0$, $f=1$ kHz, $\delta=5$ mm, $M_0=3$, and several values of θ_0. Figure 3.10 shows plots of the DFs and WNGs of the third null-steering beamformer as a function of frequency for $\theta_{\mathrm{d}}=0$, $\delta=5$ mm, $M_0=3$, and several values of θ_0. We observe that for $\theta_{\mathrm{d}}=0$, the WNG of the third null-steering beamformer increases as θ_0 increases from 90° to 180°.

A second class of beamformers is obtained by maximizing the DF instead of the WNG. Let $\mathbf{h}_2=\mathbf{h}_{2,\mathrm{DS}}$. To find the first filter, we maximize the DF by taking (3.43) into account, i.e.,

$$\min_{\mathbf{h}_1}\mathbf{h}_1^H\boldsymbol{\Gamma}_1\mathbf{h}_1\quad\text{subject to}\quad\mathbf{C}_1^H\mathbf{h}_1=\mathbf{i}_{\mathrm{c}}. \tag{3.59}$$

The solution to this problem is

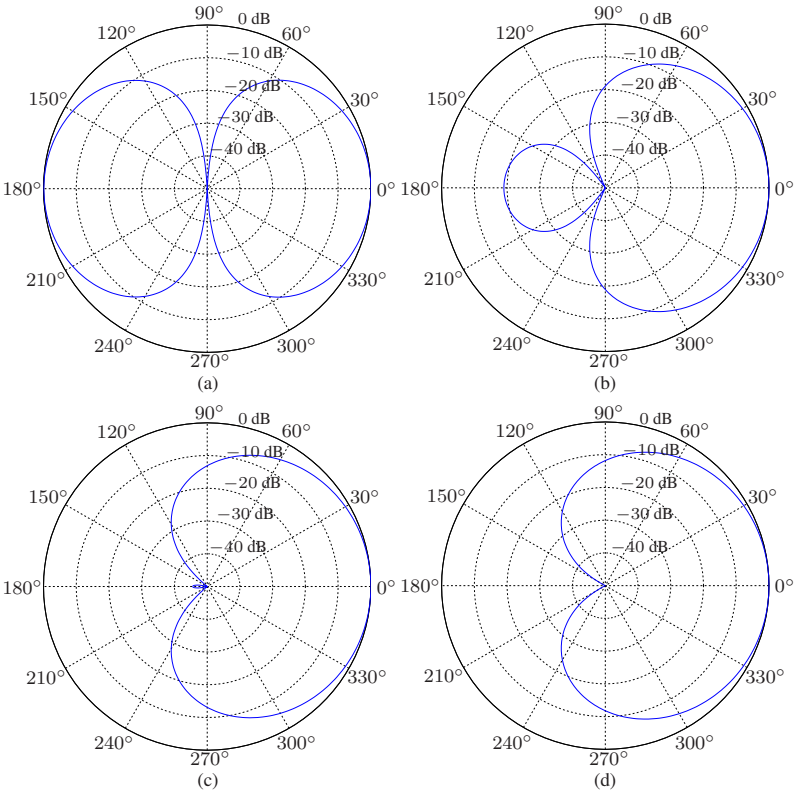

Fig. 3.9 Beampatterns of the third null-steering beamformer, $\mathbf{h}_{\mathrm{NS3}}$, for $\theta_{\mathrm{d}} = 0$, $f = 1$ kHz, $\delta = 5$ mm, $M_0 = 3$, and several values of θ_0: (a) $\theta_0 = 90°$, (b) $\theta_0 = 120°$, (c) $\theta_0 = 150°$, and (d) $\theta_0 = 180°$.

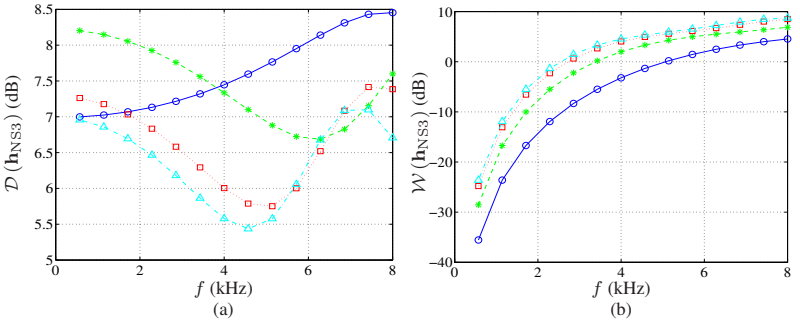

Fig. 3.10 Performance of the third null-steering beamformer, $\mathbf{h}_{\mathrm{NS3}}$, as a function of frequency for $\theta_{\mathrm{d}} = 0$, $\delta = 5$ mm, $M_0 = 3$, and several values of θ_0: $\theta_0 = 90°$ (solid line with circles), $\theta_0 = 120°$ (dashed line with asterisks), $\theta_0 = 150°$ (dotted line with squares), and $\theta_0 = 180°$ (dash-dot line with triangles). (a) DF and (b) WNG.

$$\mathbf{h}_{1,\mathrm{NS4}} = \boldsymbol{\Gamma}_1^{-1}\mathbf{C}_1\left(\mathbf{C}_1^H\boldsymbol{\Gamma}_1^{-1}\mathbf{C}_1\right)^{-1}\mathbf{i}_{\mathrm{c}}. \tag{3.60}$$

Therefore, the fourth approach is

$$\mathbf{h}_{\mathrm{NS4}} = \mathbf{h}_{1,\mathrm{NS4}} \otimes \mathbf{h}_{2,\mathrm{DS}}. \tag{3.61}$$

In the fifth approach, we choose $\mathbf{h}_1 = \mathbf{h}_{1,\mathrm{DS}}$ and to find the second filter, we maximize the DF by taking (3.44) into account. We get

$$\mathbf{h}_{2,\mathrm{NS5}} = \boldsymbol{\Gamma}_2^{-1}\mathbf{C}_2\left(\mathbf{C}_2^H\boldsymbol{\Gamma}_2^{-1}\mathbf{C}_2\right)^{-1}\mathbf{i}_{\mathrm{c}}. \tag{3.62}$$

Therefore, the global null-steering beamformer is

$$\mathbf{h}_{\mathrm{NS5}} = \mathbf{h}_{1,\mathrm{DS}} \otimes \mathbf{h}_{2,\mathrm{NS5}}. \tag{3.63}$$

In the sixth approach, we combine the two previous ones:

$$\mathbf{h}_{\mathrm{NS6}} = \mathbf{h}_{1,\mathrm{NS4}} \otimes \mathbf{h}_{2,\mathrm{NS5}}. \tag{3.64}$$

The DF of $\mathbf{h}_{\mathrm{NS6}}$ will be greater than that of $\mathbf{h}_{\mathrm{NS4}}$ and $\mathbf{h}_{\mathrm{NS5}}$.

Figure 3.11 displays the directivity patterns of the sixth null-steering beamformer, $\mathbf{h}_{\mathrm{NS6}}$, for $\theta_{\mathrm{d}} = 0$, $f = 1$ kHz, $\delta = 5$ mm, $M_0 = 3$, and several values of θ_0. Figure 3.12 shows plots of the DFs and WNGs of the sixth null-steering beamformer as a function of frequency for $\theta_{\mathrm{d}} = 0$, $\delta = 5$ mm, $M_0 = 3$, and several values of θ_0. Compared with the third null-steering beamformer, the sixth null-steering beamformer yields higher DF, but lower WNG (compare Figs 3.10 and 3.12).

To fully maximize the DF while having a null of multiplicity 2 in the direction θ_0, we need to optimize the following criteria:

$$\min_{\mathbf{h}_1^{(n)}} \left(\mathbf{h}_1^{(n)}\right)^H \boldsymbol{\Gamma}_{\mathbf{h}_2^{(n-1)}}\mathbf{h}_1^{(n)} \quad \text{subject to} \quad \mathbf{C}_1^H\mathbf{h}_1^{(n)} = \mathbf{i}_{\mathrm{c}}, \tag{3.65}$$

$$\min_{\mathbf{h}_2^{(n)}} \left(\mathbf{h}_2^{(n)}\right)^H \boldsymbol{\Gamma}_{\mathbf{h}_1^{(n)}}\mathbf{h}_2^{(n)} \quad \text{subject to} \quad \mathbf{C}_2^H\mathbf{h}_2^{(n)} = \mathbf{i}_{\mathrm{c}}, \tag{3.66}$$

where $\boldsymbol{\Gamma}_{\mathbf{h}_2^{(n-1)}}$ and $\boldsymbol{\Gamma}_{\mathbf{h}_1^{(n)}}$ are defined in (3.33) and (3.35), respectively. We easily get

$$\mathbf{h}_1^{(n)} = \boldsymbol{\Gamma}_{\mathbf{h}_2^{(n-1)}}^{-1}\mathbf{C}_1\left(\mathbf{C}_1^H\boldsymbol{\Gamma}_{\mathbf{h}_2^{(n-1)}}^{-1}\mathbf{C}_1\right)^{-1}\mathbf{i}_{\mathrm{c}} \tag{3.67}$$

and

$$\mathbf{h}_2^{(n)} = \boldsymbol{\Gamma}_{\mathbf{h}_1^{(n)}}^{-1}\mathbf{C}_2\left(\mathbf{C}_2^H\boldsymbol{\Gamma}_{\mathbf{h}_1^{(n)}}^{-1}\mathbf{C}_2\right)^{-1}\mathbf{i}_{\mathrm{c}}, \tag{3.68}$$

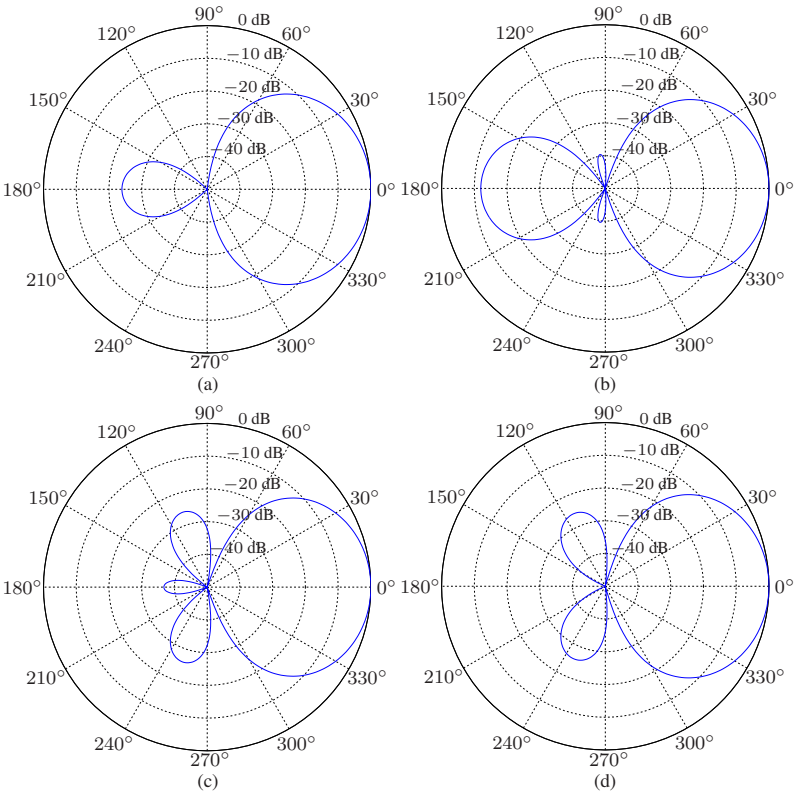

Fig. 3.11 Beampatterns of the sixth null-steering beamformer, $\mathbf{h}_{\mathrm{NS6}}$, for $\theta_{\mathrm{d}} = 0$, $f = 1$ kHz, $\delta = 5$ mm, $M_0 = 3$, and several values of θ_0: (a) $\theta_0 = 90°$, (b) $\theta_0 = 120°$, (c) $\theta_0 = 150°$, and (d) $\theta_0 = 180°$.

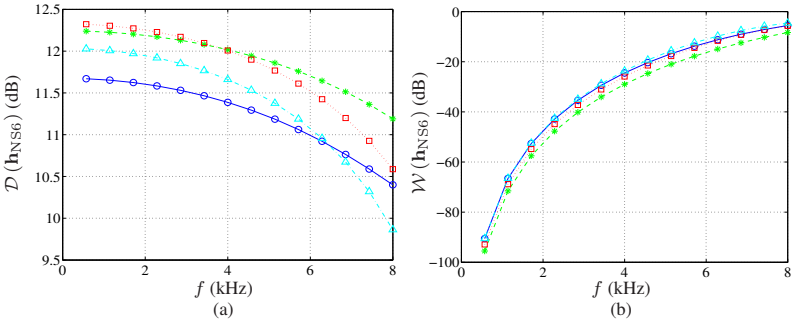

Fig. 3.12 Performance of the sixth null-steering beamformer, $\mathbf{h}_{\mathrm{NS6}}$, as a function of frequency for $\theta_{\mathrm{d}} = 0$, $\delta = 5$ mm, $M_0 = 3$, and several values of θ_0: $\theta_0 = 90°$ (solid line with circles), $\theta_0 = 120°$ (dashed line with asterisks), $\theta_0 = 150°$ (dotted line with squares), and $\theta_0 = 180°$ (dash-dot line with triangles). (a) DF and (b) WNG.

with the initialization:

$$\mathbf{h}_2^{(0)} = \mathbf{\Gamma}_2^{-1}\mathbf{C}_2\left(\mathbf{C}_2^H\mathbf{\Gamma}_2^{-1}\mathbf{C}_2\right)^{-1}\mathbf{i}_c. \tag{3.69}$$

Therefore, the seventh and last proposed null-steering beamformer is at iteration n:

$$\mathbf{h}_{\mathrm{NS7}}^{(n)} = \mathbf{h}_1^{(n)} \otimes \mathbf{h}_2^{(n)}. \tag{3.70}$$

Figure 3.13 displays the directivity patterns of the seventh null-steering beamformer, $\mathbf{h}_{\mathrm{NS7}}^{(n)}$, for $f = 1$ kHz, $\delta = 5$ mm, $\theta_{\mathrm{d}} = 0$, $\theta_0 = 180°$, and $M_0 = 3$, obtained at the iteration n for several values of n. Figure 3.14 shows plots of the DFs and WNGs of the seventh null-steering beamformer as a function of frequency for $\delta = 5$ mm, $\theta_{\mathrm{d}} = 0$, $\theta_0 = 180°$, $M_0 = 3$, and several values of n. We observe that the DF of the seventh null-steering beamformer increases at each iteration, and roughly converges after two iterations, while the WNG decreases at each iteration. Compared with the above null-steering beamformers, the seventh null-steering beamformer yields the highest DF, but the lowest WNG (compare Figs 3.12 and 3.14).

3.2 Adaptive Beamformers

Before developing some useful adaptive beamformers in our context, we first present other important performance measures that depend on the second-order statistics of the signals.

3.2.1 Other Measures

The (narrowband) noise reduction factor quantifies the amount of noise being rejected by the beamformer. It is defined as

$$\xi_{\mathrm{n}}(\mathbf{h}) = \frac{\phi_{V_1}}{\mathbf{h}^H\mathbf{\Phi}_{\mathbf{v}}\mathbf{h}}. \tag{3.71}$$

The noise reduction factor is expected to be lower bounded by 1; otherwise, the beamformer amplifies the noise. The higher the value of the noise reduction factor, the more the noise is rejected. While the output SNR is upper bounded, the noise reduction factor is not. In the distortionless case, i.e., $\mathbf{h}^H\mathbf{d}_{\theta_{\mathrm{d}}} = 1$, the noise reduction factor coincides with the array gain [defined in (2.26)].

Since the noise is reduced by the beamforming operation, so is, in general, the desired signal. This desired signal reduction (or cancellation) implies, in

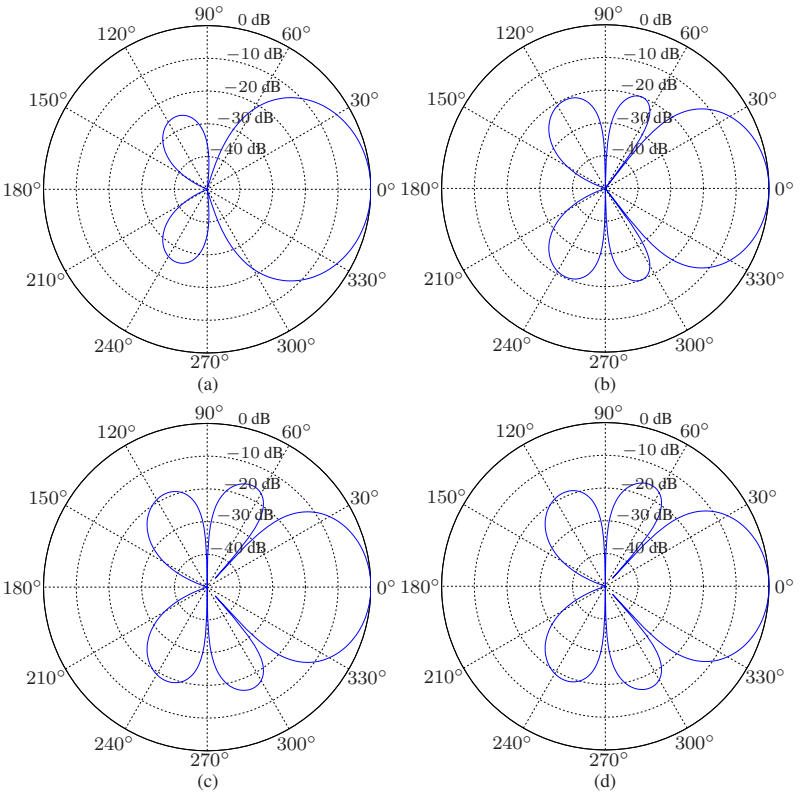

Fig. 3.13 Beampatterns of the seventh null-steering beamformer, $\mathbf{h}_{\mathrm{NS7}}^{(n)}$, for $f = 1$ kHz, $\delta = 5$ mm, $\theta_{\mathrm{d}} = 0$, $\theta_0 = 180°$, and $M_0 = 3$, obtained at the iteration n: (a) $n = 0$, (b) $n = 1$, (c) $n = 2$, and (d) $n = 10$.

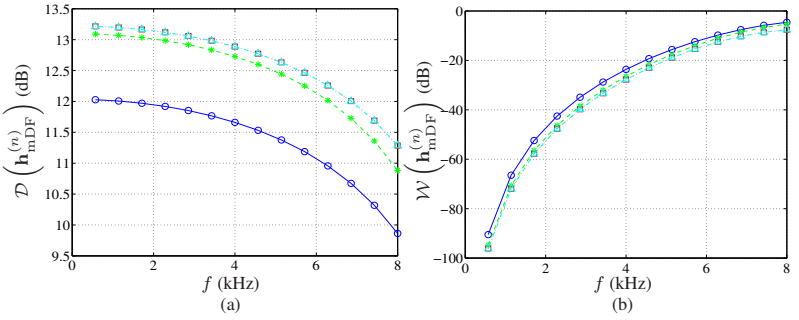

Fig. 3.14 Performance of the seventh null-steering beamformer, $\mathbf{h}_{\mathrm{NS7}}^{(n)}$, as a function of frequency for $\delta = 5$ mm, $\theta_{\mathrm{d}} = 0$, $\theta_0 = 180°$, $M_0 = 3$, and several values of n: $n = 0$ (solid line with circles), $n = 1$ (dashed line with asterisks), $n = 2$ (dotted line with squares), and $n = 10$ (dash-dot line with triangles). (a) DF and (b) WNG.

general, distortion. The (narrowband) desired signal reduction factor is

$$\begin{aligned}\xi_{\mathrm{d}}(\mathbf{h}) &= \frac{\phi_X}{\mathbf{h}^H\boldsymbol{\Phi}_{\mathbf{x}}\mathbf{h}} \\ &= \frac{1}{\left|\mathbf{h}^H\mathbf{d}_{\theta_{\mathrm{d}}}\right|^2} \\ &= \frac{1}{\left|\mathbf{h}_1^H\mathbf{d}_{1,\theta_{\mathrm{d}}}\right|^2} \times \frac{1}{\left|\mathbf{h}_2^H\mathbf{d}_{2,\theta_{\mathrm{d}}}\right|^2} \\ &= \xi_{1,\mathrm{d}}(\mathbf{h}_1) \times \xi_{2,\mathrm{d}}(\mathbf{h}_2).\end{aligned} \tag{3.72}$$

The closer the value of $\xi_{\mathrm{d}}(\mathbf{h})$ is to 1, the less distorted is the desired signal.

It is easy to verify that we have the following fundamental relation:

$$\frac{\mathrm{oSNR}(\mathbf{h})}{\mathrm{iSNR}} = \frac{\xi_{\mathrm{n}}(\mathbf{h})}{\xi_{\mathrm{d}}(\mathbf{h})}, \tag{3.73}$$

where the output and input SNRs are defined in (2.25) and (2.24), respectively. This expression indicates the equivalence between gain/loss in SNR and distortion (of both the desired and noise signals).

Another way to measure the distortion of the desired signal due to the beamforming operation is via the (narrowband) desired signal distortion index:

$$\begin{aligned}\upsilon_{\mathrm{d}}(\mathbf{h}) &= \frac{E\left(\left|X_{\mathrm{fd}} - X\right|^2\right)}{\phi_X} \\ &= \left|\mathbf{h}^H\mathbf{d}_{\theta_{\mathrm{d}}} - 1\right|^2.\end{aligned} \tag{3.74}$$

The desired signal distortion index is close to 0 if there is no distortion and expected to be greater than 0 when distortion occurs.

Error criteria play a critical role in deriving optimal beamformers. The mean-squared error (MSE) [3] is, by far, the most practical one. We define the error signal between the estimated and desired signals as

$$\begin{aligned}\mathcal{E} &= Z - X \\ &= X_{\mathrm{fd}} + V_{\mathrm{rn}} - X \\ &= \mathcal{E}_{\mathrm{d}} + \mathcal{E}_{\mathrm{n}},\end{aligned} \tag{3.75}$$

where

$$\mathcal{E}_{\mathrm{d}} = \left(\mathbf{h}^H\mathbf{d}_{\theta_{\mathrm{d}}} - 1\right)X \tag{3.76}$$

is the desired signal distortion due to the beamformer and

$$\mathcal{E}_{\mathrm{n}} = \mathbf{h}^H\mathbf{v} \tag{3.77}$$

represents the residual noise. Since $\mathcal{E}_{\mathrm{d}}$ and $\mathcal{E}_{\mathrm{n}}$ are incoherent, the (narrowband) MSE can be expressed as

$$\begin{aligned} J(\mathbf{h}) &= E\left(|\mathcal{E}|^2\right) \\ &= E\left(|\mathcal{E}_{\mathrm{d}}|^2\right) + E\left(|\mathcal{E}_{\mathrm{n}}|^2\right) \\ &= J_{\mathrm{d}}(\mathbf{h}) + J_{\mathrm{n}}(\mathbf{h}) \\ &= \phi_X + \mathbf{h}^H \mathbf{\Phi}_{\mathbf{y}} \mathbf{h} - \phi_X \mathbf{h}^H \mathbf{d}_{\theta_{\mathrm{d}}} - \phi_X \mathbf{d}_{\theta_{\mathrm{d}}}^H \mathbf{h}, \end{aligned} \tag{3.78}$$

where

$$\begin{aligned} J_{\mathrm{d}}(\mathbf{h}) &= \phi_X \left|\mathbf{h}^H \mathbf{d}_{\theta_{\mathrm{d}}} - 1\right|^2 \\ &= \phi_X \upsilon_{\mathrm{d}}(\mathbf{h}) \end{aligned} \tag{3.79}$$

and

$$\begin{aligned} J_{\mathrm{n}}(\mathbf{h}) &= \mathbf{h}^H \mathbf{\Phi}_{\mathbf{v}} \mathbf{h} \\ &= \frac{\phi_{V_1}}{\xi_{\mathrm{n}}(\mathbf{h})}. \end{aligned} \tag{3.80}$$

We have the following classical relationships:

$$\begin{aligned} \frac{J_{\mathrm{d}}(\mathbf{h})}{J_{\mathrm{n}}(\mathbf{h})} &= \mathrm{iSNR} \times \xi_{\mathrm{n}}(\mathbf{h}) \times \upsilon_{\mathrm{d}}(\mathbf{h}) \\ &= \mathrm{oSNR}(\mathbf{h}) \times \xi_{\mathrm{d}}(\mathbf{h}) \times \upsilon_{\mathrm{d}}(\mathbf{h}). \end{aligned} \tag{3.81}$$

3.2.2 Wiener

Because of the structure of $\mathbf{h}$, a closed-form Wiener beamformer cannot apparently be found but an iterative one can be derived. Using (2.40) and (2.41), we can express the MSE in (3.78) as

$$J(\mathbf{h}_1 \otimes \mathbf{h}_2) = \phi_X + \mathbf{h}_1^H \mathbf{\Phi}_{\mathbf{y},2} \mathbf{h}_1 - \phi_{X,2} \mathbf{h}_1^H \mathbf{d}_{1,\theta_{\mathrm{d}}} - \phi_{X,2}^* \mathbf{d}_{1,\theta_{\mathrm{d}}}^H \mathbf{h}_1 \tag{3.82}$$

$$= \phi_X + \mathbf{h}_2^H \mathbf{\Phi}_{\mathbf{y},1} \mathbf{h}_2 - \phi_{X,1} \mathbf{h}_2^H \mathbf{d}_{2,\theta_{\mathrm{d}}} - \phi_{X,1}^* \mathbf{d}_{2,\theta_{\mathrm{d}}}^H \mathbf{h}_2, \tag{3.83}$$

where

$$\mathbf{\Phi}_{\mathbf{y},2} = \left(\mathbf{I}_{M_0} \otimes \mathbf{h}_2\right)^H \mathbf{\Phi}_{\mathbf{y}} \left(\mathbf{I}_{M_0} \otimes \mathbf{h}_2\right), \tag{3.84}$$

$$\phi_{X,2} = \phi_X \mathbf{h}_2^H \mathbf{d}_{2,\theta_{\mathrm{d}}}, \tag{3.85}$$

and

$$\mathbf{\Phi}_{\mathbf{y},1} = \left(\mathbf{h}_1 \otimes \mathbf{I}_{M_0}\right)^H \mathbf{\Phi}_{\mathbf{y}} \left(\mathbf{h}_1 \otimes \mathbf{I}_{M_0}\right), \tag{3.86}$$

$$\phi_{X,1} = \phi_X \mathbf{h}_1^H \mathbf{d}_{1,\theta_\mathrm{d}}. \tag{3.87}$$

It is interesting to notice that the size of the matrices $\mathbf{\Phi}_{\mathbf{y},1}$ and $\mathbf{\Phi}_{\mathbf{y},2}$, which is $M_0 \times M_0$, is much smaller than the size of $\mathbf{\Phi}_{\mathbf{y}}$, which is $M_0^2 \times M_0^2$. As a result, in practice, much less observations are needed to accurately estimate $\mathbf{\Phi}_{\mathbf{y},1}$ and $\mathbf{\Phi}_{\mathbf{y},2}$ than $\mathbf{\Phi}_{\mathbf{y}}$, which is the matrix that is inverted in the conventional Wiener beamformer.

When $\mathbf{h}_2$ is fixed, we write (3.82) as

$$J\left(\mathbf{h}_1|\mathbf{h}_2\right) = \phi_X + \mathbf{h}_1^H \mathbf{\Phi}_{\mathbf{y},2} \mathbf{h}_1 - \phi_{X,2} \mathbf{h}_1^H \mathbf{d}_{1,\theta_\mathrm{d}} - \phi_{X,2}^* \mathbf{d}_{1,\theta_\mathrm{d}}^H \mathbf{h}_1, \tag{3.88}$$

and when $\mathbf{h}_1$ is fixed, we write (3.83) as

$$J\left(\mathbf{h}_2|\mathbf{h}_1\right) = \phi_X + \mathbf{h}_2^H \mathbf{\Phi}_{\mathbf{y},1} \mathbf{h}_2 - \phi_{X,1} \mathbf{h}_2^H \mathbf{d}_{2,\theta_\mathrm{d}} - \phi_{X,1}^* \mathbf{d}_{2,\theta_\mathrm{d}}^H \mathbf{h}_2. \tag{3.89}$$

Now, we have everything to derive an iterative algorithm similar to the one proposed in [4]. At iteration 0, we may take

$$\mathbf{h}_2^{(0)} = \phi_X \mathbf{\Phi}_{\mathbf{y}_2}^{-1} \mathbf{d}_{2,\theta_\mathrm{d}}, \tag{3.90}$$

where $\mathbf{\Phi}_{\mathbf{y}_2}$ is the covariance matrix of

$$\mathbf{y}_2 = \begin{bmatrix} Y_1 & Y_2 & \cdots & Y_{M_0} \end{bmatrix}^T, \tag{3.91}$$

whose elements are the M_0 first ones of $\mathbf{y}$. In fact, $\mathbf{h}_2^{(0)}$ is just the traditional Wiener beamformer applied to the second ULA. Substituting $\mathbf{h}_2^{(0)}$ into (3.84)–(3.85), we get

$$\mathbf{\Phi}_{\mathbf{y},2}^{(0)} = \left(\mathbf{I}_{M_0} \otimes \mathbf{h}_2^{(0)}\right)^H \mathbf{\Phi}_{\mathbf{y}} \left(\mathbf{I}_{M_0} \otimes \mathbf{h}_2^{(0)}\right), \tag{3.92}$$

$$\phi_{X,2}^{(0)} = \phi_X \left(\mathbf{h}_2^{(0)}\right)^H \mathbf{d}_{2,\theta_\mathrm{d}}. \tag{3.93}$$

Then, substituting these quantities into the MSE in (3.88), we obtain at iteration 1:

$$\begin{aligned} J\left(\mathbf{h}_1^{(1)}|\mathbf{h}_2^{(0)}\right) = \phi_X &+ \left(\mathbf{h}_1^{(1)}\right)^H \mathbf{\Phi}_{\mathbf{y},2}^{(0)} \mathbf{h}_1^{(1)} - \phi_{X,2}^{(0)} \left(\mathbf{h}_1^{(1)}\right)^H \mathbf{d}_{1,\theta_\mathrm{d}} \\ &- \left(\phi_{X,2}^{(0)}\right)^* \mathbf{d}_{1,\theta_\mathrm{d}}^H \mathbf{h}_1^{(1)}. \end{aligned} \tag{3.94}$$

The minimization of $J\left(\mathbf{h}_1^{(1)}|\mathbf{h}_2^{(0)}\right)$ with respect to $\mathbf{h}_1^{(1)}$ gives

$$\mathbf{h}_1^{(1)} = \phi_{X,2}^{(0)} \left(\mathbf{\Phi}_{\mathbf{y},2}^{(0)}\right)^{-1} \mathbf{d}_{1,\theta_\mathrm{d}}. \tag{3.95}$$

Using $\mathbf{h}_1^{(1)}$ into (3.86)–(3.87), we obtain

$$\mathbf{\Phi}_{\mathbf{y},1}^{(1)} = \left(\mathbf{h}_1^{(1)} \otimes \mathbf{I}_{M_0}\right)^H \mathbf{\Phi}_{\mathbf{y}} \left(\mathbf{h}_1^{(1)} \otimes \mathbf{I}_{M_0}\right), \tag{3.96}$$

$$\phi_{X,1}^{(1)} = \phi_X \left(\mathbf{h}_1^{(1)}\right)^H \mathbf{d}_{1,\theta_\mathrm{d}}. \tag{3.97}$$

With $\mathbf{\Phi}_{\mathbf{y},1}^{(1)}$ and $\phi_{X,1}^{(1)}$, we can compute the MSE in (3.89) as

$$\begin{aligned} J\left(\mathbf{h}_2^{(1)}|\mathbf{h}_1^{(1)}\right) = \phi_X + \left(\mathbf{h}_2^{(1)}\right)^H \mathbf{\Phi}_{\mathbf{y},1}^{(1)} \mathbf{h}_2^{(1)} - \phi_{X,1}^{(1)} \left(\mathbf{h}_2^{(1)}\right)^H \mathbf{d}_{2,\theta_\mathrm{d}} \\ - \left(\phi_{X,1}^{(1)}\right)^* \mathbf{d}_{2,\theta_\mathrm{d}}^H \mathbf{h}_2^{(1)}, \end{aligned} \tag{3.98}$$

whose minimization with respect to $\mathbf{h}_2^{(1)}$ gives

$$\mathbf{h}_2^{(1)} = \phi_{X,1}^{(1)} \left(\mathbf{\Phi}_{\mathbf{y},1}^{(1)}\right)^{-1} \mathbf{d}_{2,\theta_\mathrm{d}}. \tag{3.99}$$

Continuing the iterations up to the iteration n, we easily get the estimate of the first beamformer:

$$\mathbf{h}_1^{(n)} = \phi_{X,2}^{(n-1)} \left(\mathbf{\Phi}_{\mathbf{y},2}^{(n-1)}\right)^{-1} \mathbf{d}_{1,\theta_\mathrm{d}}, \tag{3.100}$$

where

$$\phi_{X,2}^{(n-1)} = \phi_X \left(\mathbf{h}_2^{(n-1)}\right)^H \mathbf{d}_{2,\theta_\mathrm{d}}, \tag{3.101}$$

$$\mathbf{\Phi}_{\mathbf{y},2}^{(n-1)} = \left(\mathbf{I}_{M_0} \otimes \mathbf{h}_2^{(n-1)}\right)^H \mathbf{\Phi}_{\mathbf{y}} \left(\mathbf{I}_{M_0} \otimes \mathbf{h}_2^{(n-1)}\right), \tag{3.102}$$

and the estimate of the second beamformer:

$$\mathbf{h}_2^{(n)} = \phi_{X,1}^{(n)} \left(\mathbf{\Phi}_{\mathbf{y},1}^{(n)}\right)^{-1} \mathbf{d}_{2,\theta_\mathrm{d}}, \tag{3.103}$$

where

$$\phi_{X,1}^{(n)} = \phi_X \left(\mathbf{h}_1^{(n)}\right)^H \mathbf{d}_{1,\theta_\mathrm{d}}, \tag{3.104}$$

$$\mathbf{\Phi}_{\mathbf{y},1}^{(n)} = \left(\mathbf{h}_1^{(n)} \otimes \mathbf{I}_{M_0}\right)^H \mathbf{\Phi}_{\mathbf{y}} \left(\mathbf{h}_1^{(n)} \otimes \mathbf{I}_{M_0}\right). \tag{3.105}$$

Finally, we deduce that the Wiener beamformer is at iteration n:

$$\mathbf{h}_\mathrm{W}^{(n)} = \mathbf{h}_1^{(n)} \otimes \mathbf{h}_2^{(n)}, \tag{3.106}$$

where $\mathbf{h}_1^{(n)}$ and $\mathbf{h}_2^{(n)}$ are defined in (3.100) and (3.103), respectively.

Example 3.1. Suppose that a desired signal impinges on the ULA from the direction $\theta_{\rm d}$, and that a statistically independent interference impinges on the ULA from the direction θ_0. Assume that the desired signal is a harmonic pulse of T samples:

$$x(t) = \begin{cases} A\sin\left(\omega_0 t + \phi\right), & 0 \le t \le T-1 \\ 0, & t < 0,\ t \ge T \end{cases},$$

with fixed amplitude A and angular frequency ω_0, and random phase ϕ, uniformly distributed on the interval from 0 to 2π. Assume that the interference $u(t)$ is white Gaussian noise, i.e., $u(t) \sim \mathcal{N}\left(0, \sigma_u^2\right)$, uncorrelated with $x(t)$. In addition, the sensors contain thermal white Gaussian noise, $w_m(t) \sim \mathcal{N}\left(0, \sigma_w^2\right)$, that are mutually uncorrelated. The noisy received signals are given by $y_m(t) = x_m(t) + v_m(t),\ m = 1, 2, \ldots, M$, where $v_m(t) = u_m(t) + w_m(t),\ m = 1, 2, \ldots, M$ are the interference-plus-noise signals. The variance of $X(\omega)$ is given by

$$\phi_X = \frac{A^2}{4} D_T^2\left[\pi\left(\omega + \omega_0\right)\right] + \frac{A^2}{4} D_T^2\left[\pi\left(\omega - \omega_0\right)\right],$$

where

$$D_T(x) = \frac{\sin\left(Tx\right)}{\sin\left(x\right)}.$$

The covariance matrices of $\mathbf{x}(\omega)$ and $\mathbf{v}(\omega)$ are given by

$$\begin{aligned} \mathbf{\Phi}_{\mathbf{x}} &= \phi_X \mathbf{d}_{\theta_{\rm d}} \mathbf{d}_{\theta_{\rm d}}^H, \\ \mathbf{\Phi}_{\mathbf{v}} &= T\sigma_u^2 \mathbf{d}_{\theta_0} \mathbf{d}_{\theta_0}^H + T\sigma_w^2 \mathbf{I}_M. \end{aligned}$$

To demonstrate the performance of the Wiener beamformer, we choose $A = 0.5$, $\omega_0 = 2\pi f_0$, $f_0 = 3$ kH, $T = 500$, $\theta_{\rm d} = 70°$, $\theta_0 = 30°$, and $\sigma_w^2 = 0.01\sigma_u^2$. Figure 3.15 displays the directivity patterns of the Wiener beamformer, $\mathbf{h}_{\rm W}^{(n)}$, for iSNR = 0 dB, $f = 3$ kHz, $\delta = 1$ cm, and $M_0 = 5$, obtained at the iteration n for several values of n. The directivity patterns converge after three iterations. The main beam is in the direction of the desired signal, i.e., $\theta_{\rm d}$, and there is a null in the direction of the interference, i.e., θ_0. Figure 3.16 shows plots of the gain in SNR, $\mathcal{G}\left(\mathbf{h}_{\rm W}^{(n)}\right)$, the noise reduction factor, $\xi_{\rm n}\left(\mathbf{h}_{\rm W}^{(n)}\right)$, the desired signal distortion index, $\upsilon_{\rm d}\left(\mathbf{h}_{\rm W}^{(n)}\right)$, and the MSE, $J\left(\mathbf{h}_{\rm W}^{(n)}\right)$, as a function of the input SNR for $f = 3$ kHz, $\delta = 1$ cm, $M_0 = 5$, and several values of n. We observe that the MSE and the desired signal distortion index obtained by the Wiener beamformer decrease at each iteration, and roughly converge after three iterations, while the gain in SNR and the noise reduction factor increase at each iteration. Figure 3.17 displays the directivity patterns of the Wiener beamformer at the iteration $n = 10$, for

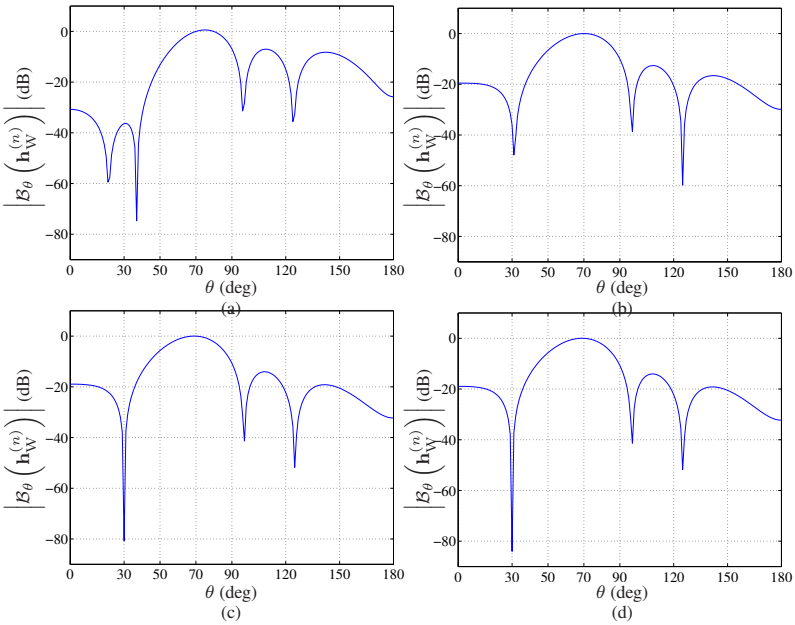

Fig. 3.15 Beampatterns of the Wiener beamformer, $\mathbf{h}_{\mathrm{W}}^{(n)}$, for iSNR = 0 dB, $f = 3$ kHz, $\delta = 1$ cm, $\theta_{\mathrm{d}} = 70°$, $\theta_0 = 30°$, and $M_0 = 5$, obtained at the iteration n: (a) $n = 1$, (b) $n = 2$, (c) $n = 3$, and (d) $n = 4$.

iSNR = 0 dB, $f = 3$ kHz, $\delta = 1$ cm, and different numbers of sensors, M. As the number of sensors increases, the width of the main beam decreases, and the null in the direction of the interference becomes deeper. Figure 3.18 shows plots of the gain in SNR, $\mathcal{G}\left(\mathbf{h}_{\mathrm{W}}^{(10)}\right)$, the noise reduction factor, $\xi_{\mathrm{n}}\left(\mathbf{h}_{\mathrm{W}}^{(10)}\right)$, the desired signal distortion index, $\upsilon_{\mathrm{d}}\left(\mathbf{h}_{\mathrm{W}}^{(10)}\right)$, and the MSE, $J\left(\mathbf{h}_{\mathrm{W}}^{(10)}\right)$, as a function of the input SNR for $f = 3$ kHz, $\delta = 1$ cm, and different numbers of sensors, M. We observe that as the number of sensors increases, the MSE and the desired signal distortion index obtained by the Wiener beamformer decrease while the gain in SNR and the noise reduction factor increase.

3.2.3 Tradeoff

In order to better compromise between noise reduction and desired signal distortion, we can minimize the desired signal distortion indices with the constraints that the noise reduction factors are equal to positive values that are greater than 1, i.e.,

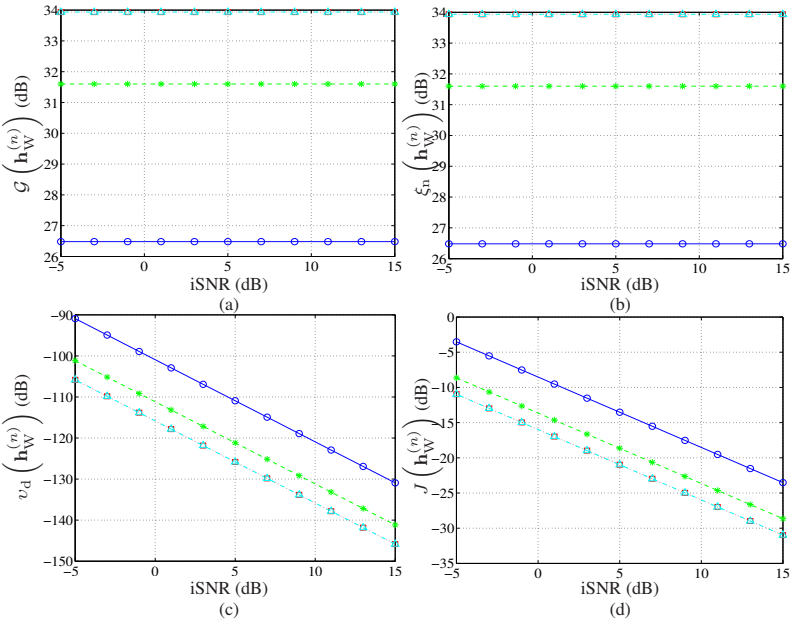

Fig. 3.16 Performance of the Wiener beamformer, $\mathbf{h}_{\mathrm{W}}^{(n)}$, as a function of the input SNR for $f = 3$ kHz, $\delta = 1$ cm, $\theta_{\mathrm{d}} = 70°$, $\theta_0 = 30°$, $M_0 = 5$, and several values of n: $n = 1$ (solid line with circles), $n = 2$ (dashed line with asterisks), $n = 3$ (dotted line with squares), and $n = 10$ (dash-dot line with triangles). (a) Gain in SNR, (b) noise reduction factor, (c) desired signal distortion index, and (d) MSE.

$$\min_{\mathbf{h}_1^{(n)}} J_{\mathrm{d}}\left(\mathbf{h}_1^{(n)}|\mathbf{h}_2^{(n-1)}\right) \quad \text{subject to} \quad J_{\mathrm{n}}\left(\mathbf{h}_1^{(n)}|\mathbf{h}_2^{(n-1)}\right) = \aleph_1\phi_{V_1}, \tag{3.107}$$

$$\min_{\mathbf{h}_2^{(n)}} J_{\mathrm{d}}\left(\mathbf{h}_2^{(n)}|\mathbf{h}_1^{(n)}\right) \quad \text{subject to} \quad J_{\mathrm{n}}\left(\mathbf{h}_2^{(n)}|\mathbf{h}_1^{(n)}\right) = \aleph_2\phi_{V_1}, \tag{3.108}$$

where $0 < \aleph_1, \aleph_2 < 1$ to insure that we get some noise reduction,

$$J_{\mathrm{d}}\left(\mathbf{h}_1^{(n)}|\mathbf{h}_2^{(n-1)}\right) = \phi_X + \left(\mathbf{h}_1^{(n)}\right)^H \mathbf{\Phi}_{\mathbf{x},2}^{(n-1)}\mathbf{h}_1^{(n)} - \phi_{X,2}^{(n-1)}\left(\mathbf{h}_1^{(n)}\right)^H \mathbf{d}_{1,\theta_{\mathrm{d}}} - \left(\phi_{X,2}^{(n-1)}\right)^* \mathbf{d}_{1,\theta_{\mathrm{d}}}^H \mathbf{h}_1^{(n)}, \tag{3.109}$$

$$J_{\mathrm{n}}\left(\mathbf{h}_1^{(n)}|\mathbf{h}_2^{(n-1)}\right) = \left(\mathbf{h}_1^{(n)}\right)^H \mathbf{\Phi}_{\mathbf{v},2}^{(n-1)}\mathbf{h}_1^{(n)}, \tag{3.110}$$

and

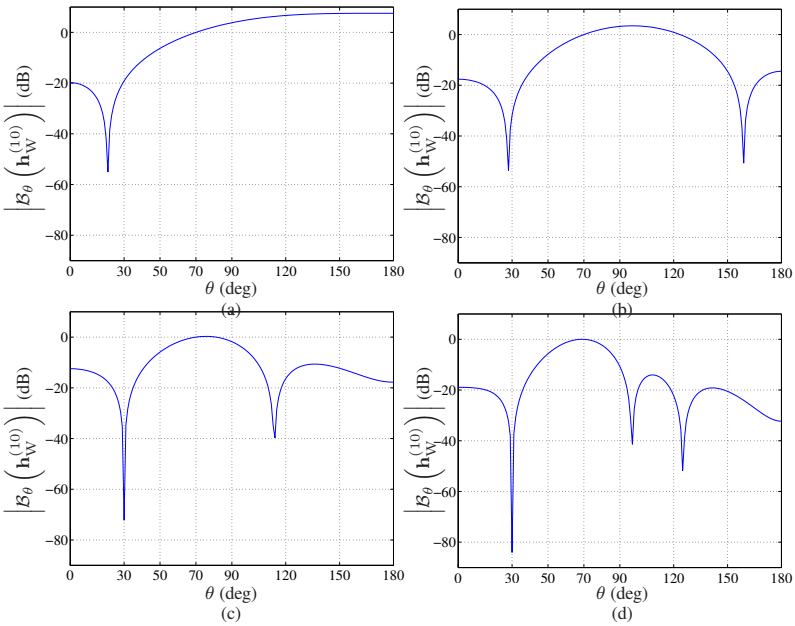

Fig. 3.17 Beampatterns of the Wiener beamformer at the iteration $n = 10$, $\mathbf{h}_{\mathrm{W}}^{(10)}$, for iSNR $= 0$ dB, $f = 3$ kHz, $\delta = 1$ cm, $\theta_{\mathrm{d}} = 70°$, $\theta_0 = 30°$, and different numbers of sensors $M = M_0^2$: (a) $M_0 = 2$, (b) $M_0 = 3$, (c) $M_0 = 4$, and (d) $M_0 = 5$.

$$J_{\mathrm{d}}\left(\mathbf{h}_2^{(n)}|\mathbf{h}_1^{(n)}\right) = \phi_X + \left(\mathbf{h}_2^{(n)}\right)^H \mathbf{\Phi}_{\mathbf{x},1}^{(n)}\mathbf{h}_2^{(n)} - \phi_{X,1}^{(n)}\left(\mathbf{h}_2^{(n)}\right)^H \mathbf{d}_{2,\theta_{\mathrm{d}}} - \left(\phi_{X,1}^{(n)}\right)^* \mathbf{d}_{2,\theta_{\mathrm{d}}}^H \mathbf{h}_2^{(n)}, \tag{3.111}$$

$$J_{\mathrm{n}}\left(\mathbf{h}_2^{(n)}|\mathbf{h}_1^{(n)}\right) = \left(\mathbf{h}_2^{(n)}\right)^H \mathbf{\Phi}_{\mathbf{v},1}^{(n)}\mathbf{h}_2^{(n)}, \tag{3.112}$$

with

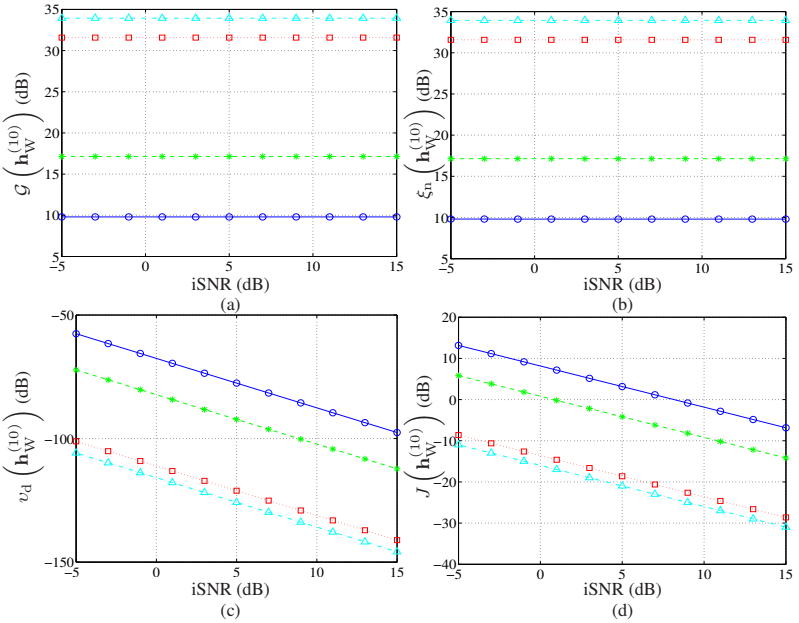

Fig. 3.18 Performance of the Wiener beamformer at the iteration $n = 10$, $\mathbf{h}_{\mathrm{W}}^{(10)}$, as a function of the input SNR for $f = 3$ kHz, $\delta = 1$ cm, $\theta_{\mathrm{d}} = 70°$, $\theta_0 = 30°$, and different numbers of sensors $M = M_0^2$: $M_0 = 2$ (solid line with circles), $M_0 = 3$ (dashed line with asterisks), $M_0 = 4$ (dotted line with squares), and $M_0 = 5$ (dash-dot line with triangles). (a) Gain in SNR, (b) noise reduction factor, (c) desired signal distortion index, and (d) MSE.

$$\begin{aligned}\mathbf{\Phi}_{\mathbf{x},2}^{(n-1)} &= \left(\mathbf{I}_{M_0} \otimes \mathbf{h}_2^{(n-1)}\right)^H \mathbf{\Phi}_{\mathbf{x}} \left(\mathbf{I}_{M_0} \otimes \mathbf{h}_2^{(n-1)}\right) \\ &= \frac{\left|\phi_{X,2}^{(n-1)}\right|^2}{\phi_X} \mathbf{d}_{1,\theta_{\mathrm{d}}} \mathbf{d}_{1,\theta_{\mathrm{d}}}^H, \end{aligned} \tag{3.113}$$

$$\mathbf{\Phi}_{\mathbf{v},2}^{(n-1)} = \left(\mathbf{I}_{M_0} \otimes \mathbf{h}_2^{(n-1)}\right)^H \mathbf{\Phi}_{\mathbf{v}} \left(\mathbf{I}_{M_0} \otimes \mathbf{h}_2^{(n-1)}\right), \tag{3.114}$$

$$\begin{aligned}\mathbf{\Phi}_{\mathbf{x},1}^{(n)} &= \left(\mathbf{h}_1^{(n)} \otimes \mathbf{I}_{M_0}\right)^H \mathbf{\Phi}_{\mathbf{x}} \left(\mathbf{h}_1^{(n)} \otimes \mathbf{I}_{M_0}\right) \\ &= \frac{\left|\phi_{X,1}^{(n)}\right|^2}{\phi_X} \mathbf{d}_{2,\theta_{\mathrm{d}}} \mathbf{d}_{2,\theta_{\mathrm{d}}}^H, \end{aligned} \tag{3.115}$$

$$\mathbf{\Phi}_{\mathbf{v},1}^{(n)} = \left(\mathbf{h}_1^{(n)} \otimes \mathbf{I}_{M_0}\right)^H \mathbf{\Phi}_{\mathbf{v}} \left(\mathbf{h}_1^{(n)} \otimes \mathbf{I}_{M_0}\right). \tag{3.116}$$

By using Lagrange multipliers, $\mu_1, \mu_2 > 0$, to adjoin the constraints to the cost functions, we get

$$\begin{aligned}\mathbf{h}_{1,\mu_1}^{(n)} &= \phi_{X,2}^{(n-1)} \left(\mathbf{\Phi}_{\mathbf{x},2}^{(n-1)} + \mu_1 \mathbf{\Phi}_{\mathbf{v},2}^{(n-1)}\right)^{-1} \mathbf{d}_{1,\theta_\mathrm{d}} \\ &= \frac{\phi_{X,2}^{(n-1)} \phi_X \left(\mathbf{\Phi}_{\mathbf{v},2}^{(n-1)}\right)^{-1} \mathbf{d}_{1,\theta_\mathrm{d}}}{\mu_1 \phi_X + \left|\phi_{X,2}^{(n-1)}\right|^2 \mathbf{d}_{1,\theta_\mathrm{d}}^H \left(\mathbf{\Phi}_{\mathbf{v},2}^{(n-1)}\right)^{-1} \mathbf{d}_{1,\theta_\mathrm{d}}}\end{aligned} \tag{3.117}$$

and

$$\begin{aligned}\mathbf{h}_{2,\mu_2}^{(n)} &= \phi_{X,1}^{(n)} \left(\mathbf{\Phi}_{\mathbf{x},1}^{(n)} + \mu_2 \mathbf{\Phi}_{\mathbf{v},1}^{(n)}\right)^{-1} \mathbf{d}_{2,\theta_\mathrm{d}} \\ &= \frac{\phi_{X,1}^{(n)} \phi_X \left(\mathbf{\Phi}_{\mathbf{v},1}^{(n)}\right)^{-1} \mathbf{d}_{2,\theta_\mathrm{d}}}{\mu_2 \phi_X + \left|\phi_{X,1}^{(n)}\right|^2 \mathbf{d}_{2,\theta_\mathrm{d}}^H \left(\mathbf{\Phi}_{\mathbf{v},1}^{(n)}\right)^{-1} \mathbf{d}_{2,\theta_\mathrm{d}}},\end{aligned} \tag{3.118}$$

with the initialization:

$$\begin{aligned}\mathbf{h}_{2,\mu_2}^{(0)} &= \phi_X \left(\phi_X \mathbf{d}_{2,\theta_\mathrm{d}} \mathbf{d}_{2,\theta_\mathrm{d}}^H + \mu_2 \mathbf{\Phi}_{\mathbf{v}_2}\right)^{-1} \mathbf{d}_{2,\theta_\mathrm{d}} \\ &= \frac{\phi_X \mathbf{\Phi}_{\mathbf{v}_2}^{-1} \mathbf{d}_{2,\theta_\mathrm{d}}}{\mu_2 + \phi_X \mathbf{d}_{2,\theta_\mathrm{d}}^H \mathbf{\Phi}_{\mathbf{v}_2}^{-1} \mathbf{d}_{2,\theta_\mathrm{d}}},\end{aligned} \tag{3.119}$$

where $\mathbf{\Phi}_{\mathbf{v}_2}$ is the covariance matrix of

$$\mathbf{v}_2 = \left[\, V_1 \; V_2 \cdots \; V_{M_0} \,\right]^T, \tag{3.120}$$

whose elements are the M_0 first ones of $\mathbf{v}$. As a matter of fact, $\mathbf{h}_{2,\mu_2}^{(0)}$ is just the traditional tradeoff beamformer applied to the second ULA. Therefore, we find that the tradeoff beamformer is at iteration n:

$$\mathbf{h}_{\mathrm{T},\mu_1,\mu_2}^{(n)} = \mathbf{h}_{1,\mu_1}^{(n)} \otimes \mathbf{h}_{2,\mu_2}^{(n)}, \tag{3.121}$$

where $\mathbf{h}_{1,\mu_1}^{(n)}$ and $\mathbf{h}_{2,\mu_2}^{(n)}$ are defined in (3.117) and (3.118), respectively. We can see that for

- $\mu_1 = \mu_2 = 1$, we get the Wiener beamformer;
- $\mu_1, \mu_2 > 1$, results in a beamformer with low residual noise at the expense of high desired signal distortion (as compared to Wiener); and
- $\mu_1, \mu_2 < 1$, results in a beamformer with high residual noise and low desired signal distortion (as compared to Wiener).

3.2.4 MVDR

The minimum variance distortionless response (MVDR) beamformer proposed by Capon [5], [6] is obtained by minimizing the MSEs of the residual

noise subject to the distortionless constraints, i.e.,

$$\min_{\mathbf{h}_1^{(n)}} \left(\mathbf{h}_1^{(n)}\right)^H \mathbf{\Phi}_{\mathbf{v},2}^{(n-1)} \mathbf{h}_1^{(n)} \quad \text{subject to} \quad \left(\mathbf{h}_1^{(n)}\right)^H \mathbf{d}_{1,\theta_\mathrm{d}} = 1, \tag{3.122}$$

$$\min_{\mathbf{h}_2^{(n)}} \left(\mathbf{h}_2^{(n)}\right)^H \mathbf{\Phi}_{\mathbf{v},1}^{(n)} \mathbf{h}_2^{(n)} \quad \text{subject to} \quad \left(\mathbf{h}_2^{(n)}\right)^H \mathbf{d}_{2,\theta_\mathrm{d}} = 1, \tag{3.123}$$

where $\mathbf{\Phi}_{\mathbf{v},2}^{(n-1)}$ and $\mathbf{\Phi}_{\mathbf{v},1}^{(n)}$ are defined in (3.114) and (3.116), respectively. From the optimization of (3.122) and (3.123), we get

$$\mathbf{h}_1^{(n)} = \frac{\left(\mathbf{\Phi}_{\mathbf{v},2}^{(n-1)}\right)^{-1} \mathbf{d}_{1,\theta_\mathrm{d}}}{\mathbf{d}_{1,\theta_\mathrm{d}}^H \left(\mathbf{\Phi}_{\mathbf{v},2}^{(n-1)}\right)^{-1} \mathbf{d}_{1,\theta_\mathrm{d}}} \tag{3.124}$$

and

$$\mathbf{h}_2^{(n)} = \frac{\left(\mathbf{\Phi}_{\mathbf{v},1}^{(n)}\right)^{-1} \mathbf{d}_{2,\theta_\mathrm{d}}}{\mathbf{d}_{2,\theta_\mathrm{d}}^H \left(\mathbf{\Phi}_{\mathbf{v},1}^{(n)}\right)^{-1} \mathbf{d}_{2,\theta_\mathrm{d}}}, \tag{3.125}$$

with the initialization:

$$\mathbf{h}_2^{(0)} = \frac{\mathbf{\Phi}_{\mathbf{v}_2}^{-1} \mathbf{d}_{2,\theta_\mathrm{d}}}{\mathbf{d}_{2,\theta_\mathrm{d}}^H \mathbf{\Phi}_{\mathbf{v}_2}^{-1} \mathbf{d}_{2,\theta_\mathrm{d}}}. \tag{3.126}$$

As a result, the MVDR beamformer is at iteration n:

$$\mathbf{h}_{\mathrm{MVDR1}}^{(n)} = \mathbf{h}_1^{(n)} \otimes \mathbf{h}_2^{(n)}. \tag{3.127}$$

This beamformer can be directly obtained from $\mathbf{h}_{\mathrm{T},\mu_1,\mu_2}^{(n)}$ by taking $\mu_1 = \mu_2 = 0$.

Another form of the MVDR beamformer is obtained from

$$\min_{\mathbf{h}_1^{(n)}} \left(\mathbf{h}_1^{(n)}\right)^H \mathbf{\Phi}_{\mathbf{y},2}^{(n-1)} \mathbf{h}_1^{(n)} \quad \text{subject to} \quad \left(\mathbf{h}_1^{(n)}\right)^H \mathbf{d}_{1,\theta_\mathrm{d}} = 1, \tag{3.128}$$

$$\min_{\mathbf{h}_2^{(n)}} \left(\mathbf{h}_2^{(n)}\right)^H \mathbf{\Phi}_{\mathbf{y},1}^{(n)} \mathbf{h}_2^{(n)} \quad \text{subject to} \quad \left(\mathbf{h}_2^{(n)}\right)^H \mathbf{d}_{2,\theta_\mathrm{d}} = 1, \tag{3.129}$$

where $\mathbf{\Phi}_{\mathbf{y},2}^{(n-1)}$ and $\mathbf{\Phi}_{\mathbf{y},1}^{(n)}$ are defined in (3.102) and (3.105), respectively. We get

$$\mathbf{h}_{\mathrm{MVDR2}}^{(n)} = \mathbf{h}_1^{(n)} \otimes \mathbf{h}_2^{(n)}, \tag{3.130}$$

where

$$\mathbf{h}_1^{(n)} = \frac{\left(\mathbf{\Phi}_{\mathbf{y},2}^{(n-1)}\right)^{-1}\mathbf{d}_{1,\theta_\mathrm{d}}}{\mathbf{d}_{1,\theta_\mathrm{d}}^H\left(\mathbf{\Phi}_{\mathbf{y},2}^{(n-1)}\right)^{-1}\mathbf{d}_{1,\theta_\mathrm{d}}} \tag{3.131}$$

and

$$\mathbf{h}_2^{(n)} = \frac{\left(\mathbf{\Phi}_{\mathbf{y},1}^{(n)}\right)^{-1}\mathbf{d}_{2,\theta_\mathrm{d}}}{\mathbf{d}_{2,\theta_\mathrm{d}}^H\left(\mathbf{\Phi}_{\mathbf{y},1}^{(n)}\right)^{-1}\mathbf{d}_{2,\theta_\mathrm{d}}}, \tag{3.132}$$

with the initialization:

$$\mathbf{h}_2^{(0)} = \frac{\mathbf{\Phi}_{\mathbf{y}_2}^{-1}\mathbf{d}_{2,\theta_\mathrm{d}}}{\mathbf{d}_{2,\theta_\mathrm{d}}^H\mathbf{\Phi}_{\mathbf{y}_2}^{-1}\mathbf{d}_{2,\theta_\mathrm{d}}}. \tag{3.133}$$

In principle, $\mathbf{h}_{\mathrm{MVDR1}}^{(n)}$ and $\mathbf{h}_{\mathrm{MVDR2}}^{(n)}$ are equivalent, but in practice, they may behave very differently.

3.2.5 LCMV

We assume that we have one interference source impinging on the array from the direction $\theta_0 \neq \theta_\mathrm{d}$ that we would like to cancel without distorting the desired signal. Then, our constraint equations are identical to the ones presented in (3.43) and (3.44). Depending on what we wish; one null of multiplicity 1 or one null of multiplicity 2 in the direction θ_0, we can derive different linearly constrained minimum variance (LCMV) beamformers [7], [8].

If one null of multiplicity 2 is desired, we should optimize

$$\min_{\mathbf{h}_1^{(n)}} \left(\mathbf{h}_1^{(n)}\right)^H \mathbf{\Phi}_{\mathbf{v},2}^{(n-1)}\mathbf{h}_1^{(n)} \quad \text{subject to} \quad \mathbf{C}_1^H\mathbf{h}_1^{(n)} = \mathbf{i}_\mathrm{c}, \tag{3.134}$$

$$\min_{\mathbf{h}_2^{(n)}} \left(\mathbf{h}_2^{(n)}\right)^H \mathbf{\Phi}_{\mathbf{v},1}^{(n)}\mathbf{h}_2^{(n)} \quad \text{subject to} \quad \mathbf{C}_2^H\mathbf{h}_2^{(n)} = \mathbf{i}_\mathrm{c}. \tag{3.135}$$

We find that

$$\mathbf{h}_1^{(n)} = \left(\mathbf{\Phi}_{\mathbf{v},2}^{(n-1)}\right)^{-1}\mathbf{C}_1\left[\mathbf{C}_1^H\left(\mathbf{\Phi}_{\mathbf{v},2}^{(n-1)}\right)^{-1}\mathbf{C}_1\right]^{-1}\mathbf{i}_\mathrm{c} \tag{3.136}$$

and

$$\mathbf{h}_2^{(n)} = \left(\mathbf{\Phi}_{\mathbf{v},1}^{(n)}\right)^{-1}\mathbf{C}_2\left[\mathbf{C}_2^H\left(\mathbf{\Phi}_{\mathbf{v},1}^{(n)}\right)^{-1}\mathbf{C}_2\right]^{-1}\mathbf{i}_\mathrm{c}, \tag{3.137}$$

with the initialization:

$$\mathbf{h}_2^{(0)} = \mathbf{\Phi}_{\mathbf{v}_2}^{-1}\mathbf{C}_2\left(\mathbf{C}_2^H\mathbf{\Phi}_{\mathbf{v}_2}^{-1}\mathbf{C}_2\right)^{-1}\mathbf{i}_{\mathrm{c}}. \tag{3.138}$$

As a consequence, the first LCMV beamformer is at iteration n:

$$\mathbf{h}_{\mathrm{LCMV1}}^{(n)} = \mathbf{h}_1^{(n)} \otimes \mathbf{h}_2^{(n)}. \tag{3.139}$$

A second LCMV beamformer (with one null of multiplicity 2) is at iteration n:

$$\mathbf{h}_{\mathrm{LCMV2}}^{(n)} = \mathbf{h}_1^{(n)} \otimes \mathbf{h}_2^{(n)}, \tag{3.140}$$

where

$$\mathbf{h}_1^{(n)} = \left(\mathbf{\Phi}_{\mathbf{y},2}^{(n-1)}\right)^{-1}\mathbf{C}_1\left[\mathbf{C}_1^H\left(\mathbf{\Phi}_{\mathbf{y},2}^{(n-1)}\right)^{-1}\mathbf{C}_1\right]^{-1}\mathbf{i}_{\mathrm{c}} \tag{3.141}$$

and

$$\mathbf{h}_2^{(n)} = \left(\mathbf{\Phi}_{\mathbf{y},1}^{(n)}\right)^{-1}\mathbf{C}_2\left[\mathbf{C}_2^H\left(\mathbf{\Phi}_{\mathbf{y},1}^{(n)}\right)^{-1}\mathbf{C}_2\right]^{-1}\mathbf{i}_{\mathrm{c}}, \tag{3.142}$$

with the initialization:

$$\mathbf{h}_2^{(0)} = \mathbf{\Phi}_{\mathbf{y}_2}^{-1}\mathbf{C}_2\left(\mathbf{C}_2^H\mathbf{\Phi}_{\mathbf{y}_2}^{-1}\mathbf{C}_2\right)^{-1}\mathbf{i}_{\mathrm{c}}. \tag{3.143}$$

If one null of multiplicity 1 is desired, we can optimize

$$\min_{\mathbf{h}_1^{(n)}}\left(\mathbf{h}_1^{(n)}\right)^H\mathbf{\Phi}_{\mathbf{v},2}^{(n-1)}\mathbf{h}_1^{(n)} \quad \text{subject to} \quad \mathbf{d}_{1,\theta_{\mathrm{d}}}^H\mathbf{h}_1^{(n)} = 1, \tag{3.144}$$

$$\min_{\mathbf{h}_2^{(n)}}\left(\mathbf{h}_2^{(n)}\right)^H\mathbf{\Phi}_{\mathbf{v},1}^{(n)}\mathbf{h}_2^{(n)} \quad \text{subject to} \quad \mathbf{C}_2^H\mathbf{h}_2^{(n)} = \mathbf{i}_{\mathrm{c}}. \tag{3.145}$$

We find that

$$\mathbf{h}_1^{(n)} = \frac{\left(\mathbf{\Phi}_{\mathbf{v},2}^{(n-1)}\right)^{-1}\mathbf{d}_{1,\theta_{\mathrm{d}}}}{\mathbf{d}_{1,\theta_{\mathrm{d}}}^H\left(\mathbf{\Phi}_{\mathbf{v},2}^{(n-1)}\right)^{-1}\mathbf{d}_{1,\theta_{\mathrm{d}}}} \tag{3.146}$$

and

$$\mathbf{h}_2^{(n)} = \left(\mathbf{\Phi}_{\mathbf{v},1}^{(n)}\right)^{-1}\mathbf{C}_2\left[\mathbf{C}_2^H\left(\mathbf{\Phi}_{\mathbf{v},1}^{(n)}\right)^{-1}\mathbf{C}_2\right]^{-1}\mathbf{i}_{\mathrm{c}}, \tag{3.147}$$

with the initialization:

$$\mathbf{h}_2^{(0)} = \mathbf{\Phi}_{\mathbf{v}_2}^{-1}\mathbf{C}_2\left(\mathbf{C}_2^H\mathbf{\Phi}_{\mathbf{v}_2}^{-1}\mathbf{C}_2\right)^{-1}\mathbf{i}_{\mathrm{c}}. \tag{3.148}$$

Therefore, the third LCMV beamformer, but with one null of multiplicity 1, is at iteration n:

$$\mathbf{h}_{\mathrm{LCMV3}}^{(n)} = \mathbf{h}_1^{(n)} \otimes \mathbf{h}_2^{(n)}. \tag{3.149}$$

The fourth LCMV beamformer with one null of multiplicity 1 is at iteration n:

$$\mathbf{h}_{\mathrm{LCMV4}}^{(n)} = \mathbf{h}_1^{(n)} \otimes \mathbf{h}_2^{(n)}, \tag{3.150}$$

where

$$\mathbf{h}_1^{(n)} = \frac{\left(\mathbf{\Phi}_{\mathbf{y},2}^{(n-1)}\right)^{-1}\mathbf{d}_{1,\theta_{\mathrm{d}}}}{\mathbf{d}_{1,\theta_{\mathrm{d}}}^H\left(\mathbf{\Phi}_{\mathbf{y},2}^{(n-1)}\right)^{-1}\mathbf{d}_{1,\theta_{\mathrm{d}}}} \tag{3.151}$$

and

$$\mathbf{h}_2^{(n)} = \left(\mathbf{\Phi}_{\mathbf{y},1}^{(n)}\right)^{-1}\mathbf{C}_2\left[\mathbf{C}_2^H\left(\mathbf{\Phi}_{\mathbf{y},1}^{(n)}\right)^{-1}\mathbf{C}_2\right]^{-1}\mathbf{i}_{\mathrm{c}}, \tag{3.152}$$

with the initialization:

$$\mathbf{h}_2^{(0)} = \mathbf{\Phi}_{\mathbf{y}_2}^{-1}\mathbf{C}_2\left(\mathbf{C}_2^H\mathbf{\Phi}_{\mathbf{y}_2}^{-1}\mathbf{C}_2\right)^{-1}\mathbf{i}_{\mathrm{c}}. \tag{3.153}$$

Another possibility is to optimize

$$\min_{\mathbf{h}_1^{(n)}}\left(\mathbf{h}_1^{(n)}\right)^H\mathbf{\Phi}_{\mathbf{v},2}^{(n-1)}\mathbf{h}_1^{(n)} \quad \text{subject to} \quad \mathbf{C}_1^H\mathbf{h}_1^{(n)} = \mathbf{i}_{\mathrm{c}}, \tag{3.154}$$

$$\min_{\mathbf{h}_2^{(n)}}\left(\mathbf{h}_2^{(n)}\right)^H\mathbf{\Phi}_{\mathbf{v},1}^{(n)}\mathbf{h}_2^{(n)} \quad \text{subject to} \quad \mathbf{d}_{2,\theta_{\mathrm{d}}}^H\mathbf{h}_2^{(n)} = 1. \tag{3.155}$$

In this case, we get

$$\mathbf{h}_1^{(n)} = \left(\mathbf{\Phi}_{\mathbf{v},2}^{(n-1)}\right)^{-1}\mathbf{C}_1\left[\mathbf{C}_1^H\left(\mathbf{\Phi}_{\mathbf{v},2}^{(n-1)}\right)^{-1}\mathbf{C}_1\right]^{-1}\mathbf{i}_{\mathrm{c}} \tag{3.156}$$

and

$$\mathbf{h}_2^{(n)} = \frac{\left(\mathbf{\Phi}_{\mathbf{v},1}^{(n)}\right)^{-1}\mathbf{d}_{2,\theta_{\mathrm{d}}}}{\mathbf{d}_{2,\theta_{\mathrm{d}}}^H\left(\mathbf{\Phi}_{\mathbf{v},1}^{(n)}\right)^{-1}\mathbf{d}_{2,\theta_{\mathrm{d}}}}, \tag{3.157}$$

with the initialization:

$$\mathbf{h}_2^{(0)} = \frac{\mathbf{\Phi}_{\mathbf{v}_2}^{-1}\mathbf{d}_{2,\theta_\mathrm{d}}}{\mathbf{d}_{2,\theta_\mathrm{d}}^H\mathbf{\Phi}_{\mathbf{v}_2}^{-1}\mathbf{d}_{2,\theta_\mathrm{d}}}. \tag{3.158}$$

Therefore, the fifth LCMV beamformer, but with one null of multiplicity 1, is at iteration n:

$$\mathbf{h}_{\mathrm{LCMV5}}^{(n)} = \mathbf{h}_1^{(n)} \otimes \mathbf{h}_2^{(n)}. \tag{3.159}$$

Finally, the last and sixth LCMV beamformer (with one null of multiplicity 1) is at iteration n:

$$\mathbf{h}_{\mathrm{LCMV6}}^{(n)} = \mathbf{h}_1^{(n)} \otimes \mathbf{h}_2^{(n)}, \tag{3.160}$$

where

$$\mathbf{h}_1^{(n)} = \left(\mathbf{\Phi}_{\mathbf{y},2}^{(n-1)}\right)^{-1}\mathbf{C}_1\left[\mathbf{C}_1^H\left(\mathbf{\Phi}_{\mathbf{y},2}^{(n-1)}\right)^{-1}\mathbf{C}_1\right]^{-1}\mathbf{i}_\mathrm{c} \tag{3.161}$$

and

$$\mathbf{h}_2^{(n)} = \frac{\left(\mathbf{\Phi}_{\mathbf{y},1}^{(n)}\right)^{-1}\mathbf{d}_{2,\theta_\mathrm{d}}}{\mathbf{d}_{2,\theta_\mathrm{d}}^H\left(\mathbf{\Phi}_{\mathbf{y},1}^{(n)}\right)^{-1}\mathbf{d}_{2,\theta_\mathrm{d}}}, \tag{3.162}$$

with the initialization:

$$\mathbf{h}_2^{(0)} = \frac{\mathbf{\Phi}_{\mathbf{y}_2}^{-1}\mathbf{d}_{2,\theta_\mathrm{d}}}{\mathbf{d}_{2,\theta_\mathrm{d}}^H\mathbf{\Phi}_{\mathbf{y}_2}^{-1}\mathbf{d}_{2,\theta_\mathrm{d}}}. \tag{3.163}$$

3.2.6 Maximum SNR

In order to maximize the output SNR, it is required to express it differently. Indeed, from its definition, it is clear that it can be rewritten as

$$\begin{aligned}\mathrm{oSNR}\left(\mathbf{h}_1 \otimes \mathbf{h}_2\right) &= \frac{\phi_X\left|\mathbf{h}_1^H\mathbf{d}_{1,\theta_\mathrm{d}}\right|^2\left|\mathbf{h}_2^H\mathbf{d}_{2,\theta_\mathrm{d}}\right|^2}{\left(\mathbf{h}_1 \otimes \mathbf{h}_2\right)^H\mathbf{\Phi}_\mathbf{v}\left(\mathbf{h}_1 \otimes \mathbf{h}_2\right)} \\ &= \frac{\left|\phi_{X,2}\right|^2\left|\mathbf{h}_1^H\mathbf{d}_{1,\theta_\mathrm{d}}\right|^2}{\phi_X\mathbf{h}_1^H\mathbf{\Phi}_{\mathbf{v},2}\mathbf{h}_1} \qquad (3.164) \\ &= \frac{\left|\phi_{X,1}\right|^2\left|\mathbf{h}_2^H\mathbf{d}_{2,\theta_\mathrm{d}}\right|^2}{\phi_X\mathbf{h}_2^H\mathbf{\Phi}_{\mathbf{v},1}\mathbf{h}_2}, \qquad (3.165)\end{aligned}$$

where

$$|\phi_{X,2}|^2 = \phi_X^2 \left|\mathbf{h}_2^H \mathbf{d}_{2,\theta_\mathrm{d}}\right|^2, \tag{3.166}$$

$$\mathbf{\Phi}_{\mathbf{v},2} = \left(\mathbf{I}_{M_0} \otimes \mathbf{h}_2\right)^H \mathbf{\Phi}_{\mathbf{v}} \left(\mathbf{I}_{M_0} \otimes \mathbf{h}_2\right), \tag{3.167}$$

and

$$|\phi_{X,1}|^2 = \phi_X^2 \left|\mathbf{h}_1^H \mathbf{d}_{1,\theta_\mathrm{d}}\right|^2, \tag{3.168}$$

$$\mathbf{\Phi}_{\mathbf{v},1} = \left(\mathbf{h}_1 \otimes \mathbf{I}_{M_0}\right)^H \mathbf{\Phi}_{\mathbf{v}} \left(\mathbf{h}_1 \otimes \mathbf{I}_{M_0}\right). \tag{3.169}$$

When $\mathbf{h}_2$ is fixed, we write (3.164) as

$$\mathrm{oSNR}\left(\mathbf{h}_1|\mathbf{h}_2\right) = \frac{|\phi_{X,2}|^2 \left|\mathbf{h}_1^H \mathbf{d}_{1,\theta_\mathrm{d}}\right|^2}{\phi_X \mathbf{h}_1^H \mathbf{\Phi}_{\mathbf{v},2} \mathbf{h}_1}, \tag{3.170}$$

and when $\mathbf{h}_1$ is fixed, we write (3.165) as

$$\mathrm{oSNR}\left(\mathbf{h}_2|\mathbf{h}_1\right) = \frac{|\phi_{X,1}|^2 \left|\mathbf{h}_2^H \mathbf{d}_{2,\theta_\mathrm{d}}\right|^2}{\phi_X \mathbf{h}_2^H \mathbf{\Phi}_{\mathbf{v},1} \mathbf{h}_2}. \tag{3.171}$$

As before, we have everything to iteratively maximize the output SNR. At iteration 0, we may take

$$\mathbf{h}_2^{(0)} = \alpha_2^{(0)} \mathbf{\Phi}_{\mathbf{v}_2}^{-1} \mathbf{d}_{2,\theta_\mathrm{d}}, \tag{3.172}$$

where $\alpha_2^{(0)} \neq 0$ is an arbitrary complex-valued number. Substituting $\mathbf{h}_2^{(0)}$ into (3.166)–(3.167), we obtain

$$\left|\phi_{X,2}^{(0)}\right|^2 = \phi_X^2 \left|\mathbf{d}_{2,\theta_\mathrm{d}}^H \mathbf{h}_2^{(0)}\right|^2, \tag{3.173}$$

$$\mathbf{\Phi}_{\mathbf{v},2}^{(0)} = \left(\mathbf{I}_{M_0} \otimes \mathbf{h}_2^{(0)}\right)^H \mathbf{\Phi}_{\mathbf{v}} \left(\mathbf{I}_{M_0} \otimes \mathbf{h}_2^{(0)}\right). \tag{3.174}$$

Using the previous expressions in the output SNR in (3.170), we get at iteration 1:

$$\mathrm{oSNR}\left(\mathbf{h}_1^{(1)}|\mathbf{h}_2^{(0)}\right) = \frac{\left|\phi_{X,2}^{(0)}\right|^2 \left|\mathbf{d}_{1,\theta_\mathrm{d}}^H \mathbf{h}_1^{(1)}\right|^2}{\phi_X \left(\mathbf{h}_1^{(1)}\right)^H \mathbf{\Phi}_{\mathbf{v},2}^{(0)} \mathbf{h}_1^{(1)}}, \tag{3.175}$$

whose maximization with respect to $\mathbf{h}_1^{(1)}$ gives

$$\mathbf{h}_1^{(1)} = \alpha_1^{(0)} \left(\mathbf{\Phi}_{\mathbf{v},2}^{(0)}\right)^{-1} \mathbf{d}_{1,\theta_\mathrm{d}}, \tag{3.176}$$

where $\alpha_1^{(0)} \neq 0$ is an arbitrary complex number. Then, using $\mathbf{h}_1^{(1)}$ in (3.168)–(3.169), we obtain

$$\left|\phi_{X,1}^{(1)}\right|^2 = \phi_X^2 \left|\mathbf{d}_{1,\theta_\mathrm{d}}^H \mathbf{h}_1^{(1)}\right|^2, \tag{3.177}$$

$$\mathbf{\Phi}_{\mathbf{v},1}^{(1)} = \left(\mathbf{h}_1^{(1)} \otimes \mathbf{I}_{M_0}\right)^H \mathbf{\Phi}_\mathbf{v} \left(\mathbf{h}_1^{(1)} \otimes \mathbf{I}_{M_0}\right), \tag{3.178}$$

which we plug into the output SNR in (3.171). We get

$$\mathrm{oSNR}\left(\mathbf{h}_2^{(1)} | \mathbf{h}_1^{(1)}\right) = \frac{\left|\phi_{X,1}^{(1)}\right|^2 \left|\mathbf{d}_{2,\theta_\mathrm{d}}^H \mathbf{h}_2^{(1)}\right|^2}{\phi_X \left(\mathbf{h}_2^{(1)}\right)^H \mathbf{\Phi}_{\mathbf{v},1}^{(1)} \mathbf{h}_2^{(1)}}. \tag{3.179}$$

The maximization of the previous expression with respect to $\mathbf{h}_2^{(1)}$ leads to

$$\mathbf{h}_2^{(1)} = \alpha_2^{(1)} \left(\mathbf{\Phi}_{\mathbf{v},1}^{(1)}\right)^{-1} \mathbf{d}_{2,\theta_\mathrm{d}}, \tag{3.180}$$

where $\alpha_2^{(1)} \neq 0$ is an arbitrary complex number.

Continuing the iterations up to the iteration n, we easily get for the first filter:

$$\mathbf{h}_1^{(n)} = \alpha_1^{(n-1)} \left(\mathbf{\Phi}_{\mathbf{v},2}^{(n-1)}\right)^{-1} \mathbf{d}_{1,\theta_\mathrm{d}}, \tag{3.181}$$

where $\alpha_1^{(n-1)} \neq 0$ is an arbitrary complex number, with

$$\mathbf{\Phi}_{\mathbf{v},2}^{(n-1)} = \left(\mathbf{I}_{M_0} \otimes \mathbf{h}_2^{(n-1)}\right)^H \mathbf{\Phi}_\mathbf{v} \left(\mathbf{I}_{M_0} \otimes \mathbf{h}_2^{(n-1)}\right), \tag{3.182}$$

and for the second filter:

$$\mathbf{h}_2^{(n)} = \alpha_2^{(n)} \left(\mathbf{\Phi}_{\mathbf{v},1}^{(n)}\right)^{-1} \mathbf{d}_{2,\theta_\mathrm{d}}, \tag{3.183}$$

where $\alpha_2^{(n)} \neq 0$ is an arbitrary complex number, with

$$\mathbf{\Phi}_{\mathbf{v},1}^{(n)} = \left(\mathbf{h}_1^{(n)} \otimes \mathbf{I}_{M_0}\right)^H \mathbf{\Phi}_\mathbf{v} \left(\mathbf{h}_1^{(n)} \otimes \mathbf{I}_{M_0}\right). \tag{3.184}$$

Finally, we deduce that the maximum SNR beamformer is at iteration n:

$$\mathbf{h}_{\max}^{(n)} = \mathbf{h}_1^{(n)} \otimes \mathbf{h}_2^{(n)}, \tag{3.185}$$

where $\mathbf{h}_1^{(n)}$ and $\mathbf{h}_2^{(n)}$ are defined in (3.181) and (3.183), respectively. There are different ways to derive the parameters $\alpha_1^{(n-1)}$ and $\alpha_2^{(n)}$. For example, if they are found in such a way that the filters $\mathbf{h}_1^{(n)}$ and $\mathbf{h}_2^{(n)}$ are distortionless, we obtain the MVDR beamformer derived in Subsection 3.2.4.

3.3 Combined Fixed/Adaptive Beamformers

Perhaps, one of the most interesting aspects of the Kronecker product formulation in beamforming (i.e., $\mathbf{h} = \mathbf{h}_1 \otimes \mathbf{h}_2$) is that, due to its decomposition and remarkable flexibility, it seems possible to combine very intelligently fixed and adaptive beamformers, so that the best of each one of these two approaches is emphasized for performance enhancement. Therefore, we hope that the global beamformer will fix the shortcomings of each one of these two classes of beamformers.

For the second ULA with the steering vector $\mathbf{d}_{2,\theta_\mathrm{d}}$, the interelement spacing, δ, can be chosen as small as desired, which is obviously good for directivity (especially at the endfires) and also good for limiting the effect of spatial aliasing. Therefore, the corresponding beamformer, $\mathbf{h}_2$, will be the fixed beamformer here and, in all this part, it will be taken as

$$\begin{aligned}\mathbf{h}_2 &= \mathbf{h}_{2,\mathrm{mDF}} \\ &= \frac{\boldsymbol{\Gamma}_2^{-1}\mathbf{d}_{2,\theta_\mathrm{d}}}{\mathbf{d}_{2,\theta_\mathrm{d}}^H \boldsymbol{\Gamma}_2^{-1}\mathbf{d}_{2,\theta_\mathrm{d}}},\end{aligned} \tag{3.186}$$

which is the maximum DF beamformer at the second ULA. Now, that $\mathbf{h}_2$ is fixed, we need to derive, accordingly, the optimal (depending on what is desired) adaptive beamformer, $\mathbf{h}_1$, which corresponds to the first ULA. Clearly, the global beamformer, $\mathbf{h}$, will inherit the features of the adaptive and fixed beamformers ($\mathbf{h}_1$ and $\mathbf{h}_2$, respectively).

Since $\mathbf{h}_2$ is fixed and distortionless, we can express the MSE as

$$J\left(\mathbf{h}_1|\mathbf{h}_2\right) = \phi_X + \mathbf{h}_1^H \boldsymbol{\Phi}_{\mathbf{y},2}\mathbf{h}_1 - \phi_X \mathbf{h}_1^H \mathbf{d}_{1,\theta_\mathrm{d}} - \phi_X \mathbf{d}_{1,\theta_\mathrm{d}}^H \mathbf{h}_1, \tag{3.187}$$

where

$$\boldsymbol{\Phi}_{\mathbf{y},2} = \left(\mathbf{I}_{M_0} \otimes \mathbf{h}_{2,\mathrm{mDF}}\right)^H \boldsymbol{\Phi}_{\mathbf{y}} \left(\mathbf{I}_{M_0} \otimes \mathbf{h}_{2,\mathrm{mDF}}\right). \tag{3.188}$$

The minimization of $J\left(\mathbf{h}_1|\mathbf{h}_2\right)$ with respect to $\mathbf{h}_1$ leads to the Wiener (adaptive) beamformer:

$$\begin{aligned}\mathbf{h}_{1,\mathrm{W}} &= \phi_X \boldsymbol{\Phi}_{\mathbf{y},2}^{-1}\mathbf{d}_{1,\theta_\mathrm{d}} \\ &= \frac{\phi_X \boldsymbol{\Phi}_{\mathbf{v},2}^{-1}\mathbf{d}_{1,\theta_\mathrm{d}}}{1 + \phi_X \mathbf{d}_{1,\theta_\mathrm{d}}^H \boldsymbol{\Phi}_{\mathbf{v},2}^{-1}\mathbf{d}_{1,\theta_\mathrm{d}}},\end{aligned} \tag{3.189}$$

where

$$\boldsymbol{\Phi}_{\mathbf{v},2} = \left(\mathbf{I}_{M_0} \otimes \mathbf{h}_{2,\mathrm{mDF}}\right)^H \boldsymbol{\Phi}_{\mathbf{v}} \left(\mathbf{I}_{M_0} \otimes \mathbf{h}_{2,\mathrm{mDF}}\right). \tag{3.190}$$

As a result, the first proposed global combined fixed/adaptive (cFA) beamformer is

$$\mathbf{h}_{\mathrm{cFA1}} = \mathbf{h}_{1,\mathrm{W}} \otimes \mathbf{h}_{2,\mathrm{mDF}}. \tag{3.191}$$

It is always possible to improve the beamforming performance by adding one more step to the previous processing, i.e, by maximizing

$$\mathcal{D}\left(\mathbf{h}_2|\mathbf{h}_{1,\mathrm{W}}\right) = \frac{\left|\mathbf{h}_2^H \mathbf{d}_{2,\theta_\mathrm{d}}\right|^2}{\mathbf{h}_2^H \mathbf{\Gamma}_{\mathbf{h}_{1,\mathrm{W}}} \mathbf{h}_2}, \tag{3.192}$$

where

$$\mathbf{\Gamma}_{\mathbf{h}_{1,\mathrm{W}}} = \left(\mathbf{h}_{1,\mathrm{W}} \otimes \mathbf{I}_{M_0}\right)^H \mathbf{\Gamma} \left(\mathbf{h}_{1,\mathrm{W}} \otimes \mathbf{I}_{M_0}\right).$$

We obtain

$$\mathbf{h}_{2,\mathrm{mDF}}^{(1)} = \frac{\mathbf{\Gamma}_{\mathbf{h}_{1,\mathrm{W}}}^{-1} \mathbf{d}_{2,\theta_\mathrm{d}}}{\mathbf{d}_{2,\theta_\mathrm{d}}^H \mathbf{\Gamma}_{\mathbf{h}_{1,\mathrm{W}}}^{-1} \mathbf{d}_{2,\theta_\mathrm{d}}}. \tag{3.193}$$

Then, instead of using $\mathbf{h}_{2,\mathrm{mDF}}$ in (3.191), we can use $\mathbf{h}_{2,\mathrm{mDF}}^{(1)}$. This leads to the second global beamformer:

$$\mathbf{h}_{\mathrm{cFA2}} = \mathbf{h}_{1,\mathrm{W}} \otimes \mathbf{h}_{2,\mathrm{mDF}}^{(1)}. \tag{3.194}$$

If we want $\mathbf{h}_1$ to be a distortionless adaptive beamformer, we can optimize the criterion:

$$\min_{\mathbf{h}_1} \mathbf{h}_1^H \mathbf{\Phi}_{\mathbf{v},2} \mathbf{h}_1 \quad \text{subject to} \quad \mathbf{h}_1^H \mathbf{d}_{1,\theta_\mathrm{d}} = 1, \tag{3.195}$$

from which we find the well-known MVDR beamformer:

$$\mathbf{h}_{1,\mathrm{MVDR}} = \frac{\mathbf{\Phi}_{\mathbf{v},2}^{-1} \mathbf{d}_{1,\theta_\mathrm{d}}}{\mathbf{d}_{1,\theta_\mathrm{d}}^H \mathbf{\Phi}_{\mathbf{v},2}^{-1} \mathbf{d}_{1,\theta_\mathrm{d}}}. \tag{3.196}$$

As a consequence, the third proposed global fixed/adaptive beamformer is

$$\mathbf{h}_{\mathrm{cFA3}} = \mathbf{h}_{1,\mathrm{MVDR}} \otimes \mathbf{h}_{2,\mathrm{mDF}}. \tag{3.197}$$

In the particular case where the noise is white, $\mathbf{h}_{1,\mathrm{MVDR}}$ simplifies to the DS beamformer, i.e., $\mathbf{h}_{1,\mathrm{DS}}$. Therefore, $\mathbf{h}_{\mathrm{cFA3}} = \mathbf{h}_{1,\mathrm{DS}} \otimes \mathbf{h}_{2,\mathrm{mDF}} = \mathbf{h}_{\mathrm{PmDF6}}$ (see Subsection 3.1.2).

If we want to better compromise between noise reduction and speech distortion, we should optimize the criterion:

$$\min_{\mathbf{h}_1} J_\mathrm{d}\left(\mathbf{h}_1|\mathbf{h}_2\right) \quad \text{subject to} \quad J_\mathrm{n}\left(\mathbf{h}_1|\mathbf{h}_2\right) = \aleph_1 \phi_{V_1}, \tag{3.198}$$

where $0 < \aleph_1 < 1$ and

$$J_{\mathrm{d}}\left(\mathbf{h}_1|\mathbf{h}_2\right) = \phi_X + \phi_X\left|\mathbf{h}_1^H\mathbf{d}_{1,\theta_{\mathrm{d}}}\right|^2 - \phi_X\mathbf{h}_1^H\mathbf{d}_{1,\theta_{\mathrm{d}}} - \phi_X\mathbf{d}_{1,\theta_{\mathrm{d}}}^H\mathbf{h}_1, \tag{3.199}$$

$$J_{\mathrm{n}}\left(\mathbf{h}_1|\mathbf{h}_2\right) = \mathbf{h}_1^H\mathbf{\Phi}_{\mathbf{v},2}\mathbf{h}_1. \tag{3.200}$$

We get the tradeoff beamformer:

$$\begin{aligned}\mathbf{h}_{1,\mathrm{T},\mu_1} &= \phi_X\left(\phi_X\mathbf{d}_{1,\theta_{\mathrm{d}}}\mathbf{d}_{1,\theta_{\mathrm{d}}}^H + \mu_1\mathbf{\Phi}_{\mathbf{v},2}\right)^{-1}\mathbf{d}_{1,\theta_{\mathrm{d}}} \\ &= \frac{\phi_X\mathbf{\Phi}_{\mathbf{v},2}^{-1}\mathbf{d}_{1,\theta_{\mathrm{d}}}}{\mu_1 + \phi_X\mathbf{d}_{1,\theta_{\mathrm{d}}}^H\mathbf{\Phi}_{\mathbf{v},2}^{-1}\mathbf{d}_{1,\theta_{\mathrm{d}}}},\end{aligned} \tag{3.201}$$

where $\mu_1 > 0$ is a Lagrange multiplier. Therefore, the fourth and last global fixed/adaptive beamformer that we propose is

$$\mathbf{h}_{\mathrm{cFA4}} = \mathbf{h}_{1,\mathrm{T},\mu_1} \otimes \mathbf{h}_{2,\mathrm{mDF}}. \tag{3.202}$$

3.4 Differential Beamformers

The family of differential beamformers is an important particular class of fixed beamformers. Arguably, beamformers belonging to this particular family are the most practical ones since the corresponding beampatterns are almost frequency invariant, which is critical when we deal with broadband signals such as speech, and they lead to the highest gains in diffuse noise. However, the main drawback of differential beamforming is white noise amplification. We will see that the flexibility of the new approach allows us to better deal with this fundamental problem. The most well-known and studied differential array beampatterns are the cardioid, the dipole, the hypercardioid, and the supercardioid. In the following, we show how they are designed in this particular context.

3.4.1 Preliminaries and Other Measures

In order that differential beamforming takes place, the following two assumptions are usually made [9], [10], [11], [12].

(i) The sensor spacing, δ, is much smaller than the acoustic wavelength, implying that $\delta \ll 2\pi c/\omega$. This assumption is required so that the true acoustic pressure differentials can be approximated by finite differences of the sensors' outputs.

(ii) The desired source signal propagates from the angle $\theta_{\mathrm{d}} = 0$ (endfire direction). Therefore, (2.6) becomes

$$\mathbf{y} = \mathbf{d}_0 X + \mathbf{v}, \tag{3.203}$$

and, at the endfire, the value of the beamformer beampattern should always be equal to 1.

Thanks to Assumption (i) frequency-invariant beamforming may be possible and thanks to Assumption (ii) any desired beampattern can be designed; in other directions (than the endfires 0 and π), the beampattern design is very limited because of the symmetry of the steering vector.

Since the interelement spacing of the second ULA is much smaller than the interelement spacing of the first ULA, the filter $\mathbf{h}_2$ will be used to design and shape the directivity pattern while $\mathbf{h}_1$ will be used to mostly maximize the WNG. Consequently, with $\mathbf{h}_2$, we will design an (M_0-1)th-order differential beamformer. Then, the global ULA will be a differential array of order certainly higher than M_0-1.

We recall that the definitions of the WNG and the DF are, respectively,

$$\begin{aligned}\mathcal{W}(\mathbf{h}) &= \frac{\left|\mathbf{h}^H\mathbf{d}_0\right|^2}{\mathbf{h}^H\mathbf{h}} \\ &= \frac{\left|\mathbf{h}_1^H\mathbf{d}_{1,0}\right|^2}{\mathbf{h}_1^H\mathbf{h}_1} \times \frac{\left|\mathbf{h}_2^H\mathbf{d}_{2,0}\right|^2}{\mathbf{h}_2^H\mathbf{h}_2}\end{aligned} \tag{3.204}$$

and

$$\begin{aligned}\mathcal{D}(\mathbf{h}) &= \frac{\left|\mathcal{B}_0(\mathbf{h})\right|^2}{\frac{1}{2}\int_0^\pi \left|\mathcal{B}_\theta(\mathbf{h})\right|^2 \sin\theta d\theta} \\ &= \frac{\left|\mathcal{B}_{1,0}(\mathbf{h}_1)\right|^2 \left|\mathcal{B}_{2,0}(\mathbf{h}_2)\right|^2}{\frac{1}{2}\int_0^\pi \left|\mathcal{B}_{1,\theta}(\mathbf{h}_1)\right|^2 \left|\mathcal{B}_{2,\theta}(\mathbf{h}_2)\right|^2 \sin\theta d\theta} \\ &= \frac{\left|\mathbf{h}^H\mathbf{d}_0\right|^2}{\mathbf{h}^H\mathbf{\Gamma}\mathbf{h}}.\end{aligned} \tag{3.205}$$

Another measure of interest in this study is the front-to-back ratio (FBR), which is defined as the ratio of the power of the output of the array to signals propagating from the front-half plane to the output power for signals arriving from the rear-half plane [13]. This ratio, for the spherically isotropic (diffuse) noise field, is mathematically defined as [13]

$$\begin{aligned}\mathcal{F}(\mathbf{h}) &= \frac{\int_0^{\pi/2} |\mathcal{B}_\theta(\mathbf{h})|^2 \sin\theta d\theta}{\int_{\pi/2}^{\pi} |\mathcal{B}_\theta(\mathbf{h})|^2 \sin\theta d\theta} \\ &= \frac{\int_0^{\pi/2} |\mathcal{B}_{1,\theta}(\mathbf{h}_1)|^2 |\mathcal{B}_{2,\theta}(\mathbf{h}_2)|^2 \sin\theta d\theta}{\int_{\pi/2}^{\pi} |\mathcal{B}_{1,\theta}(\mathbf{h}_1)|^2 |\mathcal{B}_{2,\theta}(\mathbf{h}_2)|^2 \sin\theta d\theta} \\ &= \frac{\mathbf{h}^H \mathbf{\Gamma}_{\mathrm{f}} \mathbf{h}}{\mathbf{h}^H \mathbf{\Gamma}_{\mathrm{b}} \mathbf{h}},\end{aligned} \tag{3.206}$$

where

$$\mathbf{\Gamma}_{\mathrm{f}} = \int_0^{\pi/2} \mathbf{d}_\theta \mathbf{d}_\theta^H \sin\theta d\theta, \tag{3.207}$$

$$\mathbf{\Gamma}_{\mathrm{b}} = \int_{\pi/2}^{\pi} \mathbf{d}_\theta \mathbf{d}_\theta^H \sin\theta d\theta. \tag{3.208}$$

It can be verified that the elements of the $M \times M$ matrices $\mathbf{\Gamma}_{\mathrm{f}}(\omega)$ and $\mathbf{\Gamma}_{\mathrm{b}}(\omega)$ are given, respectively, by

$$[\mathbf{\Gamma}_{\mathrm{f}}(\omega)]_{ij} = \frac{e^{\jmath\omega(j-i)\delta/c} - 1}{\jmath\omega(j-i)\delta/c} \tag{3.209}$$

and

$$[\mathbf{\Gamma}_{\mathrm{b}}(\omega)]_{ij} = \frac{1 - e^{-\jmath\omega(j-i)\delta/c}}{\jmath\omega(j-i)\delta/c}, \tag{3.210}$$

with $[\mathbf{\Gamma}_{\mathrm{f}}(\omega)]_{mm} = [\mathbf{\Gamma}_{\mathrm{b}}(\omega)]_{mm} = 1,\ m = 1, 2, \ldots, M$. Same as the DF, the FBR cannot be factorized, i.e.,

$$\mathcal{F}(\mathbf{h}) \neq \mathcal{F}_1(\mathbf{h}_1) \times \mathcal{F}_2(\mathbf{h}_2), \tag{3.211}$$

where

$$\mathcal{F}_1(\mathbf{h}_1) = \frac{\int_0^{\pi/2} |\mathcal{B}_{1,\theta}(\mathbf{h}_1)|^2 \sin\theta d\theta}{\int_{\pi/2}^{\pi} |\mathcal{B}_{1,\theta}(\mathbf{h}_1)|^2 \sin\theta d\theta} = \frac{\mathbf{h}_1^H \mathbf{\Gamma}_{\mathrm{f},1} \mathbf{h}_1}{\mathbf{h}_1^H \mathbf{\Gamma}_{\mathrm{b},1} \mathbf{h}_1}, \tag{3.212}$$

$$\mathcal{F}_2(\mathbf{h}_2) = \frac{\int_0^{\pi/2} |\mathcal{B}_{2,\theta}(\mathbf{h}_2)|^2 \sin\theta d\theta}{\int_{\pi/2}^{\pi} |\mathcal{B}_{2,\theta}(\mathbf{h}_2)|^2 \sin\theta d\theta} = \frac{\mathbf{h}_2^H \mathbf{\Gamma}_{\mathrm{f},2} \mathbf{h}_2}{\mathbf{h}_2^H \mathbf{\Gamma}_{\mathrm{b},2} \mathbf{h}_2}, \tag{3.213}$$

with

$$\mathbf{\Gamma}_{\mathrm{f},1} = \int_0^{\pi/2} \mathbf{d}_{1,\theta} \mathbf{d}_{1,\theta}^H \sin\theta d\theta, \tag{3.214}$$

$$\mathbf{\Gamma}_{\mathrm{b},1} = \int_{\pi/2}^{\pi} \mathbf{d}_{1,\theta} \mathbf{d}_{1,\theta}^H \sin\theta d\theta, \tag{3.215}$$

$$\mathbf{\Gamma}_{\mathrm{f},2} = \int_0^{\pi/2} \mathbf{d}_{2,\theta} \mathbf{d}_{2,\theta}^H \sin\theta d\theta, \tag{3.216}$$

$$\mathbf{\Gamma}_{\mathrm{b},2} = \int_{\pi/2}^{\pi} \mathbf{d}_{2,\theta} \mathbf{d}_{2,\theta}^H \sin\theta d\theta. \tag{3.217}$$

The elements of the $M_0 \times M_0$ matrices $\mathbf{\Gamma}_{\mathrm{f},1}(\omega)$, $\mathbf{\Gamma}_{\mathrm{b},1}(\omega)$, $\mathbf{\Gamma}_{\mathrm{f},2}(\omega)$, and $\mathbf{\Gamma}_{\mathrm{b},2}(\omega)$ are given, respectively, by

$$[\mathbf{\Gamma}_{\mathrm{f},1}(\omega)]_{ij} = \frac{e^{\jmath\omega(j-i)M_0\delta/c} - 1}{\jmath\omega(j-i)M_0\delta/c}, \tag{3.218}$$

$$[\mathbf{\Gamma}_{\mathrm{b},1}(\omega)]_{ij} = \frac{1 - e^{-\jmath\omega(j-i)M_0\delta/c}}{\jmath\omega(j-i)M_0\delta/c}, \tag{3.219}$$

$$[\mathbf{\Gamma}_{\mathrm{f},2}(\omega)]_{ij} = \frac{e^{\jmath\omega(j-i)\delta/c} - 1}{\jmath\omega(j-i)\delta/c}, \tag{3.220}$$

and

$$[\mathbf{\Gamma}_{\mathrm{b},2}(\omega)]_{ij} = \frac{1 - e^{-\jmath\omega(j-i)\delta/c}}{\jmath\omega(j-i)\delta/c}, \tag{3.221}$$

with $[\mathbf{\Gamma}_{\mathrm{f},1}(\omega)]_{mm} = [\mathbf{\Gamma}_{\mathrm{b},1}(\omega)]_{mm} = [\mathbf{\Gamma}_{\mathrm{f},2}(\omega)]_{mm} = [\mathbf{\Gamma}_{\mathrm{b},2}(\omega)]_{mm} = 1,\ m = 1, 2, \ldots, M_0$.

When $\mathbf{h}_2$ is fixed and given, and thanks to (2.41), we can write the FBR as

$$\mathcal{F}(\mathbf{h}_1|\mathbf{h}_2) = \frac{\mathbf{h}_1^H \mathbf{\Gamma}_{\mathrm{f},\mathbf{h}_2} \mathbf{h}_1}{\mathbf{h}_1^H \mathbf{\Gamma}_{\mathrm{b},\mathbf{h}_2} \mathbf{h}_1}, \tag{3.222}$$

where

$$\begin{aligned} \mathbf{\Gamma}_{\mathrm{f},\mathbf{h}_2} &= \int_0^{\pi/2} \mathbf{d}_{1,\theta} \mathbf{d}_{1,\theta}^H \left|\mathcal{B}_{2,\theta}(\mathbf{h}_2)\right|^2 \sin\theta d\theta \qquad (3.223)\\ &= (\mathbf{I}_{M_0} \otimes \mathbf{h}_2)^H \mathbf{\Gamma}_{\mathrm{f}} (\mathbf{I}_{M_0} \otimes \mathbf{h}_2), \\ \mathbf{\Gamma}_{\mathrm{b},\mathbf{h}_2} &= \int_{\pi/2}^{\pi} \mathbf{d}_{1,\theta} \mathbf{d}_{1,\theta}^H \left|\mathcal{B}_{2,\theta}(\mathbf{h}_2)\right|^2 \sin\theta d\theta \qquad (3.224)\\ &= (\mathbf{I}_{M_0} \otimes \mathbf{h}_2)^H \mathbf{\Gamma}_{\mathrm{b}} (\mathbf{I}_{M_0} \otimes \mathbf{h}_2). \end{aligned}$$

In the same way, when $\mathbf{h}_1$ is fixed and given, and thanks to (2.40), we can write the FBR as

$$\mathcal{F}(\mathbf{h}_2|\mathbf{h}_1) = \frac{\mathbf{h}_2^H \mathbf{\Gamma}_{\mathrm{f},\mathbf{h}_1} \mathbf{h}_2}{\mathbf{h}_2^H \mathbf{\Gamma}_{\mathrm{b},\mathbf{h}_1} \mathbf{h}_2}, \tag{3.225}$$

where

$$\begin{aligned} \mathbf{\Gamma}_{\mathrm{f},\mathbf{h}_1} &= \int_0^{\pi/2} \mathbf{d}_{2,\theta} \mathbf{d}_{2,\theta}^H \left|\mathcal{B}_{1,\theta}(\mathbf{h}_1)\right|^2 \sin\theta d\theta \qquad (3.226)\\ &= (\mathbf{h}_1 \otimes \mathbf{I}_{M_0})^H \mathbf{\Gamma}_{\mathrm{f}} (\mathbf{h}_1 \otimes \mathbf{I}_{M_0}), \\ \mathbf{\Gamma}_{\mathrm{b},\mathbf{h}_1} &= \int_{\pi/2}^{\pi} \mathbf{d}_{2,\theta} \mathbf{d}_{2,\theta}^H \left|\mathcal{B}_{1,\theta}(\mathbf{h}_1)\right|^2 \sin\theta d\theta \qquad (3.227)\\ &= (\mathbf{h}_1 \otimes \mathbf{I}_{M_0})^H \mathbf{\Gamma}_{\mathrm{b}} (\mathbf{h}_1 \otimes \mathbf{I}_{M_0}). \end{aligned}$$

3.4.2 Cardioid

The (M_0-1)th-order cardioid has a unique null of multiplicity M_0-1 in the direction π. Therefore, the ith derivative, with $i = 0, 1, \ldots, M_0 - 2$, of the beampattern of $\mathbf{h}_2$ with respect to $\cos\theta$ is equal to 0 at $\cos\pi = -1$, i.e.,

$$\left.\frac{d^i \mathcal{B}_{2,\theta}(\mathbf{h}_2)}{d\cos^i\theta}\right|_{\cos\theta=-1} = \mathcal{B}_{2,\pi}^{[i]}(\mathbf{h}_2) = 0, \tag{3.228}$$

with

$$\mathcal{B}_{2,\pi}^{[0]}\left(\mathbf{h}_2\right) = \mathcal{B}_{2,\pi}\left(\mathbf{h}_2\right).$$

We easily find that

$$\mathcal{B}_{2,\pi}^{[i]}\left(\mathbf{h}_2\right) = \left(\jmath\omega\delta/c\right)^i \left(\boldsymbol{\Sigma}^i \mathbf{d}_{2,\pi}\right)^H \mathbf{h}_2, \tag{3.229}$$

where

$$\boldsymbol{\Sigma} = \operatorname{diag}\left(0, 1, \ldots, M_0 - 1\right) \tag{3.230}$$

is a diagonal matrix of size $M_0 \times M_0$. Combining the distortionless constraint, i.e.,

$$\mathcal{B}_{2,0}\left(\mathbf{h}_2\right) = \mathbf{d}_{2,0}^H \mathbf{h}_2 = 1, \tag{3.231}$$

with the $M_0 - 1$ equations from (3.228), we obtain a linear system of M_0 equations with M_0 unknowns:

$$\mathbf{D}_{2,\pi}^H \mathbf{h}_2 = \mathbf{i}, \tag{3.232}$$

where

$$\mathbf{D}_{2,\pi}^H = \begin{bmatrix} \mathbf{d}_{2,0}^H \\ \left(\boldsymbol{\Sigma}^0 \mathbf{d}_{2,\pi}\right)^H \\ \left(\boldsymbol{\Sigma}^1 \mathbf{d}_{2,\pi}\right)^H \\ \vdots \\ \left(\boldsymbol{\Sigma}^{M_0-2} \mathbf{d}_{2,\pi}\right)^H \end{bmatrix} \tag{3.233}$$

and $\mathbf{i}$ is the first column of $\mathbf{I}_{M_0}$. Therefore, the cardioid of order $M_0 - 1$ at the second ULA is

$$\mathbf{h}_{2,\mathrm{C}} = \mathbf{D}_{2,\pi}^{-H} \mathbf{i}. \tag{3.234}$$

For the first filter, we take the DS beamformer, i.e.,

$$\mathbf{h}_{1,\mathrm{DS}} = \frac{\mathbf{d}_{1,0}}{M_0}, \tag{3.235}$$

which maximizes the WNG. As a result, the robust global cardioid of order, at least, $M_0 - 1$ is

$$\mathbf{h}_{\mathrm{C}} = \mathbf{h}_{1,\mathrm{DS}} \otimes \mathbf{h}_{2,\mathrm{C}}. \tag{3.236}$$

Figure 3.19 displays the directivity patterns of the robust global cardioid, $\mathbf{h}_{\mathrm{C}}$, for $f = 1$ kHz, $\delta = 1$ cm, and different numbers of sensors M. Figure 3.20 shows plots of the DFs and WNGs of the robust global cardioid, $\mathbf{h}_{\mathrm{C}}$, as a

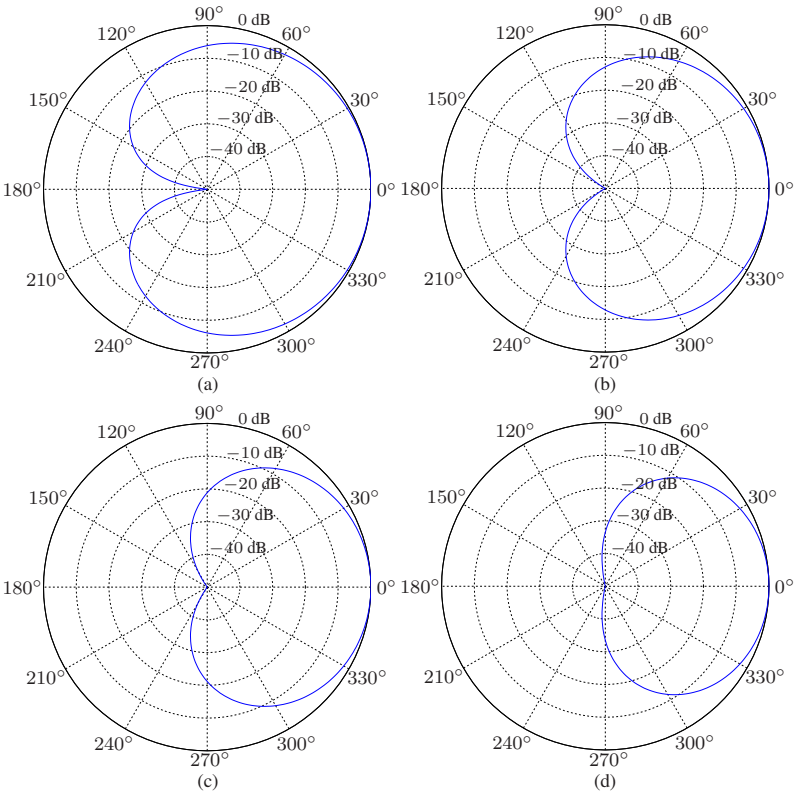

Fig. 3.19 Beampatterns of the robust global cardioid, $\mathbf{h}_{\mathrm{C}}$, for $f = 1$ kHz, $\delta = 1$ cm, and different numbers of sensors $M = M_0^2$: (a) $M_0 = 2$, (b) $M_0 = 3$, (c) $M_0 = 4$, and (d) $M_0 = 5$.

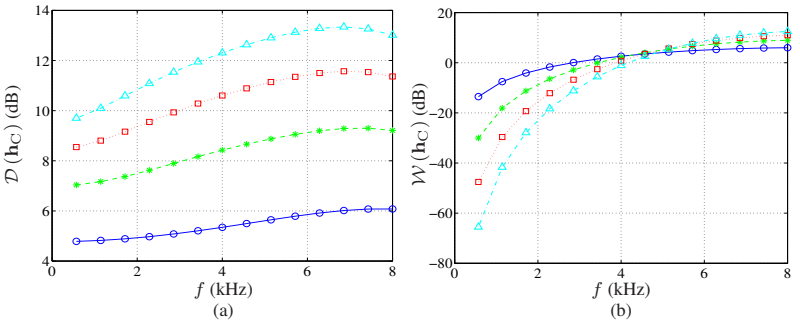

Fig. 3.20 Performance of the robust global cardioid, $\mathbf{h}_{\mathrm{C}}$, as a function of frequency for $\delta = 1$ cm, and different numbers of sensors $M = M_0^2$: $M_0 = 2$ (solid line with circles), $M_0 = 3$ (dashed line with asterisks), $M_0 = 4$ (dotted line with squares), and $M_0 = 5$ (dash-dot line with triangles). (a) DF and (b) WNG.

function of frequency. We observe that the DF increases as we increase the numbers of sensors, but the WNG decreases at low frequencies.

To get an even more robust beamformer, we may optimize

$$\min_{\mathbf{h}_2} \mathbf{h}_2^H \left(\mathbf{D}'_{2,\pi}\mathbf{D}'^H_{2,\pi} + \epsilon_2 \mathbf{I}_{M_0}\right)\mathbf{h}_2 \quad \text{subject to} \quad \mathbf{C}_{2,\pi}^H \mathbf{h}_2 = \mathbf{i}_{\mathrm{c}}, \tag{3.237}$$

where

$$\mathbf{D}'_{2,\pi} = \left[\, \boldsymbol{\Sigma}^1 \mathbf{d}_{2,\pi}\ \boldsymbol{\Sigma}^2 \mathbf{d}_{2,\pi}\ \cdots\ \boldsymbol{\Sigma}^{M_0-2}\mathbf{d}_{2,\pi}\,\right] \tag{3.238}$$

is a matrix of size $M_0 \times (M_0 - 2)$, $\epsilon_2 > 0$ is the regularization parameter, and

$$\mathbf{C}_{2,\pi}^H = \begin{bmatrix} \mathbf{d}_{2,0}^H \\ \mathbf{d}_{2,\pi}^H \end{bmatrix} \tag{3.239}$$

is the constraint matrix of size $2 \times M_0$. We see that with $\mathbf{C}_{2,\pi}$, the two main constraints are fulfilled, i.e., the distortionless one and a null in the direction π. We find that the optimal filter is

$$\begin{aligned} \mathbf{h}_{2,\mathrm{C},\epsilon_2} = &\left(\mathbf{D}'_{2,\pi}\mathbf{D}'^H_{2,\pi} + \epsilon_2 \mathbf{I}_{M_0}\right)^{-1} \mathbf{C}_{2,\pi} \\ &\times \left[\mathbf{C}_{2,\pi}^H \left(\mathbf{D}'_{2,\pi}\mathbf{D}'^H_{2,\pi} + \epsilon_2 \mathbf{I}_{M_0}\right)^{-1} \mathbf{C}_{2,\pi}\right]^{-1} \mathbf{i}_{\mathrm{c}}. \end{aligned} \tag{3.240}$$

Therefore, the more robust global cardioid is

$$\mathbf{h}_{\mathrm{C},\epsilon_2} = \mathbf{h}_{1,\mathrm{DS}} \otimes \mathbf{h}_{2,\mathrm{C},\epsilon_2}. \tag{3.241}$$

Figure 3.21 displays the directivity patterns of the robust global cardioid, $\mathbf{h}_{\mathrm{C},\epsilon_2}$, for $f = 1$ kHz, $\delta = 1$ cm, $M_0 = 4$, and several values of ϵ_2. Figure 3.22 shows plots of the DFs and WNGs of the robust global cardioid, $\mathbf{h}_{\mathrm{C},\epsilon_2}$, as a function of frequency. We observe that the WNG increases as we increase ϵ_2, but the DF decreases.

3.4.3 Dipole

The design of the global dipole is a bit different from the design of the global cardioid as explained below.

The dipole of order $M_0 - 1$ has also a unique null of multiplicity $M_0 - 1$ but in the direction $\pi/2$. Since we have a null with maximum multiplicity, the ith ($i = 0, 1, \ldots, M_0 - 2$) derivative of the beampattern of $\mathbf{h}_2$ with respect to $\cos\theta$ is equal to 0 at $\cos(\pi/2) = 0$, i.e.,

$$\left.\frac{d^i \mathcal{B}_{2,\theta}\left(\mathbf{h}_2\right)}{d\cos^i\theta}\right|_{\cos\theta=0} = \mathcal{B}^{[i]}_{2,\pi/2}\left(\mathbf{h}_2\right) = 0, \tag{3.242}$$

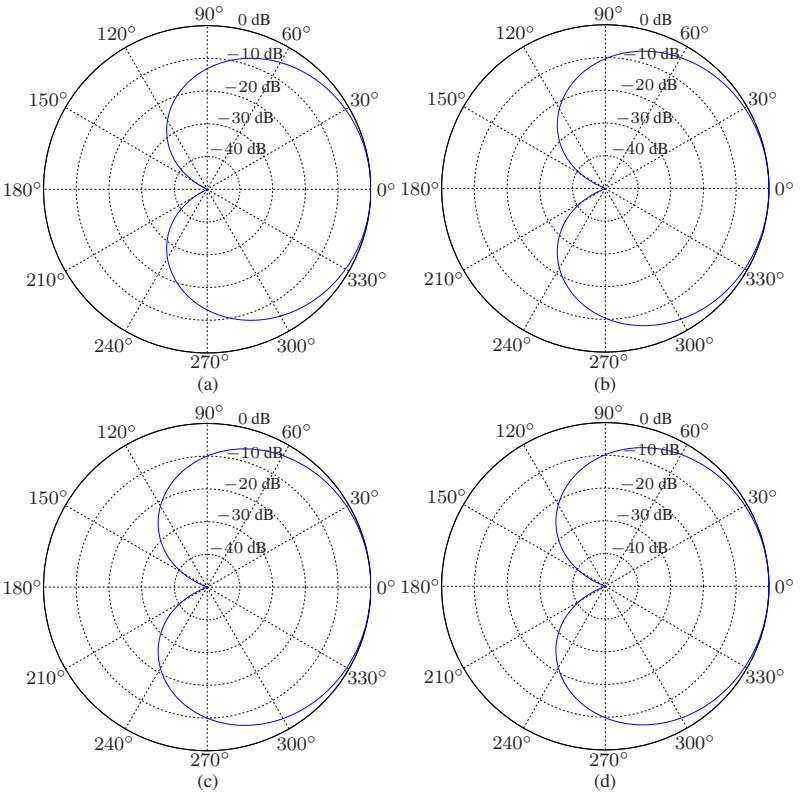

Fig. 3.21 Beampatterns of the robust global cardioid, $\mathbf{h}_{\mathrm{C},\epsilon_2}$, for $f = 1$ kHz, $\delta = 1$ cm, $M_0 = 4$, and several values of ϵ_2: (a) $\epsilon_2 = 0.001$, (b) $\epsilon_2 = 0.01$, (c) $\epsilon_2 = 0.1$, and (d) $\epsilon_2 = 1$.

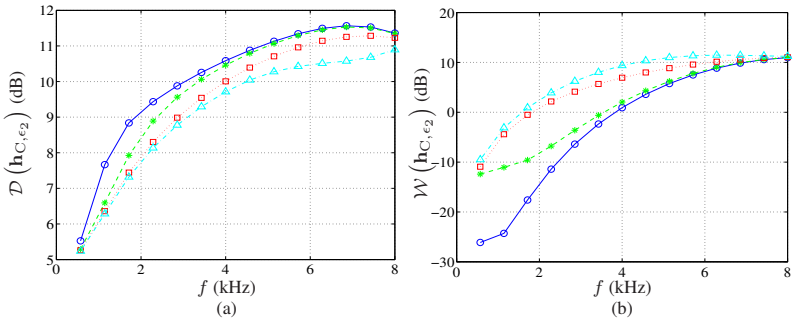

Fig. 3.22 Performance of the robust global cardioid, $\mathbf{h}_{\mathrm{C},\epsilon_2}$, as a function of frequency for $\delta = 1$ cm, $M_0 = 4$, and several values of ϵ_2: $\epsilon_2 = 0.001$ (solid line with circles), $\epsilon_2 = 0.01$ (dashed line with asterisks), $\epsilon_2 = 0.1$ (dotted line with squares), and $\epsilon_2 = 1$ (dash-dot line with triangles). (a) DF and (b) WNG.

with

$$\mathcal{B}_{2,\pi/2}^{[0]}\left(\mathbf{h}_2\right) = \mathcal{B}_{2,\pi/2}\left(\mathbf{h}_2\right).$$

We get

$$\mathcal{B}_{2,\pi/2}^{[i]}\left(\mathbf{h}_2\right) = \left(\jmath\omega\delta/c\right)^i \left(\mathbf{\Sigma}^i \mathbf{d}_{2,\pi/2}\right)^H \mathbf{h}_2, \tag{3.243}$$

where $\mathbf{\Sigma}$ is defined in (3.230). Combining the distortionless constraint with the $M_0 - 1$ constraints from (3.242), we have

$$\mathbf{D}_{2,\pi/2}^H \mathbf{h}_2 = \mathbf{i}, \tag{3.244}$$

where

$$\mathbf{D}_{2,\pi/2}^H = \begin{bmatrix} \mathbf{d}_{2,0}^H \\ \left(\mathbf{\Sigma}^0 \mathbf{d}_{2,\pi/2}\right)^H \\ \left(\mathbf{\Sigma}^1 \mathbf{d}_{2,\pi/2}\right)^H \\ \vdots \\ \left(\mathbf{\Sigma}^{M_0-2} \mathbf{d}_{2,\pi/2}\right)^H \end{bmatrix}. \tag{3.245}$$

As a result, the dipole of order $M_0 - 1$ at the second ULA is

$$\mathbf{h}_{2,\mathrm{D}} = \mathbf{D}_{2,\pi/2}^{-H} \mathbf{i}. \tag{3.246}$$

Another feature of the dipole is that it has a 1 in the direction π. To ensure that the global beampattern has also a 1 at π, we must add this constraint in the design of the first filter. We deduce that the constraint equation for $\mathbf{h}_1$ is

$$\mathbf{C}_{1,\pi}^H \mathbf{h}_1 = \begin{bmatrix} 1 \\ 1 \end{bmatrix}, \tag{3.247}$$

where

$$\mathbf{C}_{1,\pi}^H = \begin{bmatrix} \mathbf{d}_{1,0}^H \\ \mathbf{d}_{1,\pi}^H \end{bmatrix} \tag{3.248}$$

is the constraint matrix of size $2 \times M_0$. Since we want to maximize the WNG of $\mathbf{h}_1$ subject to (3.247), we find the minimum-norm beamformer:

$$\mathbf{h}_{1,\mathrm{MN}} = \mathbf{C}_{1,\pi} \left(\mathbf{C}_{1,\pi}^H \mathbf{C}_{1,\pi}\right)^{-1} \begin{bmatrix} 1 \\ 1 \end{bmatrix}. \tag{3.249}$$

Now, that the two filters are derived, we deduce that the robust global dipole of order, at least, $M_0 - 1$ is

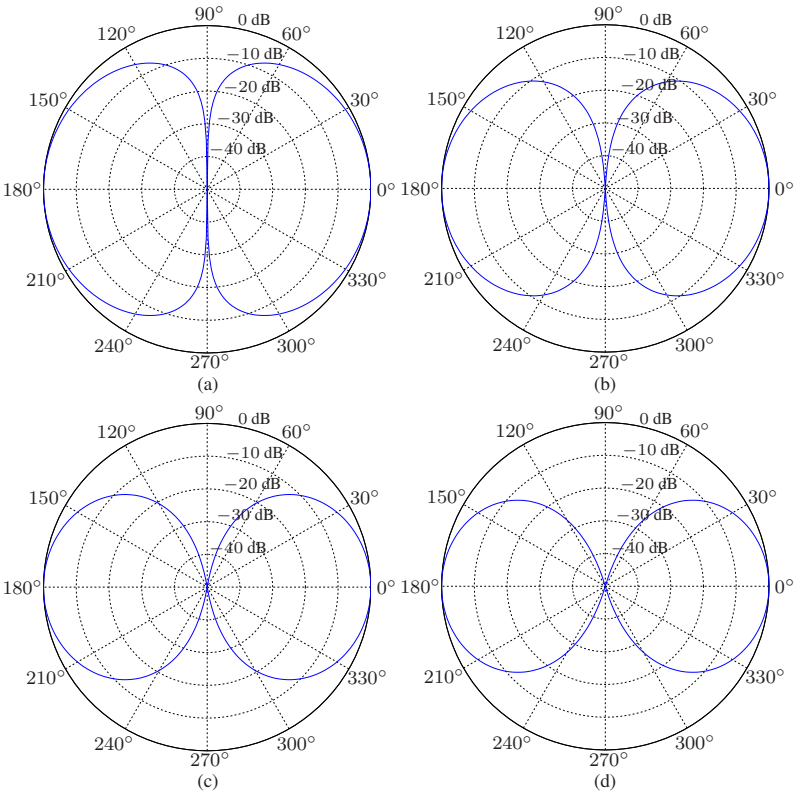

Fig. 3.23 Beampatterns of the robust global dipole, $\mathbf{h}_{\mathrm{D}}$, for $f = 1$ kHz, $\delta = 1$ cm, and different numbers of sensors $M = M_0^2$: (a) $M_0 = 2$, (b) $M_0 = 3$, (c) $M_0 = 4$, and (d) $M_0 = 5$.

$$\mathbf{h}_{\mathrm{D}} = \mathbf{h}_{1,\mathrm{MN}} \otimes \mathbf{h}_{2,\mathrm{D}}. \tag{3.250}$$

Figure 3.23 displays the directivity patterns of the robust global dipole, $\mathbf{h}_{\mathrm{D}}$, for $f = 1$ kHz, $\delta = 1$ cm, and different numbers of sensors M. Figure 3.24 shows plots of the DFs and WNGs of the robust global dipole, $\mathbf{h}_{\mathrm{D}}$, as a function of frequency. We observe that the DF generally increases as we increase the numbers of sensors, but the WNG decreases.

As we did for the cardioid, we can derive a more robust global dipole:

$$\mathbf{h}_{\mathrm{D},\epsilon_2} = \mathbf{h}_{1,\mathrm{MN}} \otimes \mathbf{h}_{2,\mathrm{D},\epsilon_2}, \tag{3.251}$$

where

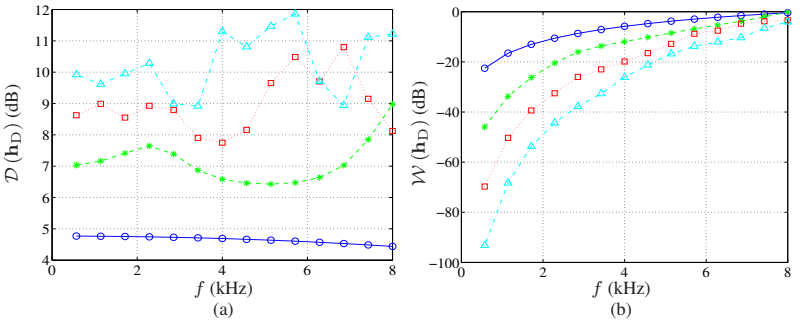

Fig. 3.24 Performance of the robust global dipole, $\mathbf{h}_{\mathrm{D}}$, as a function of frequency for $\delta = 1$ cm and different numbers of sensors $M = M_0^2$: $M_0 = 2$ (solid line with circles), $M_0 = 3$ (dashed line with asterisks), $M_0 = 4$ (dotted line with squares), and $M_0 = 5$ (dash-dot line with triangles). (a) DF and (b) WNG.

$$\mathbf{h}_{2,\mathrm{D},\epsilon_2} = \left(\mathbf{D}'_{2,\pi/2}\mathbf{D}'^{H}_{2,\pi/2} + \epsilon_2\mathbf{I}_{M_0}\right)^{-1}\mathbf{C}_{2,\pi/2} \times \left[\mathbf{C}^{H}_{2,\pi/2}\left(\mathbf{D}'_{2,\pi/2}\mathbf{D}'^{H}_{2,\pi/2} + \epsilon_2\mathbf{I}_{M_0}\right)^{-1}\mathbf{C}_{2,\pi/2}\right]^{-1}\mathbf{i}_{\mathrm{c}}, \tag{3.252}$$

with

$$\mathbf{D}'_{2,\pi/2} = \left[\,\boldsymbol{\Sigma}^1\mathbf{d}_{2,\pi/2}\ \boldsymbol{\Sigma}^2\mathbf{d}_{2,\pi/2}\ \cdots\ \boldsymbol{\Sigma}^{M_0-2}\mathbf{d}_{2,\pi/2}\,\right] \tag{3.253}$$

and

$$\mathbf{C}^{H}_{2,\pi/2} = \begin{bmatrix}\mathbf{d}^{H}_{2,0}\\ \mathbf{d}^{H}_{2,\pi/2}\end{bmatrix}. \tag{3.254}$$

Figure 3.25 displays the directivity patterns of the robust global dipole, $\mathbf{h}_{\mathrm{D},\epsilon_2}$, for $f = 1$ kHz, $\delta = 1$ cm, $M_0 = 4$, and several values of ϵ_2. Figure 3.26 shows plots of the DFs and WNGs of the robust global dipole, $\mathbf{h}_{\mathrm{D},\epsilon_2}$, as a function of frequency. We observe that the WNG increases as we increase ϵ_2.

3.4.4 Hypercardioid

The hypercardioid is usually obtained from the maximization of the DF.

For the first filter, $\mathbf{h}_1$, we take the DS beamformer, i.e., $\mathbf{h}_1 = \mathbf{h}_{1,\mathrm{DS}}$, so that its WNG is maximized. By definition, the DF of $\mathbf{h}_2$ is

$$\mathcal{D}(\mathbf{h}_2) = \frac{\left|\mathbf{h}_2^H\mathbf{d}_{2,0}\right|^2}{\mathbf{h}_2^H\boldsymbol{\Gamma}_2\mathbf{h}_2}. \tag{3.255}$$

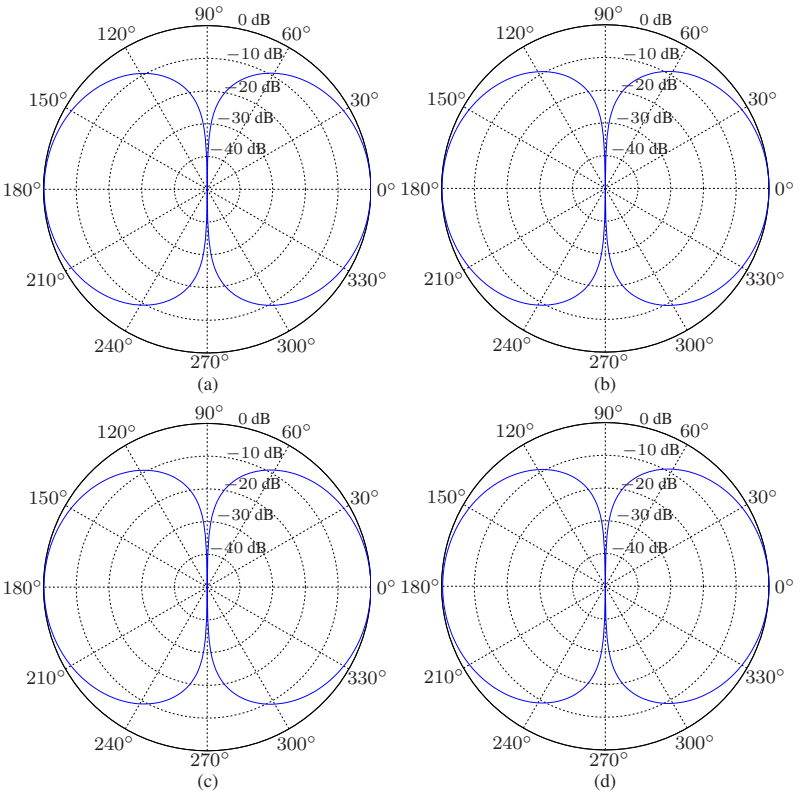

Fig. 3.25 Beampatterns of the robust global dipole, $\mathbf{h}_{\mathrm{D},\epsilon_2}$, for $f = 1$ kHz, $\delta = 1$ cm, $M_0 = 4$, and several values of ϵ_2: (a) $\epsilon_2 = 0.001$, (b) $\epsilon_2 = 0.01$, (c) $\epsilon_2 = 0.1$, and (d) $\epsilon_2 = 1$.

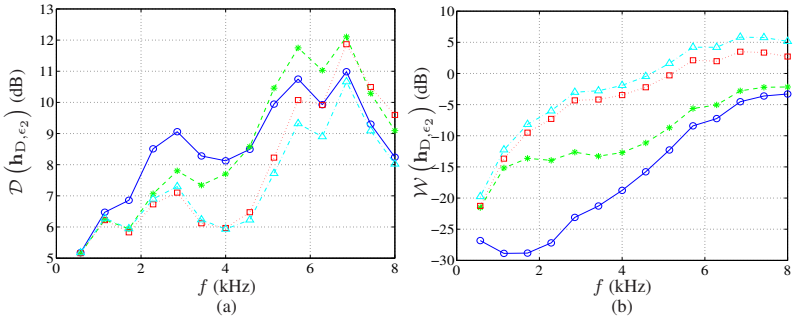

Fig. 3.26 Performance of the robust global dipole, $\mathbf{h}_{\mathrm{D},\epsilon_2}$, as a function of frequency for $\delta = 1$ cm, $M_0 = 4$, and several values of ϵ_2: $\epsilon_2 = 0.001$ (solid line with circles), $\epsilon_2 = 0.01$ (dashed line with asterisks), $\epsilon_2 = 0.1$ (dotted line with squares), and $\epsilon_2 = 1$ (dash-dot line with triangles). (a) DF and (b) WNG.

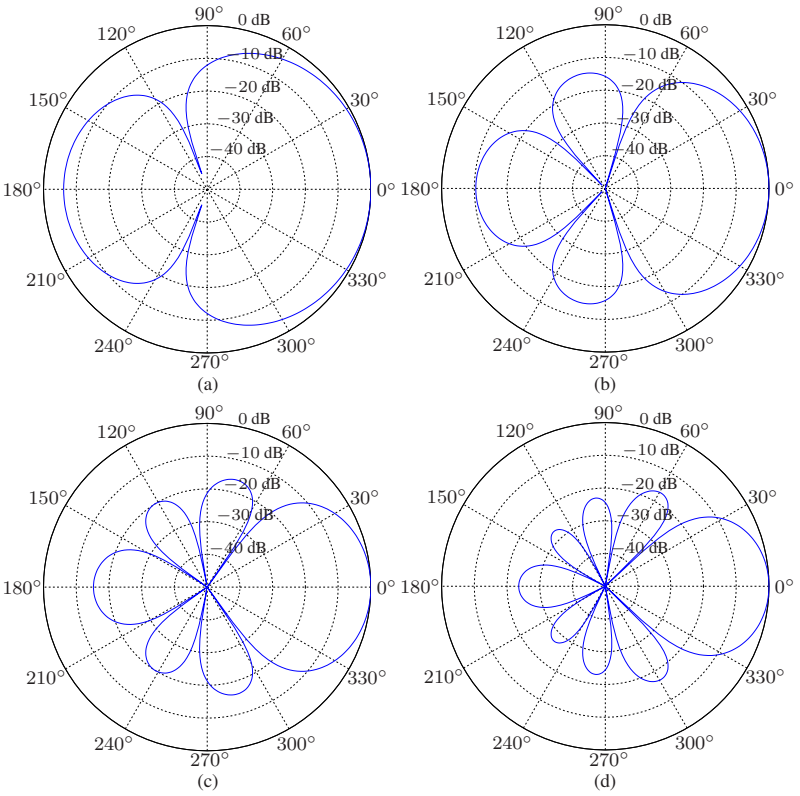

Fig. 3.27 Beampatterns of the robust global hypercardioid, $\mathbf{h}_{\mathrm{H}}$, for $f = 1$ kHz, $\delta = 5$ mm, and different numbers of sensors $M = M_0^2$: (a) $M_0 = 2$, (b) $M_0 = 3$, (c) $M_0 = 4$, and (d) $M_0 = 5$.

The maximization of $\mathcal{D}(\mathbf{h}_2)$ gives the hypercardioid of order $M_0 - 1$ at the second ULA:

$$\mathbf{h}_{2,\mathrm{H}} = \frac{\boldsymbol{\Gamma}_2^{-1}\mathbf{d}_{2,0}}{\mathbf{d}_{2,0}^H\boldsymbol{\Gamma}_2^{-1}\mathbf{d}_{2,0}}. \tag{3.256}$$

As a result, the robust global hypercardioid of order, at least, $M_0 - 1$ is

$$\mathbf{h}_{\mathrm{H}} = \mathbf{h}_{1,\mathrm{DS}} \otimes \mathbf{h}_{2,\mathrm{H}}. \tag{3.257}$$

Figure 3.27 displays the directivity patterns of the robust global hypercardioid, $\mathbf{h}_{\mathrm{H}}$, for $f = 1$ kHz, $\delta = 5$ mm, and different numbers of sensors M. Figure 3.28 shows plots of the DFs and WNGs of the robust global hypercardioid, $\mathbf{h}_{\mathrm{H}}$, as a function of frequency. We observe that the DF generally increases as we increase the numbers of sensors, but the WNG decreases.

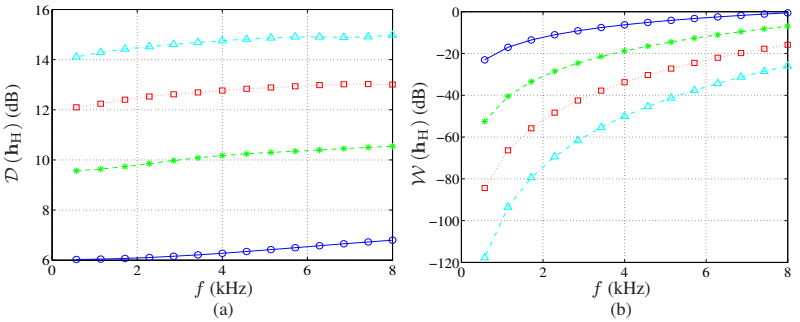

Fig. 3.28 Performance of the robust global hypercardioid, $\mathbf{h}_{\mathrm{H}}$, as a function of frequency for $\delta = 5$ mm and different numbers of sensors $M = M_0^2$: $M_0 = 2$ (solid line with circles), $M_0 = 3$ (dashed line with asterisks), $M_0 = 4$ (dotted line with squares), and $M_0 = 5$ (dash-dot line with triangles). (a) DF and (b) WNG.

To make this beamformer even more robust, we can use the following instead

$$\mathbf{h}_{\mathrm{H},\epsilon_2} = \mathbf{h}_{1,\mathrm{DS}} \otimes \mathbf{h}_{2,\mathrm{H},\epsilon_2}, \tag{3.258}$$

where

$$\mathbf{h}_{2,\mathrm{H},\epsilon_2} = \frac{\left(\mathbf{\Gamma}_2 + \epsilon_2 \mathbf{I}_{M_0}\right)^{-1} \mathbf{d}_{2,0}}{\mathbf{d}_{2,0}^H \left(\mathbf{\Gamma}_2 + \epsilon_2 \mathbf{I}_{M_0}\right)^{-1} \mathbf{d}_{2,0}}, \tag{3.259}$$

with $\epsilon_2 \geq 0$ being the regularization parameter.

Other possibilities can be borrowed from Subsection 3.1.2 by taking $\theta_{\mathrm{d}} = 0$.

Figure 3.29 displays the directivity patterns of the robust global dipole, $\mathbf{h}_{\mathrm{D},\epsilon_2}$, for $f = 1$ kHz, $\delta = 1$ cm, $M_0 = 4$, and several values of ϵ_2. Figure 3.30 shows plots of the DFs and WNGs of the robust global dipole, $\mathbf{h}_{\mathrm{D},\epsilon_2}$, as a function of frequency. We observe that the WNG increases as we increase ϵ_2, but the DF decreases.

3.4.5 Supercardioid

As we should expect, different versions of the supercardioid can be derived.

In the first version, we choose the DS beamformer for the first filter, i.e., $\mathbf{h}_1 = \mathbf{h}_{1,\mathrm{DS}}$. By definition, the FBR of $\mathbf{h}_2$ is given in (3.213) and we want to maximize this quantity. Let $\mathbf{t}_2$ be the eigenvector corresponding to the maximum eigenvalue of the matrix $\mathbf{\Gamma}_{\mathrm{b},2}^{-1}\mathbf{\Gamma}_{\mathrm{f},2}$. It is clear that the filter $\mathbf{h}_2 = \alpha\mathbf{t}_2$, where $\alpha \neq 0$ is an arbitrary complex number, maximizes this FBR. Taking the distortionless constraint into account, we deduce that the supercardioid of order $M_0 - 1$ at the second ULA is

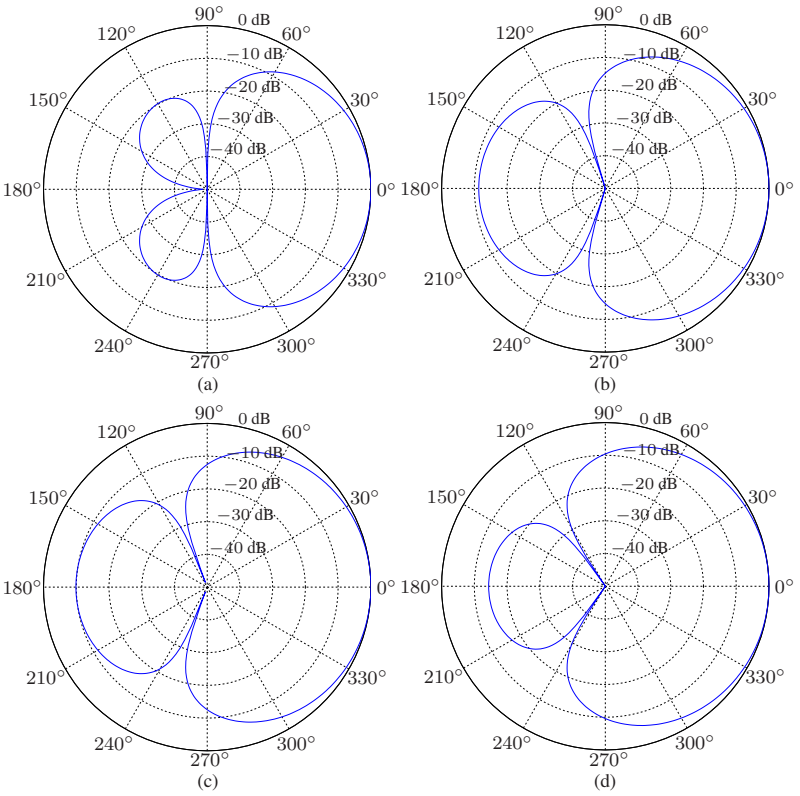

Fig. 3.29 Beampatterns of the robust global hypercardioid, $\mathbf{h}_{\mathrm{H},\epsilon_2}$, for $f = 1$ kHz, $\delta = 5$ mm, $M_0 = 4$, and several values of ϵ_2: (a) $\epsilon_2 = 10^{-5}$, (b) $\epsilon_2 = 10^{-4}$, (c) $\epsilon_2 = 10^{-3}$, and (d) $\epsilon_2 = 10^{-2}$.

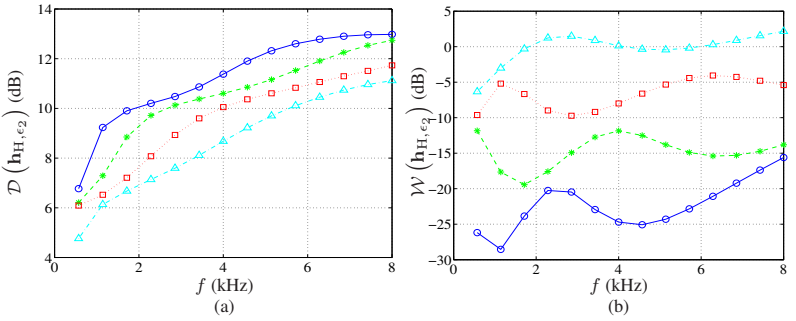

Fig. 3.30 Performance of the robust global hypercardioid, $\mathbf{h}_{\mathrm{H},\epsilon_2}$, as a function of frequency for $\delta = 5$ mm, $M_0 = 4$, and several values of ϵ_2: $\epsilon_2 = 10^{-5}$ (solid line with circles), $\epsilon_2 = 10^{-4}$ (dashed line with asterisks), $\epsilon_2 = 10^{-3}$ (dotted line with squares), and $\epsilon_2 = 10^{-2}$ (dash-dot line with triangles). (a) DF and (b) WNG.

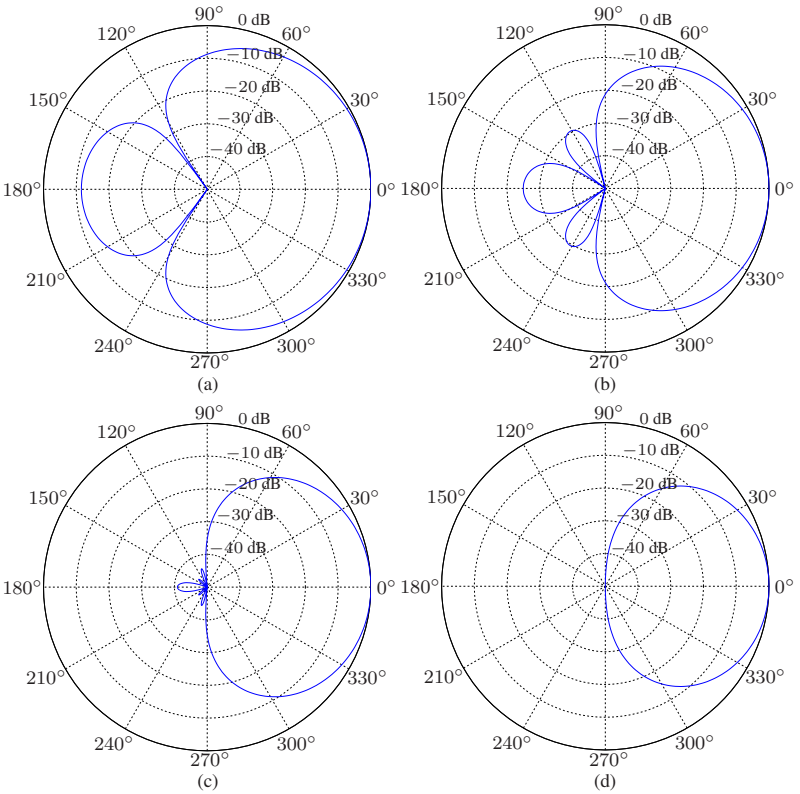

Fig. 3.31 Beampatterns of the robust global supercardioid, $\mathbf{h}_{\mathrm{S1}}$, for $f = 1$ kHz, $\delta = 5$ mm, and different numbers of sensors $M = M_0^2$: (a) $M_0 = 2$, (b) $M_0 = 3$, (c) $M_0 = 4$, and (d) $M_0 = 5$.

$$\mathbf{h}_{2,\mathrm{S}} = \frac{\mathbf{t}_2}{\mathbf{d}_{2,0}^H \mathbf{t}_2}. \tag{3.260}$$

Therefore, the robust global supercardioid of order, at least, $M_0 - 1$ is

$$\mathbf{h}_{\mathrm{S1}} = \mathbf{h}_{1,\mathrm{DS}} \otimes \mathbf{h}_{2,\mathrm{S}}. \tag{3.261}$$

Figure 3.31 displays the directivity patterns of the robust global supercardioid, $\mathbf{h}_{\mathrm{S1}}$, for $f = 1$ kHz, $\delta = 5$ mm, and different numbers of sensors M. Figure 3.32 shows plots of the DFs, WNGs, and FBRs of the robust global supercardioid, $\mathbf{h}_{\mathrm{S1}}$, as a function of frequency. We observe that the DF and FBR increase as we increase the number of sensors, but the WNG decreases.

To have a robust version of the supercardioid, $\mathbf{h}_{2,\mathrm{S}}$, we need now to consider the matrix $\left(\mathbf{\Gamma}_{\mathrm{b},2} + \epsilon_2 \mathbf{I}_{M_0}\right)^{-1} \mathbf{\Gamma}_{\mathrm{f},2}$. By taking the eigenvector corresponding to the maximum eigenvalue of this matrix that we denote $\mathbf{t}_{2,\epsilon_2}$, we find that the robust supercardioid at the second ULA is

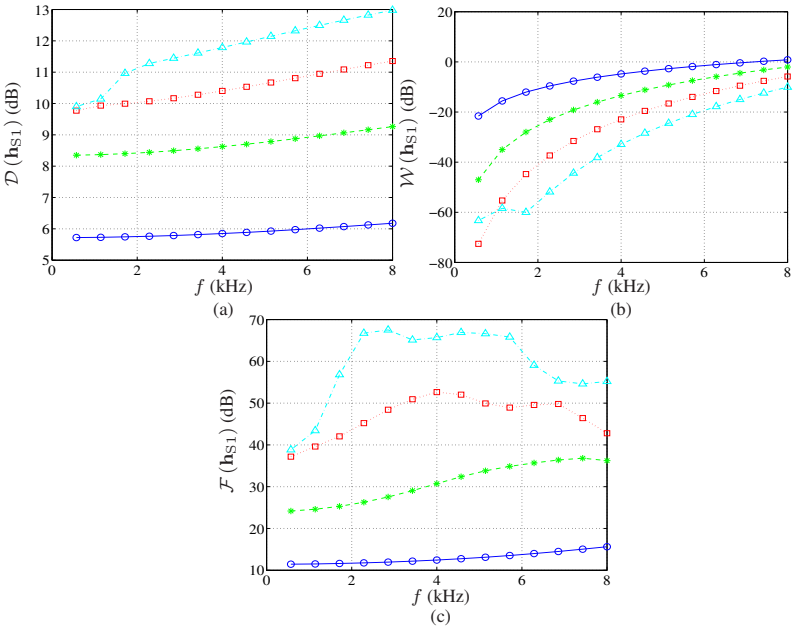

Fig. 3.32 Performance of the robust global supercardioid, $\mathbf{h}_{S1}$, as a function of frequency for $\delta = 5$ mm and different numbers of sensors $M = M_0^2$: $M_0 = 2$ (solid line with circles), $M_0 = 3$ (dashed line with asterisks), $M_0 = 4$ (dotted line with squares), and $M_0 = 5$ (dash-dot line with triangles). (a) DF, (b) WNG, and (c) FBR.

$$\mathbf{h}_{2,\mathrm{S},\epsilon_2} = \frac{\mathbf{t}_{2,\epsilon_2}}{\mathbf{d}_{2,0}^H \mathbf{t}_{2,\epsilon_2}}. \tag{3.262}$$

Then, the more robust global supercardioid is

$$\mathbf{h}_{\mathrm{S1},\epsilon_2} = \mathbf{h}_{1,\mathrm{DS}} \otimes \mathbf{h}_{2,\mathrm{S},\epsilon_2}. \tag{3.263}$$

Figure 3.33 displays the directivity patterns of the robust global supercardioid, $\mathbf{h}_{\mathrm{S1},\epsilon_2}$, for $f = 1$ kHz, $\delta = 5$ mm, $M_0 = 4$, and several values of ϵ_2. Figure 3.34 shows plots of the DFs, WNGs, and FBRs of the robust global supercardioid, $\mathbf{h}_{\mathrm{S1},\epsilon_2}$, as a function of frequency. We observe that the WNG increases as we increase ϵ_2, but the DF and FBR decrease.

Assume that $\mathbf{h}_1 = \mathbf{h}_{1,\mathrm{DS}}$. Substituting this filter into (3.225), we get

$$\mathcal{F}(\mathbf{h}_2|\mathbf{h}_{1,\mathrm{DS}}) = \frac{\mathbf{h}_2^H \boldsymbol{\Gamma}_{\mathrm{f},\mathbf{h}_{1,\mathrm{DS}}} \mathbf{h}_2}{\mathbf{h}_2^H \boldsymbol{\Gamma}_{\mathrm{b},\mathbf{h}_{1,\mathrm{DS}}} \mathbf{h}_2}, \tag{3.264}$$

where

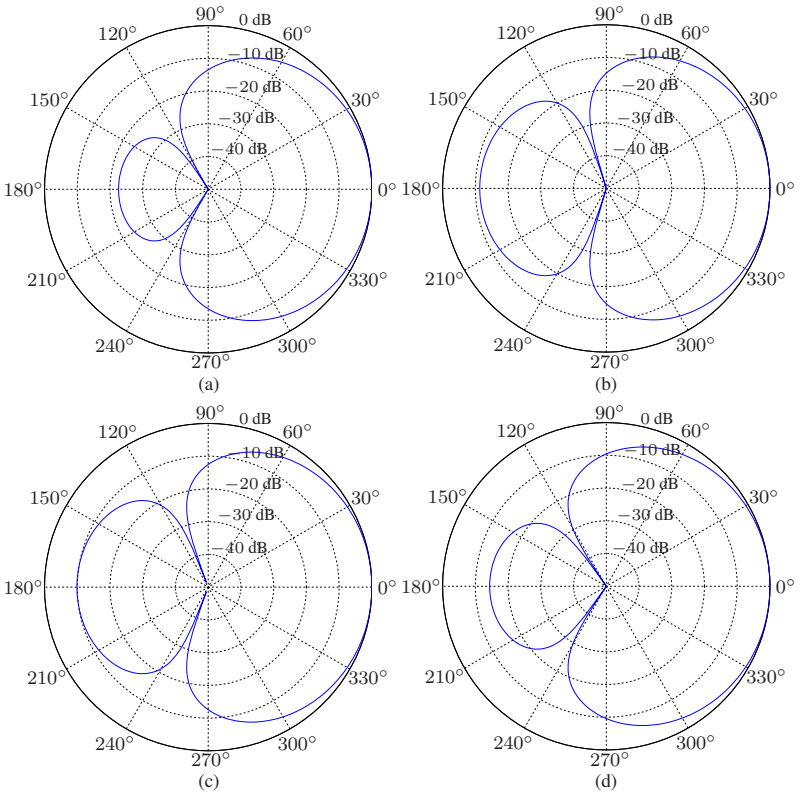

Fig. 3.33 Beampatterns of the robust global supercardioid, $\mathbf{h}_{\mathrm{S1},\epsilon_2}$, for $f = 1$ kHz, $\delta = 5$ mm, $M_0 = 4$, and several values of ϵ_2: (a) $\epsilon_2 = 10^{-5}$, (b) $\epsilon_2 = 10^{-4}$, (c) $\epsilon_2 = 10^{-3}$, and (d) $\epsilon_2 = 10^{-2}$.

$$\mathbf{\Gamma}_{\mathrm{f},\mathbf{h}_{1,\mathrm{DS}}} = \left(\mathbf{h}_{1,\mathrm{DS}} \otimes \mathbf{I}_{M_0}\right)^H \mathbf{\Gamma}_{\mathrm{f}} \left(\mathbf{h}_{1,\mathrm{DS}} \otimes \mathbf{I}_{M_0}\right), \tag{3.265}$$

$$\mathbf{\Gamma}_{\mathrm{b},\mathbf{h}_{1,\mathrm{DS}}} = \left(\mathbf{h}_{1,\mathrm{DS}} \otimes \mathbf{I}_{M_0}\right)^H \mathbf{\Gamma}_{\mathrm{b}} \left(\mathbf{h}_{1,\mathrm{DS}} \otimes \mathbf{I}_{M_0}\right). \tag{3.266}$$

Let $\mathbf{t}_{2,\mathbf{h}_{1,\mathrm{DS}}}$ be the eigenvector associated with the maximum eigenvalue of $\mathbf{\Gamma}^{-1}_{\mathrm{b},\mathbf{h}_{1,\mathrm{DS}}} \mathbf{\Gamma}_{\mathrm{f},\mathbf{h}_{1,\mathrm{DS}}}$. Then, it is clear that another supercardioid at the second ULA is

$$\mathbf{h}_{2,\mathrm{S2}} = \frac{\mathbf{t}_{2,\mathbf{h}_{1,\mathrm{DS}}}}{\mathbf{d}^H_{2,0} \mathbf{t}_{2,\mathbf{h}_{1,\mathrm{DS}}}}. \tag{3.267}$$

Therefore, another version of the robust global supercardioid is

$$\mathbf{h}_{\mathrm{S2}} = \mathbf{h}_{1,\mathrm{DS}} \otimes \mathbf{h}_{2,\mathrm{S2}}. \tag{3.268}$$

If we don't care much about white noise amplification, we can derive other supercardioid beamformers that give higher values of the FBR than the one

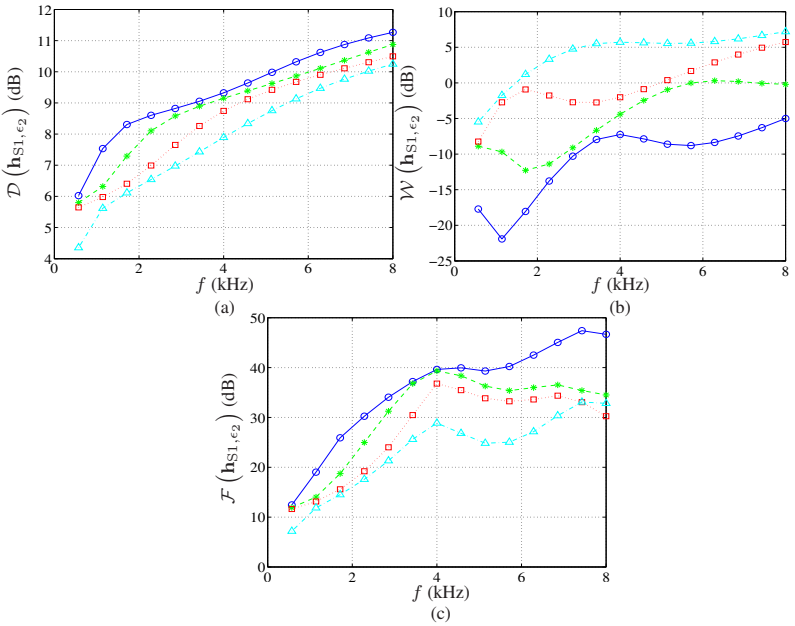

Fig. 3.34 Performance of the robust global supercardioid, $\mathbf{h}_{\mathrm{S1},\epsilon_2}$, as a function of frequency for $\delta = 5$ mm, $M_0 = 4$, and several values of ϵ_2: $\epsilon_2 = 10^{-5}$ (solid line with circles), $\epsilon_2 = 10^{-4}$ (dashed line with asterisks), $\epsilon_2 = 10^{-3}$ (dotted line with squares), and $\epsilon_2 = 10^{-2}$ (dash-dot line with triangles). (a) DF, (b) WNG, and (c) FBR.

with $\mathbf{h}_{\mathrm{S1}}$ or $\mathbf{h}_{\mathrm{S2}}$. For example, we can maximize separately the two FBRs, $\mathcal{F}_1(\mathbf{h}_1)$ and $\mathcal{F}_2(\mathbf{h}_2)$, of the subarrays. We get

$$\mathbf{h}_{1,\mathrm{S}} = \frac{\mathbf{t}_1}{\mathbf{d}_{1,0}^H \mathbf{t}_1}, \tag{3.269}$$

$$\mathbf{h}_{2,\mathrm{S}} = \frac{\mathbf{t}_2}{\mathbf{d}_{2,0}^H \mathbf{t}_2}, \tag{3.270}$$

where $\mathbf{t}_1$ and $\mathbf{t}_2$ are the eigenvectors corresponding to the maximum eigenvalues of the matrices $\mathbf{\Gamma}_{\mathrm{b},1}^{-1}\mathbf{\Gamma}_{\mathrm{f},1}$ and $\mathbf{\Gamma}_{\mathrm{b},2}^{-1}\mathbf{\Gamma}_{\mathrm{f},2}$, respectively. As a consequence, another global supercardioid is

$$\mathbf{h}_{\mathrm{S3}} = \mathbf{h}_{1,\mathrm{S}} \otimes \mathbf{h}_{2,\mathrm{S}}. \tag{3.271}$$

Figure 3.35 displays the directivity patterns of the robust global supercardioid, $\mathbf{h}_{\mathrm{S3}}$, for $f = 1$ kHz, $\delta = 5$ mm, and different numbers of sensors M. Figure 3.36 shows plots of the DFs, WNGs, and FBRs of the robust global supercardioid, $\mathbf{h}_{\mathrm{S3}}$, as a function of frequency. We observe that the FBR and DF of $\mathbf{h}_{\mathrm{S3}}$ are larger than those of $\mathbf{h}_{\mathrm{S1}}$, but the WNG of $\mathbf{h}_{\mathrm{S3}}$ is lower than that of $\mathbf{h}_{\mathrm{S1}}$ (compare Figs 3.32 and 3.36). As we increase the number of sen-

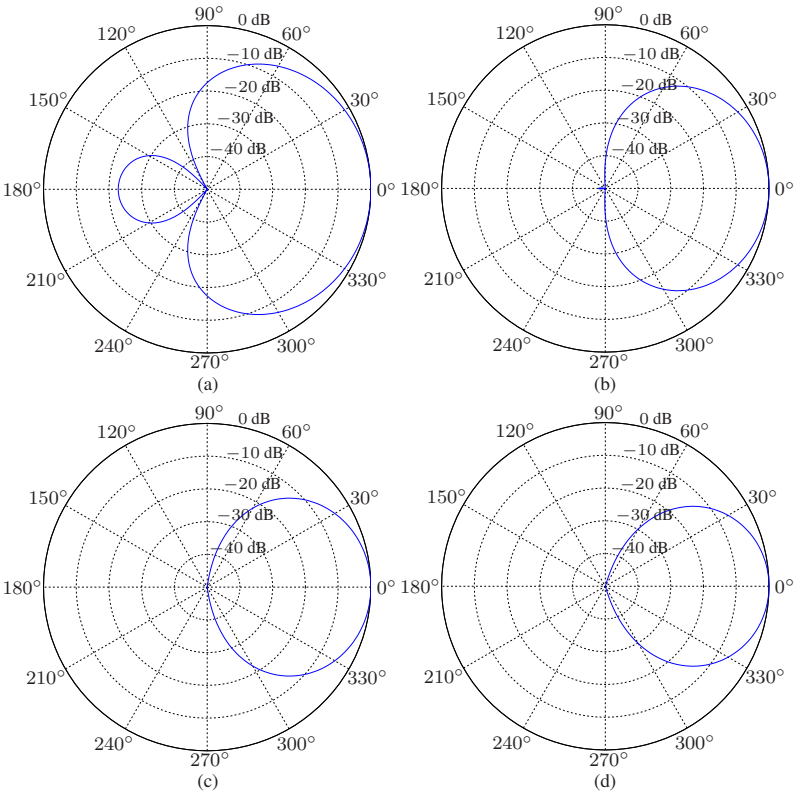

Fig. 3.35 Beampatterns of the robust global supercardioid, $\mathbf{h}_{\mathrm{S3}}$, for $f = 1$ kHz, $\delta = 5$ mm, and different numbers of sensors $M = M_0^2$: (a) $M_0 = 2$, (b) $M_0 = 3$, (c) $M_0 = 4$, and (d) $M_0 = 5$.

sors, the DF and FBR of the robust global supercardioid increase for the mid-range frequencies, but the WNG decreases.

Now, if we want to fully maximize the FBR in (3.206), we need to derive an iterative algorithm.

At iteration 0, we may take

$$\begin{aligned}\mathbf{h}_2^{(0)} &= \mathbf{h}_{2,\mathrm{S}} \\ &= \frac{\mathbf{t}_2}{\mathbf{d}_{2,0}^H \mathbf{t}_2}.\end{aligned} \tag{3.272}$$

Substituting $\mathbf{h}_2^{(0)}$ into (3.223) and (3.224), we get

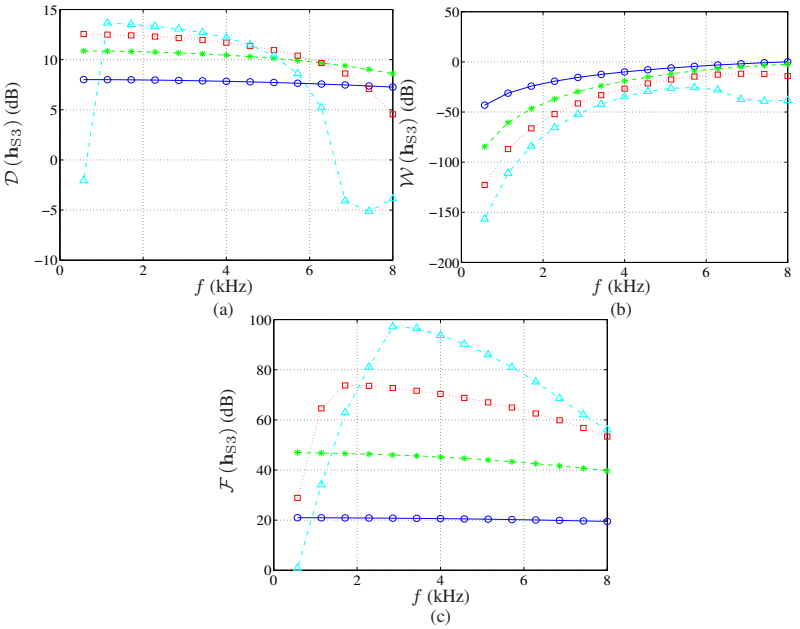

Fig. 3.36 Performance of the robust global supercardioid, $\mathbf{h}_{S3}$, as a function of frequency for $\delta = 5$ mm and different numbers of sensors $M = M_0^2$: $M_0 = 2$ (solid line with circles), $M_0 = 3$ (dashed line with asterisks), $M_0 = 4$ (dotted line with squares), and $M_0 = 5$ (dash-dot line with triangles). (a) DF, (b) WNG, and (c) FBR.

$$\mathbf{\Gamma}_{\mathrm{f},\mathbf{h}_2^{(0)}} = \left(\mathbf{I}_{M_0} \otimes \mathbf{h}_2^{(0)}\right)^H \mathbf{\Gamma}_{\mathrm{f}} \left(\mathbf{I}_{M_0} \otimes \mathbf{h}_2^{(0)}\right), \tag{3.273}$$

$$\mathbf{\Gamma}_{\mathrm{b},\mathbf{h}_2^{(0)}} = \left(\mathbf{I}_{M_0} \otimes \mathbf{h}_2^{(0)}\right)^H \mathbf{\Gamma}_{\mathrm{b}} \left(\mathbf{I}_{M_0} \otimes \mathbf{h}_2^{(0)}\right). \tag{3.274}$$

Now, plugging these expressions into the FBR in (3.222), we obtain at iteration 1:

$$\mathcal{F}\left(\mathbf{h}_1^{(1)}|\mathbf{h}_2^{(0)}\right) = \frac{\left(\mathbf{h}_1^{(1)}\right)^H \mathbf{\Gamma}_{\mathrm{f},\mathbf{h}_2^{(0)}} \mathbf{h}_1^{(1)}}{\left(\mathbf{h}_1^{(1)}\right)^H \mathbf{\Gamma}_{\mathrm{b},\mathbf{h}_2^{(0)}} \mathbf{h}_1^{(1)}}. \tag{3.275}$$

The maximization of $\mathcal{F}\left(\mathbf{h}_1^{(1)}|\mathbf{h}_2^{(0)}\right)$ with respect of $\mathbf{h}_1^{(1)}$ leads to

$$\mathbf{h}_1^{(1)} = \frac{\mathbf{t}_1^{(0)}}{\mathbf{d}_{1,0}^H \mathbf{t}_1^{(0)}}, \tag{3.276}$$

where $\mathbf{t}_1^{(0)}$ is the eigenvector corresponding to the maximum eigenvalue of the matrix $\mathbf{\Gamma}^{-1}_{\mathrm{b},\mathbf{h}_2^{(0)}}\mathbf{\Gamma}_{\mathrm{f},\mathbf{h}_2^{(0)}}$. Using $\mathbf{h}_1^{(1)}$ in (3.226) and (3.227), we get

$$\mathbf{\Gamma}_{\mathrm{f},\mathbf{h}_1^{(1)}} = \left(\mathbf{h}_1^{(1)} \otimes \mathbf{I}_{M_0}\right)^H \mathbf{\Gamma}_{\mathrm{f}} \left(\mathbf{h}_1^{(1)} \otimes \mathbf{I}_{M_0}\right), \tag{3.277}$$

$$\mathbf{\Gamma}_{\mathrm{b},\mathbf{h}_1^{(1)}} = \left(\mathbf{h}_1^{(1)} \otimes \mathbf{I}_{M_0}\right)^H \mathbf{\Gamma}_{\mathrm{b}} \left(\mathbf{h}_1^{(1)} \otimes \mathbf{I}_{M_0}\right). \tag{3.278}$$

As a result, the FBR in (3.225) is

$$\mathcal{F}\left(\mathbf{h}_2^{(1)}|\mathbf{h}_1^{(1)}\right) = \frac{\left(\mathbf{h}_2^{(1)}\right)^H \mathbf{\Gamma}_{\mathrm{f},\mathbf{h}_1^{(1)}} \mathbf{h}_2^{(1)}}{\left(\mathbf{h}_2^{(1)}\right)^H \mathbf{\Gamma}_{\mathrm{b},\mathbf{h}_1^{(1)}} \mathbf{h}_2^{(1)}}, \tag{3.279}$$

whose maximization with respect to $\mathbf{h}_2^{(1)}$ gives

$$\mathbf{h}_2^{(1)} = \frac{\mathbf{t}_2^{(1)}}{\mathbf{d}_{2,0}^H \mathbf{t}_2^{(1)}}, \tag{3.280}$$

where $\mathbf{t}_2^{(1)}$ is the eigenvector corresponding to the maximum eigenvalue of the matrix $\mathbf{\Gamma}^{-1}_{\mathrm{b},\mathbf{h}_1^{(1)}}\mathbf{\Gamma}_{\mathrm{f},\mathbf{h}_1^{(1)}}$.

Continuing to iterate up to iteration n, we easily get for the first filter:

$$\mathbf{h}_1^{(n)} = \frac{\mathbf{t}_1^{(n-1)}}{\mathbf{d}_{1,0}^H \mathbf{t}_1^{(n-1)}}, \tag{3.281}$$

where $\mathbf{t}_1^{(n-1)}$ is the eigenvector corresponding to the maximum eigenvalue of the matrix $\mathbf{\Gamma}^{-1}_{\mathrm{b},\mathbf{h}_2^{(n-1)}}\mathbf{\Gamma}_{\mathrm{f},\mathbf{h}_2^{(n-1)}}$, with

$$\mathbf{\Gamma}_{\mathrm{f},\mathbf{h}_2^{(n-1)}} = \left(\mathbf{I}_{M_0} \otimes \mathbf{h}_2^{(n-1)}\right)^H \mathbf{\Gamma}_{\mathrm{f}} \left(\mathbf{I}_{M_0} \otimes \mathbf{h}_2^{(n-1)}\right), \tag{3.282}$$

$$\mathbf{\Gamma}_{\mathrm{b},\mathbf{h}_2^{(n-1)}} = \left(\mathbf{I}_{M_0} \otimes \mathbf{h}_2^{(n-1)}\right)^H \mathbf{\Gamma}_{\mathrm{b}} \left(\mathbf{I}_{M_0} \otimes \mathbf{h}_2^{(n-1)}\right), \tag{3.283}$$

and for the second filter:

$$\mathbf{h}_2^{(n)} = \frac{\mathbf{t}_2^{(n)}}{\mathbf{d}_{2,0}^H \mathbf{t}_2^{(n)}}, \tag{3.284}$$

where $\mathbf{t}_2^{(n)}$ is the eigenvector corresponding to the maximum eigenvalue of the matrix $\mathbf{\Gamma}^{-1}_{\mathrm{b},\mathbf{h}_1^{(n)}}\mathbf{\Gamma}_{\mathrm{f},\mathbf{h}_1^{(n)}}$, with

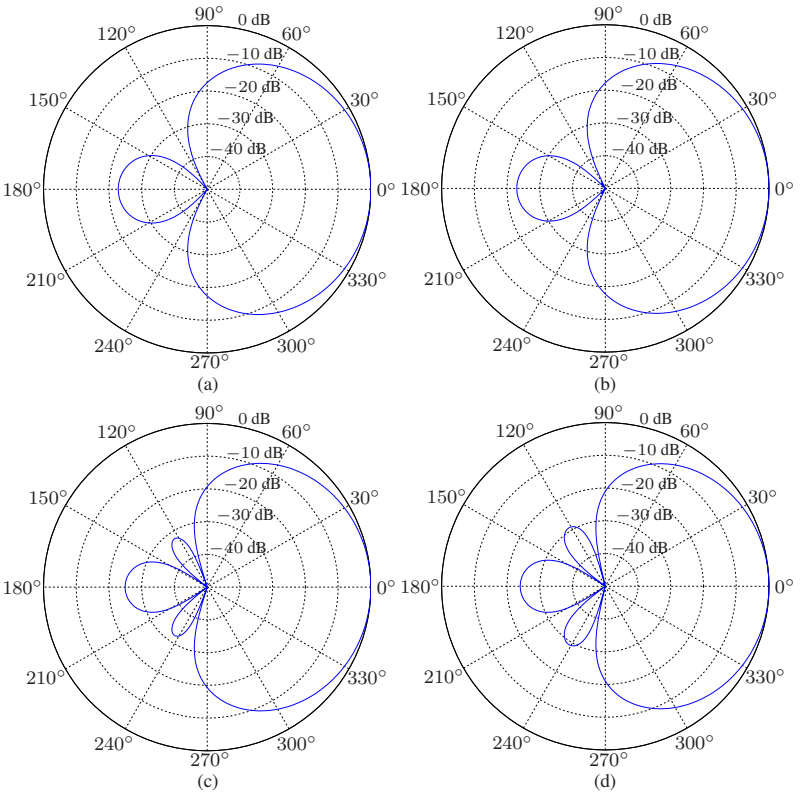

Fig. 3.37 Beampatterns of the supercardioid beamformer, $\mathbf{h}_{\mathrm{S}}^{(n)}$, for $M_0 = 2$, $f = 1$ kHz, and $\delta = 5$ mm, obtained at the iteration n: (a) $n = 0$, (b) $n = 1$, (c) $n = 2$, and (d) $n = 5$.

$$\mathbf{\Gamma}_{\mathrm{f},\mathbf{h}_1^{(n)}} = \left(\mathbf{h}_1^{(n)} \otimes \mathbf{I}_{M_0}\right)^H \mathbf{\Gamma}_{\mathrm{f}} \left(\mathbf{h}_1^{(n)} \otimes \mathbf{I}_{M_0}\right), \tag{3.285}$$

$$\mathbf{\Gamma}_{\mathrm{b},\mathbf{h}_1^{(n)}} = \left(\mathbf{h}_1^{(n)} \otimes \mathbf{I}_{M_0}\right)^H \mathbf{\Gamma}_{\mathrm{b}} \left(\mathbf{h}_1^{(n)} \otimes \mathbf{I}_{M_0}\right). \tag{3.286}$$

Finally, we deduce that the supercardioid beamformer is at iteration n:

$$\mathbf{h}_{\mathrm{S}}^{(n)} = \mathbf{h}_1^{(n)} \otimes \mathbf{h}_2^{(n)}. \tag{3.287}$$

Figure 3.37 displays the directivity patterns of the supercardioid beamformer, $\mathbf{h}_{\mathrm{S}}^{(n)}$, for $M_0 = 2$, $f = 1$ kHz, and $\delta = 5$ mm, obtained at the iteration n for several values of n. Figure 3.38 shows plots of the DFs, WNGs, and FBRs of the supercardioid beamformer, $\mathbf{h}_{\mathrm{S}}^{(n)}$, as a function of frequency. The iteration $n = 0$ corresponds to the robust global supercardioid, $\mathbf{h}_{\mathrm{S3}}$. We observe that the FBR and DF of the supercardioid beamformer, $\mathbf{h}_{\mathrm{S}}^{(n)}$, are larger than those of $\mathbf{h}_{\mathrm{S3}}$ and $\mathbf{h}_{\mathrm{S1}}$, but the WNGs of $\mathbf{h}_{\mathrm{S}}^{(n)}$ and $\mathbf{h}_{\mathrm{S3}}$ are lower

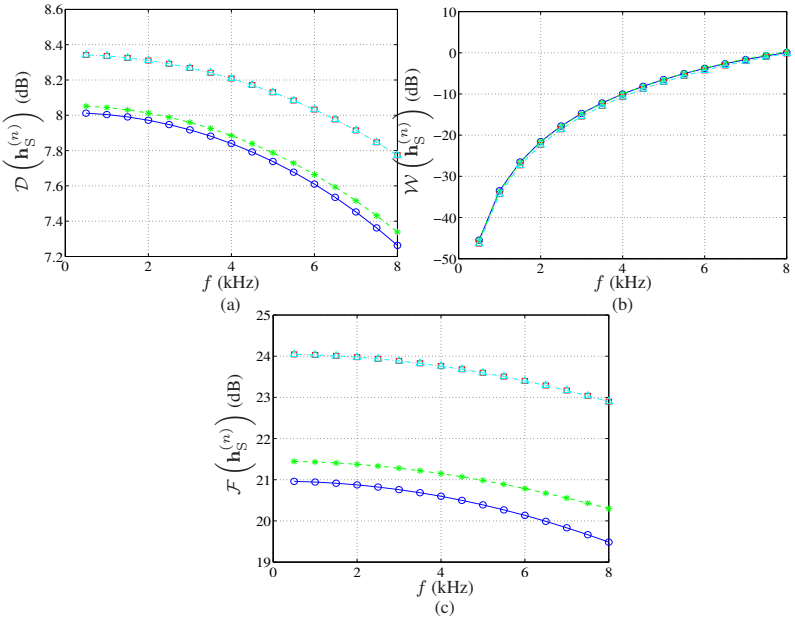

Fig. 3.38 Performance of the supercardioid beamformer, $\mathbf{h}_{\mathrm{S}}^{(n)}$, as a function of frequency for $M_0 = 2$, $\delta = 5$ mm, and several values of n: $n = 0$ (solid line with circles), $n = 1$ (dashed line with asterisks), $n = 3$ (dotted line with squares), and $n = 10$ (dash-dot line with triangles). (a) DF, (b) WNG, and (c) FBR.

than that of $\mathbf{h}_{\mathrm{S1}}$ (compare Figs 3.38, 3.36 and 3.32). Furthermore, the DF and FBR of the supercardioid beamformer, $\mathbf{h}_{\mathrm{S}}^{(n)}$, increase at each iteration, and roughly converge after three iterations, while the WNG remains almost the same at each iteration.

References

1. H. L. Van Trees, *Optimum Array Processing: Part IV of Detection, Estimation, and Modulation Theory*. New York, NY: John Wiley & Sons, Inc., 2002.
2. J. Benesty, I. Cohen, and J. Chen, *Fundamentals of Signal Enhancement and Array Signal Processing*. Singapore: Wiley–IEEE Press, 2018.
3. S. Haykin, *Adaptive Filter Theory*. Fourth Edition, Upper Saddle River, NJ: Prentice-Hall, 2002.
4. J. Benesty, C. Paleologu, and S. Ciochina, "On the identification of bilinear forms with the Wiener filter," *IEEE Signal Process. Lett.*, vol. 24, pp. 653–657, May 2017.
5. J. Capon, "High resolution frequency-wavenumber spectrum analysis," *Proc. IEEE*, vol. 57, pp. 1408–1418, Aug. 1969.
6. R. T. Lacoss, "Data adaptive spectral analysis methods," *Geophysics*, vol. 36, pp. 661–675, Aug. 1971.

7. A. Booker and C. Y. Ong, "Multiple constraint adaptive filtering," *Geophysics*, vol. 36, pp. 498–509, June 1971.
8. O. Frost, "An algorithm for linearly constrained adaptive array processing," *Proc. IEEE*, vol. 60, pp. 926–935, Jan. 1972.
9. G. W. Elko and J. Meyer, "Microphone arrays," in *Springer Handbook of Speech Processing*, J. Benesty, M. M. Sondhi, and Y. Huang, Eds., Berlin, Germany: Springer-Verlag, 2008, Chapter 50, pp. 1021–1041.
10. G. W. Elko, "Superdirectional microphone arrays," in *Acoustic Signal Processing for Telecommunication*, S. L. Gay and J. Benesty, Eds. Boston, MA: Kluwer Academic Publishers, 2000, Chapter 10, pp. 181–237.
11. J. Benesty and J. Chen, *Study and Design of Differential Microphone Arrays*. Berlin, Germany: Springer-Verlag, 2012.
12. J. Chen, J. Benesty, and C. Pan "On the design and implementation of linear differential microphone arrays," *J. Acoust. Soc. Am.*, vol. 136, pp. 3097–3113, Dec. 2014.
13. R. N. Marshall and W. R. Harry, "A new microphone providing uniform directivity over an extended frequency range," *J. Acoust. Soc. Am.*, vol. 12, pp. 481–497, 1941.